2021

# Biofabricated platforms for wound healing and skin regeneration

Lingzhi Kang
*University of Wollongong*

**Australian Research Council Centre of Excellence for Electromaterials Science**

**The Intelligent Polymer Research Institute**

**The Australian Institute for Innovative Materials**

# Biofabricated platforms for wound healing and skin regeneration

Lingzhi Kang

Supervisors:

Prof. Gordon G. Wallace, Dr, Zhilian Yue, Dr, Xiao Liu and A/Prof. Chris Baker

This thesis is presented as part of the requirement for the conferral of the degree:

**Doctor of Philosophy**

University of Wollongong

The Intelligent Polymer Research Institute

May 2021

# Dedication

*To my parents:*

*Aizhi Li and Xinlin Kang, for their support, encouragement, and constant love.*

*To my uncle:*

*Maishou Li, you were the one who inspired me to go abroad and to pursue a Ph.D. degree.*

*To my baby in my belly:*

*Shanshui Liu, thanks for sitting patiently in my womb and giving me the feeling of pure delight.*

*To my husband:*

*Chuhao Liu, who walked me through the challenges of Ph.D. life with endless love and persistent encouragement.*

*Without you, this would not have been possible.*

# Certification

*I, Lingzhi Kang, declare that this thesis submitted in fulfilment of the requirements for the conferral of the degree Doctor of Philosophy, from the University of Wollongong, is wholly my own work unless otherwise referenced or acknowledged. This document has not been submitted for qualifications at any other academic institution.*

_____

***Lingzhi Kang***

*May 2021*

# Acknowledgments

I would like to express my deepest gratitude to my supervisors Prof. Gordon G. Wallace, Dr. Zhilian Yue, Dr. Xiao Liu, and Prof. Chris Baker, who gave me the valuable opportunity to work in a highly interdisciplinary research center in IPRI where I could learn from many talented colleagues and join innovative collaborations. Especially thanks to Prof. Gordon Wallace, it's a great honor to work as his PhD student. His outstanding professionalism, valuable advice, and patient guidance has encouraged and helped me so much along my PhD journey. He also inspired me a lot in scientific communication skills, which inspired me to take part in the 2019 UOW 3 Minute Thesis Competition and won the People's Choice Award. He also offered us a valuable opportunity to finish the entrepreneurship course, which will undoubtedly be a massive advantage for our future career. The achievements during my PhD study would have been impossible without his guidance and help.

I would like to thank Dr. Zhilian Yue for her immense knowledge and tremendous mentoring in my research. Over the past three and a half years, she has always encouraged me to explore my research interests and allowed me to grow. Her guidance helped me so much on the experiments conduction, data analysis and manuscripts revision. Her knowledge and suggestions have helped me tremendously in my thesis writing and publications. Without her precious support and guidance, it would not be possible for me to finish this research.

I would like to thank Dr. Xiao Liu, for her patience, motivation, and constant support all along the way. She has always been able to provide instant support during my entire PhD period, making it possible for me to perform my research efficiently. I sincerely appreciate all her efforts and ideas contributed to my PhD periods.

I would specifically like to thank my clinic mentor Prof. Chris Baker from the Department of Dermatology, St Vincent's Hospital Melbourne, who sponsored my research and involved

significantly with the cell work and translational issues. As an experienced and eminent dermatologist and qualified cell biologist, he always encouraged me, gave many valuable feedbacks and suggestions, and put considerable effort in reviewing manuscripts.

Great appreciation to my collaborator, Dr. Pia C. Winberg, from Venus Shell Systems Pty Ltd., who kindly offered the materials needed for my first research project as well as for reviewing our publications. Thanks to my colleagues in IPRI: Dr. Zhi Chen, Xifang Chen, Ying Zhou, for publishing manuscripts together and review papers.

I would also like to thank all the IPRI numbers. Thanks to Toni Campbell and FIL4IT, who have always helped keep all the paper works and meetings highly organized. Also, thanks to lab supervisors Dr. Kerry Gilmore, Dr. Johnson Chung, Dr. Kalani Ruberu, and Dr. Eva Tomaskovic-Crook, for their enormous effort to provide us an excellent experimental environment. And thanks to my friends and colleagues at IPRI: Prof. Jun Chen, Dr. Caiyun Wang, Dr. Qi Gu, Dr. Dan Yang, Dr. Zhi Chen, Dr. Yang Xiao, Dr. Jiangfeng Li, Liang Wu, Yuchao Fan, Kezhong Wang, Ying Zhou, Yu Hou, for all the support and growing together. The lab will be different without them.

Lingzhi Kang

# Abstract

Skin is the largest organ of the our body, and wound healing is an issue of some critical concern. This study aims to fabricate scaffolds to facilitate wound healing. The major extracellular matrix (ECM) components, including collagen, elastin, glycosaminoglycans (GAGs, including hyaluronic acid), and GAG-like marine polysaccharides-ulvan, were explored here to mimic the compositional property of natural skin. Electrocompaction, which is a technique used to fabricate densely packed and highly ordered collagen structures, was utilized in this research to mimic the structural property of natural skin ECM. It is worth noting that, the work described in this thesis is the first example of utilizing the technique of electrocompaction in the area of skin regeneration.

To test the feasibility of collagen electrocompaction and evaluate its ability to support skin regeneration, two types of skin scaffolds were fabricated and evaluated. In the first study, a collagen/sulfated xylorhamnoglycuronan (SXRGlu) scaffold was built. The fabricated electrocompacted collagen/SXRGlu matrices (ECLCU) were characterized in terms of micromorphology, mechanical property, water uptake, and degradability. The viability, proliferation, and morphology of human dermal fibroblasts (HDFs) cells on the fabricated structures were also evaluated. The results indicated that the electrocompaction process could promote structures that support HDFs proliferation, and the introduce of SXRGlu improves the water uptake ability and improves stability against collagenase degradation, also supporting fibroblast spreading. Therefore, all these results suggest that the electrocompacted collagen/SXRGlu scaffold is a potential candidate as a dermal substitute with enhanced biostability and biocompatibility.

Then, to better mimic the compositional property of natural skin ECM, an ECM-like scaffold comprising the structural protein collagen I (COL) and elastin (ELN), and glycosaminoglycans (GAGs) hyaluronan (HA) were fabricated and evaluated. Specifically, collagen and elastin were electrochemically aligned to mimic the morphological and mechanical properties of the dermal matrix. HA was incorporated into the electrocompacted collagen-elastin (CE) matrices via physical

adsorption and chemical linking, to achieve a final composition of 7:2:1 between collagen, elastin, and HA. This produced a final collagen/elastin/hyaluronic acid scaffold (CEH) that recapitulated compositional characteristics of the native skin ECM. In this research, we analyzed the effect of CEH composition on the cultivation of human dermal fibroblast cells (HDFs) and immortalized human keratinocytes (HaCaTs). We showed that the CEH scaffold supported dermal regeneration by promoting HDFs proliferation, ECM deposition, and differentiation into myofibroblasts. The CEH scaffold also supported epidermis growth by supporting HaCaT proliferation, differentiation, stratification. A double-layered epidermal-dermal skin structure was also constructed on the CEH scaffold supporting its ability to promote skin cell function and skin regeneration.

Taken together, ECM-like skin scaffolds that mimic the compositional and structural characteristics of natural skin ECM were fabricated and evaluated in this thesis. The results confirmed the feasibility of utilizing the method of electrocompaction for skin scaffold fabrication. The fabricated skin scaffolds, especially the ECM-like CEH scaffold, may serve as a promising candidate for skin regeneration and wound healing application.

Keywords: collagen; glycosaminoglycans (GAGs); electrocompaction; biomimicry; skin scaffold; skin regeneration; wound healing;

# Publications

1. **Lingzhi Kang**, Ying Zhou, Xifang Chen, Zhilian Yue, Xiao Liu, Chris Baker, Gordon G. Wallace. “Fabrication and characterization of an electrocompacted collagen/elastin/hyaluronic acid sheet as a potential skin scaffold” (Under revision by supervisors).

2. **Lingzhi Kang**, Zhilian Yue, Xiao Liu, Chris Baker, and Gordon Wallace. “Collagen and glycosaminoglycan (GAG) based platforms for skin regeneration” (In preparation).

3. **Lingzhi Kang**, Xiao Liu, Zhilian Yue, Zhi Chen, Chris Baker, Pia Winberg, and Gordon Wallace. "Fabrication and in vitro characterization of electrochemically compacted collagen/sulfated xylorhamnoglycuronan matrix for wound healing applications." Polymers 10, no. 4 (2018): 415.

4. Zhou, Ying, **Lingzhi Kang**, Zhilian Yue, Xiao Liu, and Gordon G. Wallace. "Composite tissue adhesive containing catechol-modified hyaluronic acid and poly-L-lysine." ACS Applied Bio Materials (2019).

5. Hadis Khakbaz, Kalani Ruberu, **Lingzhi Kang,** Sepehr Talebian, Sepidar Sayyar, Benjamin Filippi, Mehdi Khatamifar, Stephen Beirne, and Peter C. Innis. “3D Printing of Highly Flexible, Cytocompatible Nanocomposites for Thermal Management” (Submitted to Advanced Functional Materials, 2020).

# Conference Presentations

1. 2019 TERMIS (Tissue Engineering & Regenerative Medicine International Society – Asian Pacific Chapter and the 7th Asian Biomaterials Congress), "Fabrication and characterization of an electrocompacted collagen/elastin/hyaluronic acid sheet as a potential skin scaffold", Brisbane Convention and Exhibition Centre, Brisbane, Queensland, Australia, Oct 14 - 18, 2019

2. International Conference on Biofabrication, "Fabrication and in vitro characterization of electrochemically compacted collagen/sulfated xylorhamnoglycuronan matrix for wound healing applications" (Poster presentation), Wurzburg, Germany, 28-31 October, 2018.

3. 2018 ACES Full Centre Meeting, "Electro-compacted collagen for skin repair and regeneration" (Poster presentation), Innovation Campus, University of Wollongong, 30 June-01 July 2018.

4. 2018 International Conference On Nanoscience and Nanotechnology (ICONN), "Electro-compacted collagen for skin repair and regeneration" (Poster presentation), University of Wollongong, 29 Jan -2 Feb 2018.

5. ACES Clinical Connections Workshop, "Collage-based platforms for wound healing and skin regeneration" (Oral presentation), Wollongong Private Hospital, Wollongong, Australia, 30 January 2017.

# List of Abbreviations

| | |
|---|---|
| 2D | Two-dimensional |
| 3D | Three-dimensional |
| mg | Milligram |
| ml | Milliliter |
| mm | Millimeter |
| µg | Microgram |
| µL | Microliter |
| α-SMA | Alpha-smooth muscle actin |
| BM | Basement membrane |
| bFGF | Basic fibroblast growth factor |
| DMEM/F-12 | Dulbecco's Modified Eagle Medium: Nutrient Mixture F-12 |
| ECM | Extracellular matrix (ECM) |
| EDC | 1-Ethyl-3-(3-dimethylaminopropyl)-carbodiimide |
| NHS | N-hydroxysuccinimide |
| FGF-2 | Fibroblast growth factor (FGF-2) |
| HA | Hyaluronic acid |
| HEPES | (4-(2-hydroxyethyl)-1-piperazineethanesulfonic acid) |

| | |
|---|---|
| MMP | Matrix metalloprotease |
| NaCl | Sodium chloride |
| PFA | Paraformaldehyde |
| PI | Propidium iodide |
| RT-qPCR | Reverse transcription-quantitative PCR |
| SEM | Scanning electron microscope |
| TCP | Tissue culture plastic |
| TGF-b3 | Transforming growth factors-beta3 |
| FGF | Fibroblast growth factor |
| GAGs | Glycosaminoglycans |
| PDGF | Platelet-derived growth factor |
| EGF | Epidermal growth factors |
| KGF | Keratinocyte growth factors |
| TGF α/β | Transforming growth factors α and β |
| αSMA | α-smooth muscle actin |
| VEGF | Vascular endothelial growth factor |
| TBSA | Total burned surface area |
| KCs | Keratinocytes |
| FBs | Fibroblasts |

| | |
|---|---|
| RGD | Arginine-glycine-aspartic acid |
| HMWHA | High molecular weight hyaluronic acid |
| HS | Heparan sulfate |
| LMWHs | Low molecular weight heparins |
| CS | Chondroitin sulfate |
| CTAB | Cetyltrimethylammonium bromide |
| DS | Dermatan sulfate |
| CNC | Cellulose nanocrystals |
| CE | Co-electrocompacted collagen and elastin |
| CEH | CE coated with hyaluronic acid |
| DMMB | Dimethylmethylene blue |
| KS | Keratan sulfate |
| HDFs | Human dermal fibroblast cells |
| HaCaTs | Human immortalized keratinocytes |
| FBS | Fetal bovine serum |
| ALI | Air liquid interface cell culture |
| FTIR | Fourier-transform infrared spectroscopy |
| NMR | Nuclear Magnetic Resonance |
| PI | Propidium iodide |

| | |
|---|---|
| SXRGlu | Sulfated xylorhamnoglycuronan |
| ECL | Electrochemically aligned collagen |
| ECLCU | SXRGlu conjugated-ECL |
| HMDS | Hexamethyldisilane |
| DAPI | 4′,6-diamidino-2-phenylin |

# List of Figures

**Figure 5.8** Expression of proteins of reconstructed epidermis on CEH scaffolds: involucrin & loricrin (green, late differentiation marker), K10 (green, early differentiation marker), E-cadherin (a cell-junction protein), Ki-67 (red, proliferation maker), and DAPI (blue, nuclei) stained sections of reconstructed epidermis.

**Figure 5.9** H&E staining of co-cultured HDFs and HaCaTs after 4 weeks.

**Figure 5.10** Immunostaining of E-cadherin, collagen I, loricrin, involucrin and cell nuclei (DAPI) in co-cultured HDFs and HaCaTs after 4 weeks.

# List of Tables

# Table of Contents

# Chapter 1

# General Introduction

## CONTENT

## 1.1 Human skin structure and function

Skin is the largest organ in the human body and acts as a physical barrier against the external environment, such as chemicals, UV-radiation, temperature, and pathogens [1]. Human skin is made up of three main layers (Figure 1.1): the epidermis, dermis, and hypodermis or subcutaneous [1].

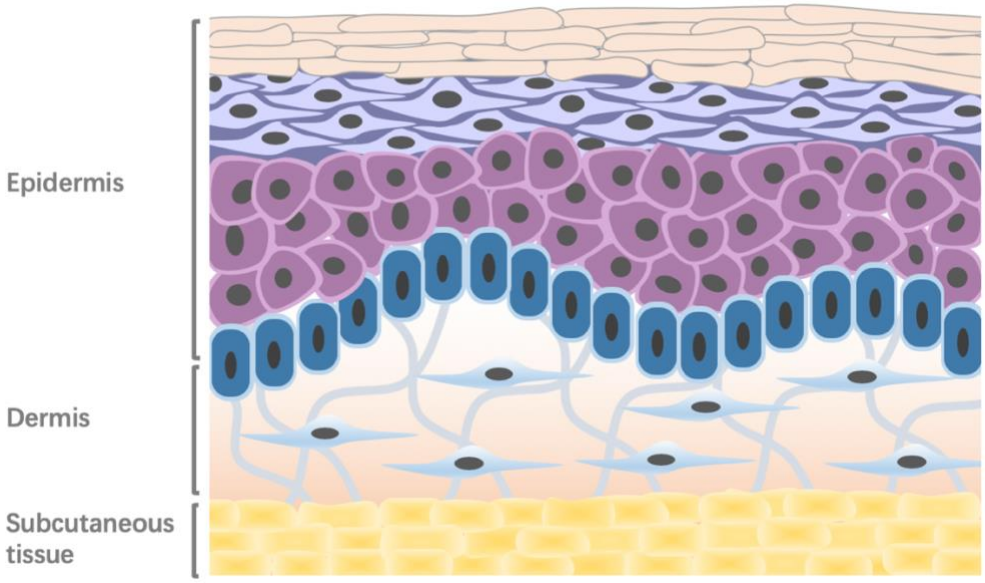


**Figure 1.1.** Human skin structure.

The epidermis contains mainly keratinocytes, which acts as the first barrier against harmful pathogens and environmental hazards. Underneath the epidermal region is the dermis, which is predominantly extracellular matrix with fibroblasts. The dermis can be categorized into two layers, an upper papillary dermal layer and a lower reticular dermal layer [2]. The ECM of the papillary dermis is mainly composed of thin, randomly oriented collagen fibers. The reticular dermis comprises type I collagen fibers that are thick and highly organized, and elastic fibers produced by dermal fibroblasts. Dermis houses nerves, blood vessels, and vital ECM components such as collagen, elastin, and glycosaminoglycans (GAGs). The layer connecting the dermis and the superficial

epidermis is the basement membrane (BM), which enables the remodeling of damaged skin in vitro [3]. The hypodermis consists mostly of connective tissues and fats. This layer is vital in the maintenance of homoeostasis and thermoregulation [4].

Apart from the three main layers in the skin, there are also affiliated skin structures such as melanin and hair follicles, which are crucial to the functions of the integumentary system [5]. Although skin mainly consists of fibroblasts, keratinocytes, and adipose tissue, there are also other cell types such as melanocytes, which can produce melanin [6], and immune cells [7, 8]. Once the skin is impaired, these cells start to repair the wound through a complicated wound healing procedure.

### 1.2 Wounds and wound healing process

In healthy skin, the epidermis and dermis form a protective barrier against the external environment. Once damaged, the complex wound healing process that involves growth factors, chemokines, and cytokines will be triggered to reconstitute skin function. The wound healing process is mainly composed of 3 overlapping stages (Figure 1.2): hemostatic, proliferative, and remodeling phases [8].

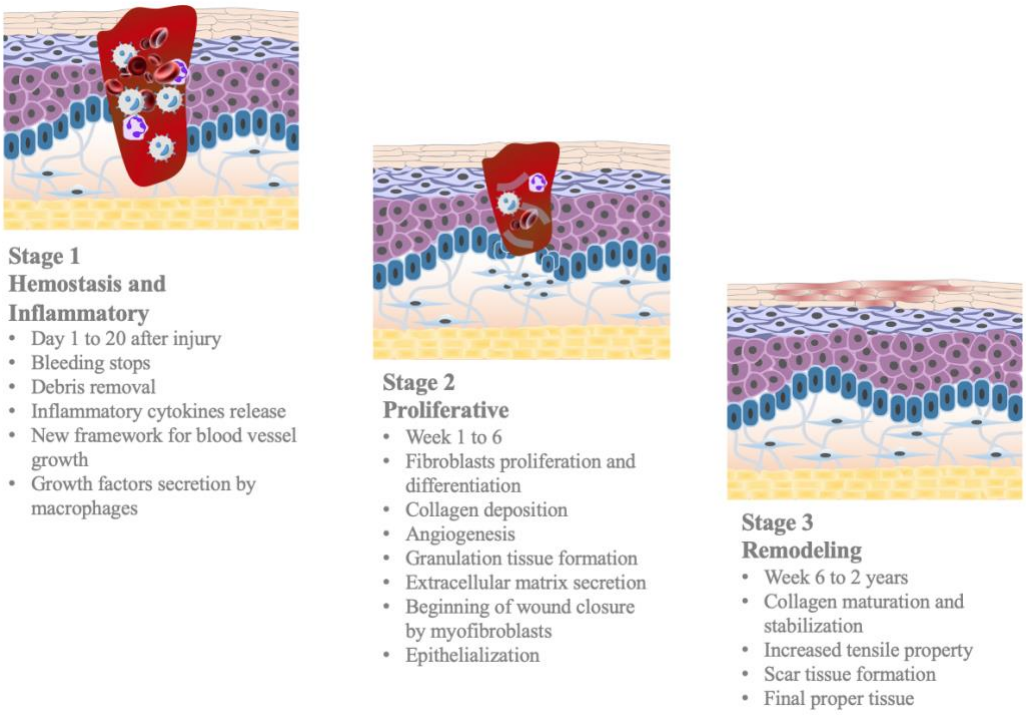


**Figure 1.2.** Wound healing stages.

### 1.2.1 Hemostasis and inflammation

The first stage in wound healing is the hemostasis stage during which platelets play a vital role in clot formation to stop bleeding. This is mainly accomplished by the aggregation and release of cytokines, chemokines, and hormones [2]. Once aggregated and attached to the exposed collagen surface, the platelets will be activated. This activation will further enable platelets to degranulate and release growth factors, such as platelet-derived growth factor (PDGF) [9]. Fibrin will also be activated under the effect of thrombin and forms a mesh as "glue" to interact with platelets. This interaction will produce clots that serve to plug the breakage in the blood vessels to further slowing the bleeding. Besides, vasoconstriction [10] occurs under the effect of vasoactive mediators such as serotonin, epinephrine, prostaglandins, and thromboxane to prevent blood loss [11].

Also, the release of these components will attract circulating immunologic cells that are responsible for clearing out damaged and dead cells together with bacteria and other debris. Among these cells, macrophages and neutrophils [12] are the primary immune cells and are essential in the early stage of wound healing process. Macrophages are responsible for clearing out the debris and bacteria, secreting 5 collagenase and elastases to break down injured tissue. Besides, macrophages will also release PDGF to stimulates fibroblast proliferation, migration and division, as well as smooth muscle cell proliferation [12].

During the inflammatory phase, T lymphocytes, which are attracted by the interleukin 1, also migrate into the wound and contributes to the production of collagenase [13]. Lymphocytes secrete wound healing related growth factors such as heparin-binding epidermal growth factor and basic fibroblast growth factor (bFGF) [14]. Lymphocytes are also crucial in antibody production and cellular immunity.

Hemostasis and inflammation are complicated stages that complement each other with hemostasis responsible for limiting bleeding and tissue damage, and inflammation accountable for repairing the damaged tissue and preparing the wound bed for the growth of new tissue.

### 1.2.2 Proliferation

In the proliferation phase, angiogenesis, epithelialization, collagen deposition, formation of granulation tissue, and wound contraction will occur [11]. Among all these activities, the formation of granulation tissue is a central part. This includes accumulation of inflammatory cells and fibroblasts, and new blood vessel formation in a matrix composed of collagen, fibronectin, glycosaminoglycans, and proteoglycans [15].

Granulation tissue is a newly formed connective tissue on the surface of a wound and is capable of filling in the wounds during the healing process. It is made up of tissue matrix

consisting of type I & III collagen, glycosaminoglycans, and fibronectin. This granulation tissue supports different types of cells, most of which can be associated with one of the following functions: formation of extracellular matrix, immunity, or vascularization [16]. As an essential component of the granulation tissue, fibroblasts are responsible for the secretion of vital skin components, including collagen, elastin, glycosaminoglycans, fibronectin, and proteases. During the proliferation stage, fibroblasts proliferate in response to different variety of growth factors produced by platelets and macrophages during the inflammation phase [17]. These growth factors include fibroblast growth factors (FGF), epidermal growth factors (EGF), and platelets derived growth factors (PDGF), which causes fibroblast to deposit granulation tissue in the wound [16]. Keratinocytes respond to EGF produced by the macrophages and keratinocyte growth factors (KGF) that are produced by fibroblasts.

Epithelization is the development of an epithelium layer over a denuded skin surface. This process happens within hours of an initial wound and epithelial cells must have a healthy bed of granulation tissue to migrate across [18]. At the beginning of epithelization, basal epithelial cells go through conformational changes to enable them to detach from other epidermal cells. Then these detached epithelial cells produce intracellular actin microfilaments, migrate across the open wound. At the same time, they will secret mediators, such as transforming growth factors α and β (TGF α/β) [19]. Under the influence of TGF-β, fibroblasts in large wounds will differentiate into myofibroblasts. Myofibroblasts is a phenotype expressing α-smooth muscle actin thus able to decrease the wound size by gripping the wound edges and contracting [19]. Epidermal cells also secret collagenase that breaks down collagen as well as plasminogen activator to stimulate the plasmin formation. This promotes clot dissolution during epithelial cell migration. Even though epithelial cells migrate in random directions, the migration will be inhibited when

contact is formed between epithelial cells. Also, moist environments could provide a faster epithelialization process [20].

Angiogenesis is another critical issue in the proliferation stage of wound healing [10]. Macrophages and keratinocytes are crucial to angiogenesis by producing macrophage-derived angiogenic factors [12]. Keratinocytes are the most essential source of vascular endothelial growth factor (VEGF) in response to the oxygen environment resulting from damaged blood vessels [21]. These growth factors are essential to angiogenesis.

Collagen synthesis and deposition are essential events in the proliferation stage. The abundant hydroxylysine and hydroxyproline moieties inside collagen make it possible to form stable crosslinks between the proline and lysine residues [22]. This crosslink happens in the presence of vitamin C, oxygen, and ferrous iron; thus, deficiencies of oxygen and vitamin C will result in weak crosslink of collagen. Therefore, it is more vulnerable to breakdown [23]. Elastin also appears in the wound site in a smaller amount than collagen. Elastin enables skin with stretch and recoil properties because of the random coils inside this structural protein [24].

### 1.2.3 Remodeling

The remodeling stage, which is also called the maturation stage, is characterized by the transmission of granulation tissue from a random network into an organized collection of collagen and proteoglycans with higher tensile properties [25]. During the collagen remodeling, collagenases, and matrix metalloproteinase coordinate to make a balance between the collagen synthesis and destruction [26]. Type III collagen will be replaced by collagen I, and fibronectin will disappear gradually. At the same time, hyaluronic acid, dermatan sulfate, heparin sulfate, chondroitin sulfate, and glycosaminoglycans will be replaced by proteoglycans, water is restored, all these events enables collagen fibers to be

adjacently promoting collagen crosslink, which finally decreases scar thickness and makes it resistant to destruction [12].

### 1.3 Conventional treatments

Depending on the extent of tissue damage, location, wound size, phase of healing, and the level of the exudates, the strategies for the treatment of skin lesions are different [27]. Among these strategies wound dressing, skin autografts and allografts are widely used methods.

The use of wound dressings, such as bandages, cotton, or wool, is still deployed for wound healing, providing a clean cover to protect the wound from the external environment and stimulate wound healing [28]. Some drawbacks of this strategy include low adhesion to the lesion and damage induced upon removal leading to impairment of wound healing [29].

Modern wound dressings with improved properties in keeping the environment moist, alleviating pain, fitting in different shapes and sizes, allowing non-traumatic removal, and anti-inflammatory properties have been developed to overcome the drawbacks mentioned above. Example compositions include alginate dressings [29], gelling cellulose fibers [30], foams [31], hydrocolloids [32], hydrogels [33], paraffin gauze dressings [34], silicone dressing [35], and silver dressings [36]. Alginates from seaweed are highly absorbent and turn into a gel-like substance on contact with the wound fluid. This provides a moist environment that can keep nerve endings moist, reduce pain, and promote the formation of new tissue. Some alginate dressings have haemostatic properties, thus are ideal for bleeding wounds [37].

In the case of large full-thickness wounds or where the skin lesion extends to the dermis or hypodermis region, skin autografts, allografts, or xenografts would be used in the surgical

treatment. Among these strategies, skin autografts remain the current gold standard [38]. Full-thickness skin autografts have excellent adhesion to the wound bed, limited immunological rejection, and provides pain relief. But this method is limited by donor site shortage and may cause secondary injury. In general, autografts require the surgical removal of skin from another site of a person's body [39], and autologous full-thickness skin transfer can only be performed for injured areas < 2% of total burned surface area (TBSA). Although skin allografts could prevent the wound from dehydration and contamination, it may lead to immune rejection.

### 1.4 Skin tissue engineering

Skin tissue engineering, which is the combination of material science and cell biology, offers a promising approach to produce artificial skin substitutes [40]. Skin tissue engineering alleviated the issue of donor shortage and prompted the wound management from using passive wound dressings to bioactive cell-material complex scaffolds. Ideally, a tissue-engineered skin substitute is a multi-layered, fully functional skin substitute that might fulfill all the different functions of the dermis and epidermis [41].

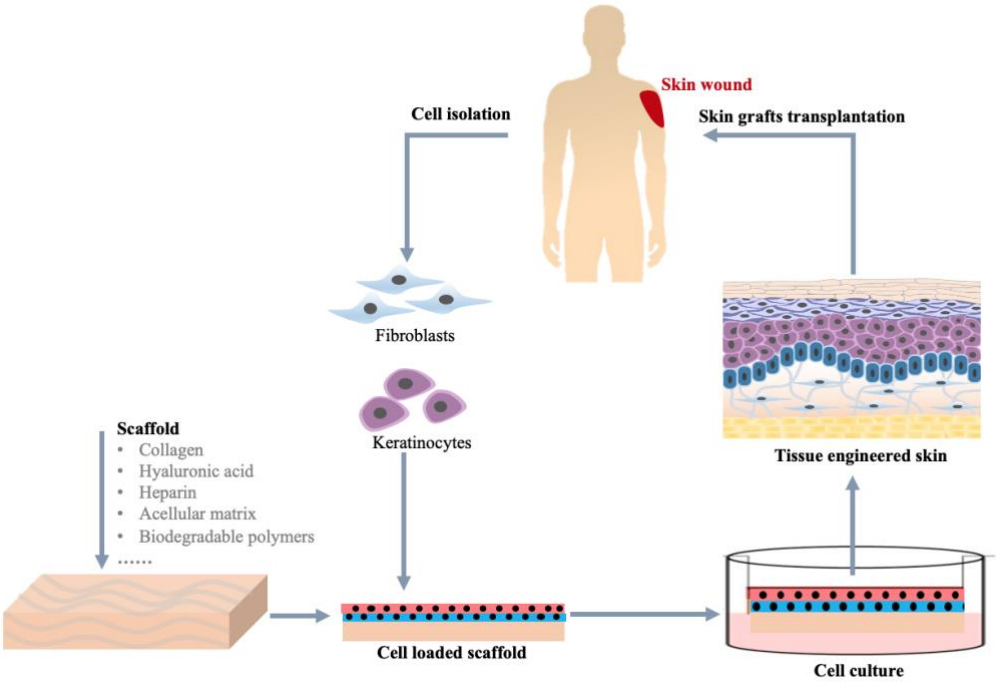


**Figure 1.3.** Skin tissue engineering.

A typical approach to a tissue-engineered skin is to produce a two-compartment cellular construct with a scaffold base to simulate the native structure and organization of skin (Figure 1.3). The top compartment is a multi-layered epidermis-mimic that consists of keratinocytes (KCs). The underlying compartment, dermis-mimics, is typically composed of synthetic scaffolds and fibroblasts (FBs). The temporary scaffold could promote cellular attachment and growth. Then skin cells on it will secret extracellular matrix (ECM) to remodel neighboring ECM [42].

Although the skin was the first tissue to be successfully tissue-engineered and implemented back into the clinical routine, there are still some disadvantages to overcome, including poor vascularization, pigmentation, and so on. Addressing these challenges requires effective and appropriate integration of key technologies in biomaterials, cells, biofactors, and advanced biomanufacturing.

## 1.5 Biopolymers in skin tissue engineering

ECM components play a crucial role in every stage of the wound healing process [43, 44]. By providing the microenvironment for skin cells, the ECM regulates wound repair by influencing the development, phenotype, genetic expression, and function of all skin cells [45]. As such, when designing skin substitutes, bioengineered skin scaffolds should aim to mimic the function of natural ECM by incorporating appropriate biomaterials and cytokines at physiological quantities and durations [46]. Researchers have explored using ECM components, such as collagen, elastin, and glycosaminoglycans, as materials for tissue-engineered skin scaffolds. These naturally occurred biomaterials are summarized and reviewed here in terms of their properties and performance as skin tissue engineering scaffold materials.

### 1.5.1 Collagen

Collagens are the most abundant proteins by weight in the extracellular matrix and in connective tissue of most animals. There are several different types of collagen that are composed of similar or of different α chains in the triple helix of collagen fibers [22]. Among them, type I collagen is a significant and most abundant component of most extracellular material. Collagen fibers could be covalently crosslinked at their lysine sites, which contributes to the modulated mechanical properties of tissues with aging [47].

Collagen scaffolds have been used in a variety of applications due to a series of essential properties, such as low antigenicity, hemostatic effect, and good biocompatibilities for use in wound dressings and skin regeneration applications [22]. During normal wound healing process, collagen deposition by fibroblasts is one of the pivotal milestones in cell-material interaction and extracellular matrix reconstitution. Besides, collagen scaffolds were shown to promote cell attachment and growth. In particular, collagen contains critical residues,

such as lysine and arginine, and crucial integrin-binding sequences - the arginine-glycine-aspartic acid (RGD) groups [48]. The RGD groups actively bind to integrin receptors, and this interaction contributes significantly to cell growth, differentiation, and overall regulation of cell functions. Collagen has thus been pursued in wound healing for several decades for its excellent biocompatibility and biodegradability. However, its fast biodegradation in vivo and limited mechanical strength are limitations for further use. The stability of a collagen-based scaffold could be improved by several approaches, such as adding chemical crosslinkers, or through the incorporation of synthetic polymers, or by engineering methods such as electrocompaction. A balance between material stiffness and biocompatibility should be met for a successful skin-scaffold design.

### 1.5.2 Elastin

Elastin is another principal extracellular matrix constituent providing elasticity to tissues. It is crucial to the elasticity and resilience of many tissues including tendon, cartilage, ligament, arteries, lung, and skin [49]. Especially, elastin is essential for skin structural integrity and is enriched in the deep dermis. Due to its densely crosslinked property, elastin is highly insoluble and usually exists as particles. In severe wound healing, it takes 4 – 5 years for the burned wounds/scar tissues to re-commence elastin expression [50]. The lack of elastin is one of the causes of functional and spatial disorganization in scar tissue. Despite the apparent significance of elastin in wound healing and healthy skin function, few explorations of the use of elastin in dermal and skin regeneration exist.

Although elastin is mainly known for its structural role, elastin and elastin-derived peptides have shown to be beneficial on wound healing and regeneration. Within skin wounds, various proteases act on elastin to liberate these fiber-forming proteins. This leads to increased collagen type I deposition, accelerated fibroblast growth and proliferation, and

increased tropoelastin [51]. During the skin wound healing process, dermal fibroblasts can differentiate into myofibroblasts to close the wound by contraction. Elastin can influence fibroblasts cell phenotype and function, thus affecting its differentiation [52]. Elastin is also required in the terminal differentiation and stratification of human keratinocytes, which is necessary for the reconstruction of the epidermis and the barrier function of the skin. A silk/elastin scaffold showed faster re-epithelialization, accelerated wound closure, and improved wound healing by the incorporation of elastin [53].

### 1.5.3 Proteoglycans and GAGs

Glycosaminoglycans (GAGs) are a major group of natural compounds that exists in the ECM, and they play a pivotal role in providing cell-surface receptors and binding to growth factors and cytokines that are required for cell growth. GAGs are unbranched polysaccharides made up of repeating disaccharide units. The disaccharide units contain either of modified *N*-acetylgalactosamine (GalNAc) or *N*-acetylglucosamine (GlcNAc), and a uronic acid such as glucuronate (GlcA) or iduronate (IdoA).

GAGs that are of well-known physiological importance including hyaluronic acid, heparin, chondroitin sulfate, heparan sulfate, dermatan sulfate, and keratan sulfate. Most of these GAGs are sulphated GAGs based on the type of the disaccharide units inside and are conjugated to a protein backbone that is expressed as proteoglycans. One molecule of a proteoglycan may carry more than one kind of GAG chain. GAGs are highly negatively charged, and a small number of GAGs can trap a large amount of water into a gel. Among these GAGs, hyaluronic acid is unique, as it does not contain any sulfated group and is not covalently connected to any protein forming a proteoglycan. HA is composed of repeating disaccharides of glucuronic acid and N-acetyl glucosamine. It is synthesized by enzymes at the plasma membrane and is abundant in many tissues.

GAGs are attractive bioactive polymers for tissue engineering because of their highly polar and water-absorbing property. In natural skin, polysaccharides are also important native components with functions, including maintaining moisture environment, promoting angiogenesis, regulating cell differentiation, and offering binding sites for drugs or growth factors [44]. Their negatively charged sulpho and carboxyl groups are believed to be critical to these functions [54]. GAGs can bind and modulate various proteins, including cytokines, growth factors, and extracellular matrix proteins. These interactions are essential for cell functions, including proliferation, adhesion, and motility [55]. As a consequence, GAGs are gaining more and more attention as potential components in tissue engineering and regenerative medicine.

**Table 1.1.** Structure of glycosaminoglycans.

| Glycosaminoglycans in skin | GAG-like polysaccharides |
|---|---|
| 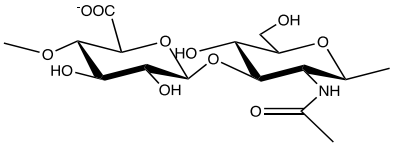 | 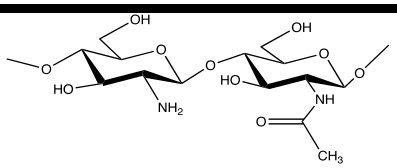 |
| HA | Chitosan |
| 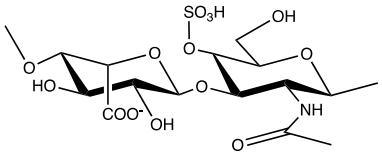 | 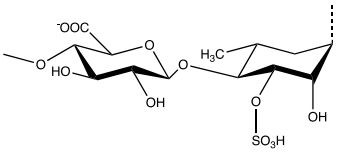 |
| Dermatan sulphate | Ulvan |
| 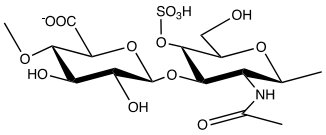 | 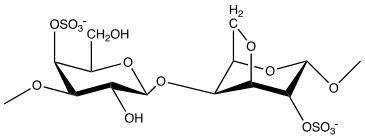 |
| Chondroitin sulphate | Carrageenan |
| 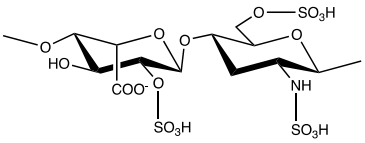 | 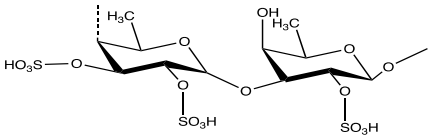 |
| Heparin sulphate | Fucoidan |
| 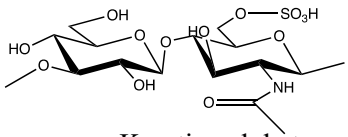 | 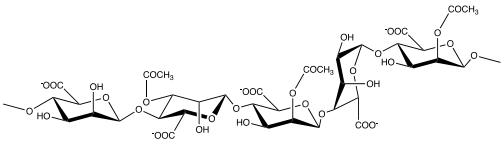 |
| Keratin sulphate | Alginate |

## 1.6 Roles of GAGs in wound healing

**Table 1.2.** Collagen and/or GAGs based scaffolds for skin regeneration.

| Biomaterial | Fabrication method | Cell(s)/ Models | Performance | Ref. |
|---|---|---|---|---|
| Collagen | Freeze-dry VS. electrospinning | HDF, HEK | Electrospinning resulted in impaired wound contraction | [56] |
| Collagen - Elastin | Laser-assisted bioprinting | NIH-3T3, HaCaT | Multilayered epidermis was formed from the printed keratinocytes; In vitro model showed promoted angiogenesis from the wound bed and wound edges | [57] |
| Collagen-C6S | Freeze-drying | HDF, HEK | Formation of a stratified epidermis and a mature dermis | [58] |
| Collagen-HA | Freeze-drying | HDF | Improved HDF proliferation, collagen synthesis and epithelial regeneration | [59] |

| | | | | |
|---|---|---|---|---|
| Collagen - Chitosan | Freeze Drying and Crosslinking | L929 (mouse fibroblasts) | Enhanced scaffold biostability and promoted fibroblast cells proliferation | [42] |
| Collagen - Ulvan | Electrocompaction | HDF | Strengthened scaffold stiffness and HDFs spreading on the ulvan-conjugated scaffold than collagen only scaffold | [60] |
| Collagen - Heparin | Mixture and crosslinking | Rat and guinea pig dermal wound models | Improved fibroblasts invasion and angiogenesis than collagen only implants | [61] |
| Carrageenan | Hydrogel | Skin-derived multipotent stromal cells | Reduced inflammatory process, faster initial recovery of wounded area, and improved extracellular matrix deposition. | [62] |
| Collagen-Alginate | Dopamine modify, crosslink | Mouse fibroblast cells (L929) | Chaotic interconnected scaffold structure; good mechanical properties, skin tissue adhesion, water absorption, accelerated wound healing in vivo | [63] |

| | | | | |
|---|---|---|---|---|
| Chitosan-fucoidan | Solvent dropping & Freeze-drying | Superficial dermal burns model | Dermal papillary formation, reepithelization, and the accelerated wounds closure were found | [64] |

Abbreviations: C6S: chondroitin 6-sulfate; HDFs: human dermal fibroblast cells; HEKs: human epidermal keratinocyte cells; HaCaT: human

### 1.6.1 HA

HA is a significant component in skin ECM and plays an important biological role in the wound healing process by influencing inflammation, granulation, and re-epithelialization [65]. Hyaluronic acid (HA) is a non-sulfated linear polysaccharide that contains a repeating disaccharide of β-1,3-*N*-acetyl-d-glucosamine and β-1,4-d-glucuronic acid. It originates throughout the body, from the vitreous of the eye to the ECM of cartilage tissues.

HA is synthesized by a family of hyaluronan synthases (HAS1, HAS2, and HAS3), of which HAS2 is the most critical synthase [66]. It is well known that HA is an information-rich polymer system based purely on chain size [67]. During the wound healing process, HA is continuously being produced in a high molecular weight (HMWHA) form, which can reach over $10^{6\sim7}$ Da in molecular mass. In the inflammation stage of wound healing, the level of HMWHA increases quickly at the wound site, especially in the cytoplasm of the platelets [66]. By binding with fibronectin and its fibrin product, the HMWHA contributes to bleeding control by the formation and deposition of the clotted fibrin. Besides, HMWHA is associated with decreased inflammation by its stimulation in leukocyte response [68]. In the later stage of wound healing, fragmented HA (<400 kDa) becomes dominant, and the function of fragmented HA in wound healing involves

increased inflammation, higher collagen I deposition, and increased proliferation of fibroblasts [69].

### 1.6.2 Heparin/ heparin sulfate

Heparin and heparan sulfate (HS) are naturally occurring glycosaminoglycans (GAGs). Heparin is only produced by mast cells and functions as an anticoagulant. Heparan sulfate (HS) is a component of the extracellular matrix that appeared in all animal tissues. Heparin and HS are both linear polysaccharides composed of two basic saccharides: a uronic acid and an amino sugar. The uronic acid is typically either D-glucuronic acid (D-GlcA) or L-iduronic acid (L-IdoA). The amino sugar is either N-acetyl-D-glucosamine (D-GlcNAc) or N-acetyl-D-galactosamine (D-GalNAc). These basic saccharides will be further modified by sulfation, epimerization, and deacetylation during biosynthesis.

HS typically occurs as a proteoglycan (HSPG) with multiple HS side chains covalently connected to core proteins. In the skin, HSPGs are usually presented in basement membranes where they cooperate with other matrix materials to define basement membrane structure and to provide a matrix for cell function [70]. The high charge density of heparin makes it attractive for growth factor related-cell encapsulation because heparin helps to stabilize and localize these growth factors. Upon injured, heparin could relieve pain, inhibit clotting and inflammation, restore blood flow, thus accelerate the wound healing process [70]. Low molecular weight heparins (LMWHs) are sometimes used instead of heparin [71]. In an abdominal rat wound-healing model, applying LMWHs to wounds resulted in a significant increase in collagen production at the wound site [72]. LMWHs induced accelerated wound healing in dorsal wound-healing models in rats in terms of collagen fiber thickness, epidermal regeneration, numbers of fibroblasts, and vascularity [70].

### 1.6.3 Chondroitin sulfate

Chondroitin sulfate (CS) is a component of the extracellular matrix of all vertebrates. Chondroitin sulphate (CS) is a linear polysaccharide composed of (1–3)-β-*N*-acetyl-d-galactosamine and (1–4)-β-glucuronic acid. Chondroitin sulfates A and C are the chondroitin sulfates that contain glucuronic acid in the disaccharide units instead of iduronic acid. CS, as well as dermatan sulfate (DS), are usually covalently connected to proteoglycans or as a receptor on basement membranes. CS plays a vital role in processes including wound repair, central nervous system, and chondrogenesis [73]. Chondroitin sulphate is also a vital structural component of cartilage providing resistance to compression. Chondroitin sulphate is a surrogate ECM and an important bio-entity for wound healing.

To allow for polymerization and hydrogel formation, CS has been modified with different functional groups such as methacrylate [74] and thiols [75]. Prepared CS hydrogel was shown to stimulate wound healing by providing structural support for fibroblasts and epithelial regeneration. Chondroitin-6-sulfate (C6S) modified collagen gels were reported to be able to alter the scarring process and strengthen the mechanical characteristic of the matrix in the wound healing phase [76].

### 1.6.4 Dermatan sulfate

Dermatan sulfate (DS), formerly referred to as chondroitin sulfate B, is a glycosaminoglycan exists mostly in skin, but also in tendons, blood vessels, heart valves and lungs. DS was shown to be the most common soluble GAG that appeared in acute human wounds [77]. DS and CS are slightly different in structure, with DS distinguishing itself only by the presence of iduronic acid.

During the earlier phases of wound healing, DS is indispensable for the modification of CD44 and fibroblast migration in the granulation tissue. Besides, DS is known to bind with fibroblast growth factors (FGF) and mediating FGF responsiveness in the fibroblast through the modulation of the iduronic acid in DS [78]. CS and DS were also suspected to be essential factors in scarless fetal wound healing, as proteoglycans isolated from human fetal skin were shown to consist of much longer GAG chains compared with those from the adult human skin [79].

### 1.6.5 Keratan sulfates

Keratan sulfate (KS), also called keratosulfate, is a glycosaminoglycan that occurs in the ECM and on the cell membrane surface. The basic disaccharide unit of KS is N-acetyllactosamine and Gal(b1-4)GlcNAc(b1-3), with C-6 of GlcNAc and Gal as residues for sulfate esters. Keratan sulfate exists as a proteoglycan (KSPG) in which KS chains are attached to core proteins on cell-surface or extracellular matrix proteins, including lumican, aggrecan, fibromodulin, mimecan, osteoadherin, and keratocan. KS has been found in the cornea, skin, cartilage, and bone. KS are long, highly hydrated molecules that can perform as a cushion to absorb mechanical shock in joints. KS also plays a role in the nervous system metabolism and acting as an essential factor in the tissue damage repair [80].

### 1.6.6 Newly explored GAG-like polysaccharides

Apart from above mentioned naturally occurred GAGs, GAG-like polysaccharides from other sources, such as marine biomass, have gained increasing attention as an abundant and sustainable source of polysaccharides. Some of these newly explored GAGs, including alginate, carrageenan, fucoidan, chitosan, and ulvan. These marine polysaccharides share similar chemical structure and functional groups as those GAGs found in ECM. They are also reported to have important biological properties such as biodegradability,

biocompatibility, anti-inflammatory, promoting wound healing, antimicrobial, as well as adhesive activity [81].

Among these marine polysaccharides, there is one particular group that gains more attention: sulfated polysaccharides [82]. Ulvan is a sulphated polysaccharide extracted from the cell wall of specific green algae. It shares chemical similarities with dermatan sulfate and hyaluronic acid in the skin [83]. Ulvan has been shown to have a strong binding affinity to fibroblast cells and collagen, helping stabilize the scaffold, as well as accelerating fibroblast cell growth and cell spreading [60]. Carrageenan is a thermoreversible polymer originated from the red seaweed that presents a glycosaminoglycan-like structure. In a mouse full-thickness skin wound model, the carrageenan hydrogel was reported to reduce the inflammatory process, accelerate the initial recovery of the wounded area, and promote extracellular matrix deposition [62]. Fucoidan is a sulfated polysaccharide found in many species of brown seaweed. It has been shown to slow blood clotting, promote wound healing, possess anti-inflammatory and antioxidant activities [64]. In a low molecular weight fucoidan (LMF) treated dermal wounds, collagen deposition and angiogenesis were elevated in the granular tissue post-treatment [84].

### 1.6.7 Conclusion of GAGs in wound healing

Wound healing is a complex biological process involving a series of continuous stages. Skin tissue engineering offered great potential for the reconstruction of skin function. Among the wide range of available materials for skin tissue engineering, only limited have been extensively used in the laboratories or clinical, such as collagen. GAGs are naturally occurred biopolymers and main components in skin ECM. The fact that GAGs are water-absorbing, growth - factor trapping, biocompatible, biodegradable, and nontoxic makes

them suitable raw materials for the construction of the skin scaffolding system**.** Yet, due to their size-dependent and informative property, most of these GAGs are underexploited. Recently, there are more and more researches on GAGs in wound healing as well as other specific biological processes like angiogenesis, bone regeneration, and tumor growth. In this review, we summarized the function of GAGs in wound healing. A greater understanding of the function, especially the glycode provided by GAGs, will further enrich our understanding of wounds and finally advance the wound treatment strategies.

### 1.7 Electrocompaction of collagen-based skin scaffold

In skin tissue engineering, scaffolds are of pivotal importance in guiding cell behavior and controlling the transportation of nutrients and wastes. To fabricate such skin scaffolds, many fabrication technologies have been developed and reported. Generally, they can be classified into two main categories: conventional and advanced [85]. Conventional techniques include freeze-drying [86], casting [87], and particulate-leaching [88]. With these methods, scaffolds with interconnected porous structures can be created. However, they offer little control over pore geometry, or size, and cannot allow for the construction of internal channels inside the scaffolds [85].

As an alternative to conventional methods, there are recently developed advanced fabrication techniques, such as 3D printing or bioprinting [89], and electrical signal guided fabrication methods [90] which includes electrospinning, electro-writing, and electrocompaction. In this research, we are particularly interested in the electrically-based fabrication methods. Electrical signals are especially convenient for fabrication. They can be controllably imposed to promote the electrophoresis, alignment, self-assembly, and functionalization of macromolecules to generate hierarchically organized material systems [90].

Collagen is the most famous candidate for skin scaffold fabrication. Often the most challenging part for collagen fabrication is to recapitulate the aligned structure that is critical in matching the mechanical property of the scaffold with the neighboring tissue. A method named electrocompaction for the fabrication of the collagen matrix with improved mechanical properties was reported in 2008 [91].

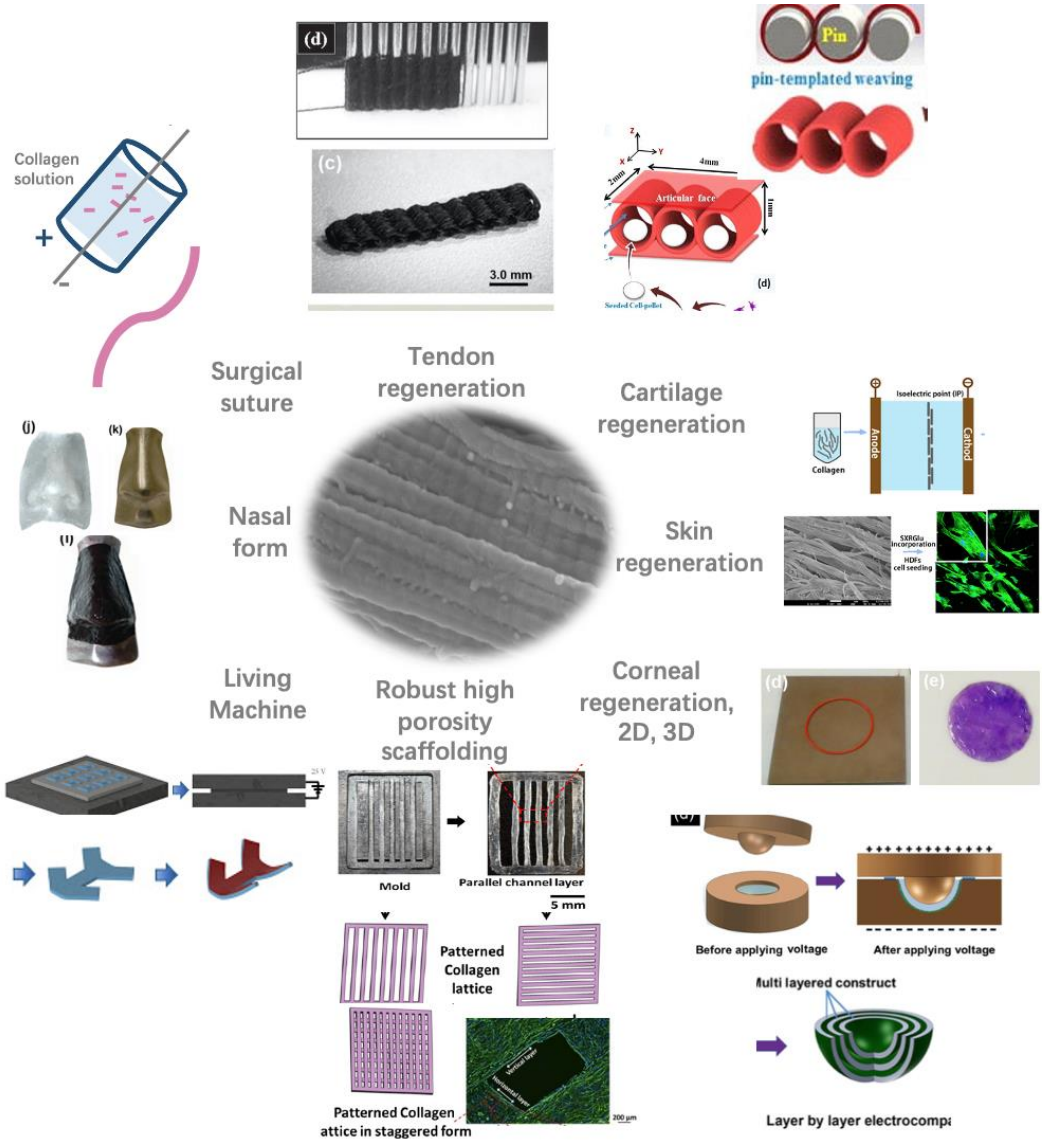


**Figure 1.4.** Application of collagen electrocompaction in tissue engineering. Electrocompaction has been researched in areas, including surgical suture [92], tendon regeneration [93], cartilage regeneration [94], skin regeneration

[60], corneal regeneration (2D [95] and 3D [96]), robust high porosity scaffolding system [97], living machine [98], and free standing nasal form [96].

During the electrocompaction process, the collagen solution was loaded between two oppositely charged electrodes. Upon application of an electric field, an electrochemically induced pH gradient will be formed. Due to the amphoteric nature of the collagen molecules, they will be aligned along the isoelectric point (pI) to create highly oriented densely packed collagen fibers that form into sheets. Variations in the electrodes size and shapes can help to achieve controllable and diverse structures. As such, electrocompacted collagen sheets or threads were applied in various areas (Figure 1.4) such as tendon regeneration [92], corneal regeneration [95], cartilage repair [94], conduits for nerve guidance [99], skin grafts [60], and orthopedic implants [100].

**Table 1.3.** Collagen electrocompaction and application.

| Material | Form | Function | Cells used | Application | Year |
|---|---|---|---|---|---|
| Collagen | 2D complex structure | Organic living machines with electrocompacted collagen as skeletons; cell powered devices; | Chicken primary cardiomyocyte | Organic living machines, bio-robot | 2016 [101] |
| Collagen-Ulvan | Sheet | Good biocompatibility and stability; support cell | Human dermal | Wound healing | 2018 [102] |

| | | | | | |
|---|---|---|---|---|---|
| | | growth and spreading; support skin regeneration | fibroblasts | | |
| Collagen-Cellulose | Fiber/ Sheet | Significant enhancement of the tensile property | NO | Composites biopolymers | 2017 [103] |
| Collagen | complex curved topography | Versatile, robust collagen-based structure with good biocompatibility and cell-matrix interaction | No | Mechanically robust shell structures | 2015 [96] |
| Collagen | Sheet | Support cell growth and promote cell attachment | Human corneal epithelial cells | Corneal bioengineering | 2019 [104] |
| Collagen | Woven arcade | Developed a microporous scaffold with high compressive modulus; achieved robust chondrogenesis | Micromass cell pellets of mesenchymal cell | Cartilage regeneration | 2016 [94] |
| Collagen | Thread | Aligned and highly ordered collagen thread as directional orientation; support neurite outgrowth | PC12 | Nerve guidance conduits, | 2011 [99] |

| | | | | | |
|---|---|---|---|---|---|
| | | | | spinal cord recovery | |
| Collagen-Elastin | Thread | Match the mechanical property of native vessel; support smooth muscle cell growth and differentiation | Smooth muscle cell | Vascular regeneration | 2016 [105] |
| Collagen-Decorin | Thread | Enhanced ultimate stress and ultimate strain of the thread; | No | Tendon tissue engineering | 2011 [106] |
| Collagen | 3D-biotextile woven scaffold | Similar mechanical properties and load-displacement behavior to native tendon; | Mesenchymal stem cells | Tendon and ligaments repair | 2014 [93] |
| Collagen | Highly porous patterned scaffolds | Resulted in collagen scaffolds of high strength, high porosity and good biocompatibility | Mesenchymal stem cells | Load-bearing applications | 2015 [97] |

| | | | | | |
|---|---|---|---|---|---|
| Collagen-Heparin | Thread | Increased mechanical property; Sustained release of growth factors; Support cell proliferation | Tendon-derived cells | Suture for tendon repair | 2016 [92] |

## 1.8 Conclusion and aims of the thesis

Wound healing is a crucial issue in massive skin lesions. Skin tissue engineering offers excellent potential for the fabrication of bioactive skin grafts. Among the many available candidates for the fabrication of skin scaffold, collagen is the most popular and extensively explored biomaterial. Some limitations of collagen-based scaffold include weak mechanical properties and the inability to mimic the aligned microstructure of collagen in natural skin. Electrocompaction, which is an electrochemical alignment technique to control collagen assemble, offered an alternative way to fabricate highly ordered, densely packed collagen bundles that mimic the microstructure of natural skin quite well. Apart from collagen, glycosaminoglycans are also crucial components with functions that include keeping moisture environment, promoting angiogenesis, offering binding sites for drugs or growth factors.

This project aims to fabricate bio mimicking skin scaffolds and explore the application of such scaffolds in supporting dermis, epidermis, and full skin regeneration. Main materials used in this project are collagen and glycosaminoglycans including ulvan and hyaluronic acid. The main fabrication technique used here is electrocompaction. The proposed study will provide a strong base for further in vivo studies to advance development of tissue engineered skin grafts.

## 1.9 References


1. G.K. Menon, New insights into skin structure: scratching the surface, Advanced drug delivery reviews 2002, 54, S3-S17.

2. B.K. Sun, Z. Siprashvili, P.A. Khavari, Advances in skin grafting and treatment of cutaneous wounds, Science 2014, 346, 941-945.

3. D. Breitkreutz, I. Koxholt, K. Thiemann, R. Nischt, Skin basement membrane: the foundation of epidermal integrity—BM functions and diverse roles of bridging molecules nidogen and perlecan, BioMed research international 2013, 2013.

4. R.R. Driskell, F.M. Watt, Understanding fibroblast heterogeneity in the skin, Trends in cell biology 2015, 25, 92-99.

5. C. Huang, Y. Du, C.S. Nabzdyk, R. Ogawa, T. Koyama, D.P. Orgill, X. Fu, Regeneration of hair and other skin appendages: A microenvironment-centric view, Wound Repair and Regeneration 2016, 24, 759-766.

6. M. Cichorek, M. Wachulska, A. Stasiewicz, A. Tymińska, Skin melanocytes: biology and development, Advances in Dermatology and Allergology/Postępy Dermatologii I Alergologii 2013, 30, 30.

7. B. Malissen, S. Tamoutounour, S. Henri, The origins and functions of dendritic cells and macrophages in the skin, Nature Reviews Immunology 2014, 14, 417-428.

8. K. Vig, A. Chaudhari, S. Tripathi, S. Dixit, R. Sahu, S. Pillai, V. Dennis, S. Singh, Advances in skin regeneration using tissue engineering, International journal of molecular sciences 2017, 18, 789.

9. R. Mittermayr, L. Branski, M. Moritz, M.G. Jeschke, D.N. Herndon, D. Traber, J. Schense, J. Gampfer, A. Goppelt, H. Redl, Fibrin biomatrix-conjugated platelet-derived growth factor AB accelerates wound healing in severe thermal injury, Journal of tissue engineering and regenerative medicine 2016, 10, E275-E285.

10. N.S. Greaves, K.J. Ashcroft, M. Baguneid, A. Bayat, Current understanding of molecular and cellular mechanisms in fibroplasia and angiogenesis during acute wound healing, Journal of dermatological science 2013, 72, 206-217.

11. H. Sinno, S. Prakash, Complements and the wound healing cascade: an updated review, Plastic surgery international 2013, 2013.

12. R.A. Clark, The molecular and cellular biology of wound repair, Springer Science & Business Media2013.

13. T. Zhou, N. Wang, Y. Xue, T. Ding, X. Liu, X. Mo, J. Sun, Electrospun tilapia collagen nanofibers accelerating wound healing via inducing keratinocytes proliferation and differentiation, Colloids and Surfaces B: Biointerfaces 2016, 143, 415-422.

14. S.J. Coleman, C. Bruce, A.-M. Chioni, H.M. Kocher, R.P. Grose, The ins and outs of fibroblast growth factor receptor signalling, Clinical science 2014, 127, 217-231.

15. C.G. Decker, Y. Wang, S.J. Paluck, L. Shen, J.A. Loo, A.J. Levine, L.S. Miller, H.D. Maynard, Fibroblast growth factor 2 dimer with superagonist in vitro activity improves granulation tissue formation during wound healing, Biomaterials 2016, 81, 157-168.

16. M.M. Martino, P.S. Briquez, E. Güç, F. Tortelli, W.W. Kilarski, S. Metzger, J.J. Rice, G.A. Kuhn, R. Müller, M.A. Swartz, Growth factors engineered for super-affinity to the extracellular matrix enhance tissue healing, Science 2014, 343, 885-888.

17. V. Moulin, The role of myofibrolasts in normal skin wound healing, Myofibroblasts: origin, function and role in disease 2016.

18. I. Pastar, O. Stojadinovic, N.C. Yin, H. Ramirez, A.G. Nusbaum, A. Sawaya, S.B. Patel, L. Khalid, R.R. Isseroff, M. Tomic-Canic, Epithelialization in wound healing: a comprehensive review, Advances in wound care 2014, 3, 445-464.

19. I.A. Darby, B. Laverdet, F. Bonté, A. Desmoulière, Fibroblasts and myofibroblasts in wound healing, Clinical, cosmetic and investigational dermatology 2014, 7, 301.

20. J.P. Junker, R.A. Kamel, E. Caterson, E. Eriksson, Clinical impact upon wound healing and inflammation in moist, wet, and dry environments, Advances in wound care 2013, 2, 348-356.

21. K.E. Johnson, T.A. Wilgus, Vascular endothelial growth factor and angiogenesis in the regulation of cutaneous wound repair, Advances in wound care 2014, 3, 647-661.

22. S. Chattopadhyay, R.T. Raines, Review collagen-based biomaterials for wound healing, Biopolymers 2014, 101, 821-833.

23. P. Li, G. Wu, Roles of dietary glycine, proline, and hydroxyproline in collagen synthesis and animal growth, Amino acids 2018, 50, 29-38.

24. B.K. Boekema, M. Vlig, L.O. Damink, E. Middelkoop, L. Eummelen, A.V. Bühren, M.M. Ulrich, Effect of pore size and cross-linking of a novel collagen-elastin dermal substitute on wound healing, Journal of Materials Science: Materials in Medicine 2014, 25, 423-433.

25. A.C.d.O. Gonzalez, T.F. Costa, Z.d.A. Andrade, A.R.A.P. Medrado, Wound healing-A literature review, Anais brasileiros de dermatologia 2016, 91, 614-620.

26. M.G. Rohani, W.C. Parks, Matrix remodeling by MMPs during wound repair, Matrix Biology 2015, 44, 113-121.

27. J. Boateng, O. Catanzano, Advanced therapeutic dressings for effective wound healing—a review, Journal of pharmaceutical sciences 2015, 104, 3653-3680.

28. S. Dhivya, V.V. Padma, E. Santhini, Wound dressings–a review, BioMedicine 2015, 5.

29. R. Pereira, A. Carvalho, D.C. Vaz, M. Gil, A. Mendes, P. Bártolo, Development of novel alginate based hydrogel films for wound healing applications, International journal of biological macromolecules 2013, 52, 221-230.

30. J.M. Gladman, B. Griffiths, Wound dressing material, Google Patents, 2014.

31. N. Santamaria, M. Gerdtz, S. Sage, J. McCann, A. Freeman, T. Vassiliou, S. De Vincentis, A.W. Ng, E. Manias, W. Liu, A randomised controlled trial of the effectiveness of soft silicone multi-layered foam dressings in the prevention of sacral and heel pressure ulcers in trauma and critically ill patients: the border trial, International wound journal 2015, 12, 302-308.

32. S.G. Jin, A.M. Yousaf, K.S. Kim, D.W. Kim, D.S. Kim, J.K. Kim, C.S. Yong, Y.S. Youn, J.O. Kim, H.-G. Choi, Influence of hydrophilic polymers on functional properties and wound healing efficacy of hydrocolloid based wound dressings, International journal of pharmaceutics 2016, 501, 160-166.

33. J.S. Gonzalez, L.N. Ludueña, A. Ponce, V.A. Alvarez, Poly (vinyl alcohol)/cellulose nanowhiskers nanocomposite hydrogels for potential wound dressings, Materials Science and Engineering: C 2014, 34, 54-61.

34. D. Kaiser, J. Hafner, D. Mayer, L.E. French, S. Läuchli, Alginate dressing and polyurethane film versus paraffin gauze in the treatment of split-thickness skin graft donor sites: a randomized controlled pilot study, Advances in skin & wound care 2013, 26, 67-73.

35. R. Xu, G. Luo, H. Xia, W. He, J. Zhao, B. Liu, J. Tan, J. Zhou, D. Liu, Y. Wang, Novel bilayer wound dressing composed of silicone rubber with particular micropores enhanced wound re-epithelialization and contraction, Biomaterials 2015, 40, 1-11.

36. B. Boonkaew, M. Kempf, R. Kimble, P. Supaphol, L. Cuttle, Antimicrobial efficacy of a novel silver hydrogel dressing compared to two common silver burn wound dressings: Acticoat™ and PolyMem Silver®, Burns 2014, 40, 89-96.

37. G.D. Mogoşanu, A.M. Grumezescu, Natural and synthetic polymers for wounds and burns dressing, International journal of pharmaceutics 2014, 463, 127-136.

38. A.G. Haddad, G. Giatsidis, D.P. Orgill, E.G. Halvorson, Skin substitutes and bioscaffolds: temporary and permanent coverage, Clinics in plastic surgery 2017, 44, 627-634.

39. T.T. Nyame, H.A. Chiang, D.P. Orgill, Clinical applications of skin substitutes, Surgical Clinics 2014, 94, 839-850.

40. A.A. Chaudhari, K. Vig, D.R. Baganizi, R. Sahu, S. Dixit, V. Dennis, S.R. Singh, S.R. Pillai, Future prospects for scaffolding methods and biomaterials in skin tissue engineering: a review, International journal of molecular sciences 2016, 17, 1974.

41. N. Bhardwaj, D. Chouhan, B. B Mandal, Tissue engineered skin and wound healing: current strategies and future directions, Current pharmaceutical design 2017, 23, 3455-3482.

42. C. Tangsadthakun, S. Kanokpanont, N. Sanchavanakit, T. Banaprasert, S. Damrongsakkul, Properties of collagen/chitosan scaffolds for skin tissue engineering, Journal of Metals, Materials and Minerals 2017, 16.

43. P.P. Bonvallet, M.J. Schultz, E.H. Mitchell, J.L. Bain, B.K. Culpepper, S.J. Thomas, S.L. Bellis, Microporous dermal-mimetic electrospun scaffolds pre-seeded with fibroblasts promote tissue regeneration in full-thickness skin wounds, PLoS One 2015, 10.

44. L.E. Tracy, R.A. Minasian, E. Caterson, Extracellular matrix and dermal fibroblast function in the healing wound, Advances in wound care 2016, 5, 119-136.

45. P. Olczyk, Ł. Mencner, K. Komosinska-Vassev, The role of the extracellular matrix components in cutaneous wound healing, BioMed research international 2014, 2014.

46. R.A. Kamel, J.F. Ong, E. Eriksson, J.P. Junker, E.J. Caterson, Tissue engineering of skin, Journal of the American College of Surgeons 2013, 217, 533-555.

47. V. Kahan, M. Andersen, J. Tomimori, S. Tufik, Stress, immunity and skin collagen integrity: evidence from animal models and clinical conditions, Brain, behavior, and immunity 2009, 23, 1089-1095.

48. A.M. Wojtowicz, A. Shekaran, M.E. Oest, K.M. Dupont, K.L. Templeman, D.W. Hutmacher, R.E. Guldberg, A.J. García, Coating of biomaterial scaffolds with the collagen-mimetic peptide GFOGER for bone defect repair, Biomaterials 2010, 31, 2574-2582.

49. S.M. Mithieux, A.S. Weiss, Elastin, Advances in protein chemistry, Elsevier2005, pp. 437-461.

50. I. Jones, L. Currie, R. Martin, A guide to biological skin substitutes, British journal of plastic surgery 2002, 55, 185-193.

51. F. Antonicelli, G. Bellon, S. Lorimier, W. Hornebeck, Role of the elastin receptor complex (S-Gal/Cath-A/Neu-1) in skin repair and regeneration, Wound repair and regeneration 2009, 17, 631-638.

52. J.F. Almine, D.V. Bax, S.M. Mithieux, L. Nivison-Smith, J. Rnjak, A. Waterhouse, S.G. Wise, A.S. Weiss, Elastin-based materials, Chemical Society Reviews 2010, 39, 3371-3379.

53. A. Vasconcelos, A.C. Gomes, A. Cavaco-Paulo, Novel silk fibroin/elastin wound dressings, Acta Biomaterialia 2012, 8, 3049-3060.

54. A. Weyers, R.J. Linhardt, Neoproteoglycans in tissue engineering, The FEBS journal 2013, 280, 2511-2522.

55. A.D. Theocharis, S.S. Skandalis, G.N. Tzanakakis, N.K. Karamanos, Proteoglycans in health and disease: novel roles for proteoglycans in malignancy and their pharmacological targeting, The FEBS journal 2010, 277, 3904-3923.

56. H.M. Powell, D.M. Supp, S.T. Boyce, Influence of electrospun collagen on wound contraction of engineered skin substitutes, Biomaterials 2008, 29, 834-843.

57. S. Michael, H. Sorg, C.-T. Peck, L. Koch, A. Deiwick, B. Chichkov, P.M. Vogt, K. Reimers, Tissue engineered skin substitutes created by laser-assisted bioprinting form skin-like structures in the dorsal skin fold chamber in mice, PloS one 2013, 8.

58. I. Yannas, E. Lee, D.P. Orgill, E. Skrabut, G.F. Murphy, Synthesis and characterization of a model extracellular matrix that induces partial regeneration of adult mammalian skin, Proceedings of the National Academy of Sciences 1989, 86, 933-937.

59. S.-N. Park, H.J. Lee, K.H. Lee, H. Suh, Biological characterization of EDC-crosslinked collagen–hyaluronic acid matrix in dermal tissue restoration, Biomaterials 2003, 24, 1631-1641.

60. L. Kang, X. Liu, Z. Yue, Z. Chen, C. Baker, P.C. Winberg, G.G. Wallace, Fabrication and in vitro characterization of electrochemically compacted collagen/sulfated xylorhamnoglycuronan matrix for wound healing applications, Polymers 2018, 10, 415.

61. J.M. Mcpherson, P.W. Ledger, G. Ksander, S.J. Sawamura, A. Conti, S. Kincaid, D. Michaeli, R.A. Clark, The influence of heparin on the wound healing response to collagen implants in vivo, Collagen and related research 1988, 8, 83-100.

62. M.P. Rode, A.B. Batti Angulski, F.A. Gomes, M.M. da Silva, T.d.S. Jeremias, R.G. de Carvalho, D.G. Iucif Vieira, L.F.C. Oliveira, L. Fernandes Maia, A.G. Trentin, Carrageenan hydrogel as a scaffold for skin-derived multipotent stromal cells delivery, Journal of biomaterials applications 2018, 33, 422-434.

63. Z. Bai, W. Dan, G. Yu, Y. Wang, Y. Chen, Y. Huang, C. Yang, N. Dan, Tough and tissue-adhesive polyacrylamide/collagen hydrogel with dopamine-grafted oxidized sodium alginate as crosslinker for cutaneous wound healing, RSC advances 2018, 8, 42123-42132.

64. A.D. Sezer, F. Hatipoglu, E. Cevher, Z. Oğurtan, A.L. Bas, J. Akbuğa, Chitosan film containing fucoidan as a wound dressing for dermal burn healing: preparation and in vitro/in vivo evaluation, Aaps Pharmscitech 2007, 8, E94-E101.

65. J.S. Frenkel, The role of hyaluronan in wound healing, International wound journal 2014, 11, 159-163.

66. K.L. Aya, R. Stern, Hyaluronan in wound healing: rediscovering a major player, Wound repair and regeneration 2014, 22, 579-593.

67. R. Stern, A.A. Asari, K.N. Sugahara, Hyaluronan fragments: an information-rich system, European journal of cell biology 2006, 85, 699-715.

68. N. Mambetsariev, T. Mirzapoiazova, B. Mambetsariev, S. Sammani, F.E. Lennon, J.G. Garcia, P.A. Singleton, Hyaluronic acid binding protein 2 is a novel regulator of vascular integrity, Arteriosclerosis, thrombosis, and vascular biology 2010, 30, 483-490.

69. G. Majno, G. Gabbiani, B. Hirschel, G. Ryan, P. Statkov, Contraction of granulation tissue in vitro: similarity to smooth muscle, Science 1971, 173, 548-550.

70. C.E. Durmaz, A. Ozkan, B. Senel, H.A. Uyar, Comparison of effects of unfractionated heparin and low molecular weight heparin on skin wound healing of rats, Acta cirurgica brasileira 2012, 27, 639-644.

71. M.J. Saliba Jr, Heparin in the treatment of burns: a review, Burns 2001, 27, 349-358.

72. E. Kus, A. Bienkiewicz, Subcutaneous low molecular weight heparin administration promotes wound healing in rats, Pathophysiology 2006, 13, 81-84.

73. X.H. Zou, Y.Z. Jiang, G.R. Zhang, H.M. Jin, N.T.M. Hieu, H.W. Ouyang, Specific interactions between human fibroblasts and particular chondroitin sulfate molecules for wound healing, Acta biomaterialia 2009, 5, 1588-1595.

74. N.J. Steinmetz, S.J. Bryant, Chondroitin sulfate and dynamic loading alter chondrogenesis of human MSCs in PEG hydrogels, Biotechnol Bioeng 2012, 109, 2671-82.

75. R.A. Peattie, D.B. Pike, B. Yu, S. Cai, X.Z. Shu, G.D. Prestwich, M.A. Firpo, R.J. Fisher, Effect of gelatin on heparin regulation of cytokine release from hyaluronan-based hydrogels, Drug Delivery 2008, 15, 389-397.

76. M.E. Gilbert, K.R. Kirker, S.D. Gray, P.D. Ward, J.G. Szakacs, G.D. Prestwich, R.R. Orlandi, Chondroitin sulfate hydrogel and wound healing in rabbit maxillary sinus mucosa, The Laryngoscope 2004, 114, 1406-1409.

77. S.F. Penc, B. Pomahac, T. Winkler, R.A. Dorschner, E. Eriksson, M. Herndon, R.L. Gallo, Dermatan sulfate released after injury is a potent promoter of fibroblast growth factor-2 function, Journal of Biological Chemistry 1998, 273, 28116-28121.

78. K.A. Radek, K.R. Taylor, R.L. Gallo, FGF-10 and specific structural elements of dermatan sulfate size and sulfation promote maximal keratinocyte migration and cellular proliferation, Wound Repair and Regeneration 2009, 17, 118-126.

79. D.A. Carrino, P. Önnerfjord, J.D. Sandy, G. Cs-Szabo, P.G. Scott, J.M. Sorrell, D. Heinegård, A.I. Caplan, Age-related changes in the proteoglycans of human skin Specific cleavage of decorin to yield a major catabolic fragment in adult skin, Journal of Biological Chemistry 2003, 278, 17566-17572.

80. B. Olgierd, A. Sklarek, P. Siwek, E. Waluga, Methods of Biomaterial-Aided Cell or Drug Delivery: Extracellular Matrix Proteins as Biomaterials, Stem Cells and Biomaterials for Regenerative Medicine, Elsevier2019, pp. 163-189.

81. M.J. Cardoso, R.R. Costa, J.F. Mano, Marine origin polysaccharides in drug delivery systems, Marine drugs 2016, 14, 34.

82. I. Wijesekara, R. Pangestuti, S.-K. Kim, Biological activities and potential health benefits of sulfated polysaccharides derived from marine algae, Carbohydrate polymers 2011, 84, 14-21.

83. F. Chiellini, A. Morelli, Ulvan: A versatile platform of biomaterials from renewable resources, Biomaterials—Physics and Chemistry 2011, 75-98.

84. J.-H. Park, S.-H. Choi, S.-J. Park, Y.J. Lee, J.H. Park, P.H. Song, C.-M. Cho, S.-K. Ku, C.-H. Song, Promoting wound healing using low molecular weight fucoidan in a full-thickness dermal excision rat model, Marine drugs 2017, 15, 112.

85. N. Zhu, X. Chen, Biofabrication of tissue scaffolds, Advances in biomaterials science and biomedical applications 2013, 315-328.

86. F.J. O'Brien, B.A. Harley, I.V. Yannas, L. Gibson, Influence of freezing rate on pore structure in freeze-dried collagen-GAG scaffolds, Biomaterials 2004, 25, 1077-1086.

87. S. Deville, E. Saiz, A.P. Tomsia, Freeze casting of hydroxyapatite scaffolds for bone tissue engineering, Biomaterials 2006, 27, 5480-5489.

88. S.H. Oh, S.G. Kang, E.S. Kim, S.H. Cho, J.H. Lee, Fabrication and characterization of hydrophilic poly (lactic-co-glycolic acid)/poly (vinyl alcohol) blend cell scaffolds by melt-molding particulate-leaching method, Biomaterials 2003, 24, 4011-4021.

89. S.V. Murphy, A. Atala, 3D bioprinting of tissues and organs, Nature biotechnology 2014, 32, 773.

90. J. Li, S. Wu, E. Kim, K. Yan, H. Liu, C. Liu, H. Dong, X. Qu, X. Shi, J. Shen, Electrobiofabrication: electrically based fabrication with biologically derived materials, Biofabrication 2019, 11, 032002.

91. X. Cheng, U.A. Gurkan, C.J. Dehen, M.P. Tate, H.W. Hillhouse, G.J. Simpson, O. Akkus, An electrochemical fabrication process for the assembly of anisotropically oriented collagen bundles, Biomaterials 2008, 29, 3278-3288.

92. M. Younesi, B.O. Donmez, A. Islam, O. Akkus, Heparinized collagen sutures for sustained delivery of PDGF-BB: delivery profile and effects on tendon-derived cells in-vitro, Acta biomaterialia 2016, 41, 100-109.

93. M. Younesi, A. Islam, V. Kishore, J.M. Anderson, O. Akkus, Tenogenic induction of human MSCs by anisotropically aligned collagen biotextiles, Advanced functional materials 2014, 24, 5762-5770.

94. M. Younesi, V.M. Goldberg, O. Akkus, A micro-architecturally biomimetic collagen template for mesenchymal condensation based cartilage regeneration, Acta biomaterialia 2016, 30, 212-221.

95. V. Kishore, R. Iyer, A. Frandsen, T.-U. Nguyen, In vitro characterization of electrochemically compacted collagen matrices for corneal applications, Biomedical Materials 2016, 11, 055008.

96. M. Younesi, A. Islam, V. Kishore, S. Panit, O. Akkus, Fabrication of compositionally and topographically complex robust tissue forms by 3D-electrochemical compaction of collagen, Biofabrication 2015, 7, 035001.

97. A. Islam, K. Chapin, M. Younesi, O. Akkus, Computer aided biomanufacturing of mechanically robust pure collagen meshes with controlled macroporosity, Biofabrication 2015, 7, 035005.

98. V.A. Webster, E.L. Hawley, O. Akkus, H.J. Chiel, R.D. Quinn, Fabrication of electrocompacted aligned collagen morphs for cardiomyocyte powered living machines, Conference on Biomimetic and Biohybrid Systems, Springer, 2015, pp. 429-440.

99. M.T. Abu-Rub, K.L. Billiar, M.H. Van Es, A. Knight, B.J. Rodriguez, D.I. Zeugolis, S. McMahon, A.J. Windebank, A. Pandit, Nano-textured self-assembled aligned collagen hydrogels promote directional neurite guidance and overcome inhibition by myelin associated glycoprotein, Soft Matter 2011, 7, 2770-2781.

100. T. Ling, J. Lin, J. Tu, S. Liu, W. Weng, K. Cheng, H. Wang, P. Du, G. Han, Mineralized collagen coatings formed by electrochemical deposition, Journal of Materials Science: Materials in Medicine 2013, 24, 2709-2718.

101. V.A. Webster, E.L. Hawley, O. Akkus, H.J. Chiel, R.D. Quinn, Effect of actuating cell source on locomotion of organic living machines with electrocompacted collagen skeleton, Bioinspiration & biomimetics 2016, 11, 036012.

102. L. Kang, X. Liu, Z. Yue, Z. Chen, C. Baker, P. Winberg, G. Wallace, Fabrication and in vitro characterization of electrochemically compacted collagen/sulfated xylorhamnoglycuronan matrix for wound healing applications, Polymers 2018, 10, 415.

103. E. Cudjoe, M. Younesi, E. Cudjoe, O. Akkus, S.J. Rowan, Synthesis and fabrication of nanocomposite fibers of collagen-cellulose nanocrystals by coelectrocompaction, Biomacromolecules 2017, 18, 1259-1267.

104. Z. Chen, Electro-compacted collagen for corneal bioengineering, 2019.

105. T.-U. Nguyen, C.A. Bashur, V. Kishore, Impact of elastin incorporation into electrochemically aligned collagen fibers on mechanical properties and smooth muscle cell phenotype, Biomedical Materials 2016, 11, 025008.

106. V. Kishore, J.E. Paderi, A. Akkus, K.M. Smith, D. Balachandran, S. Beaudoin, A. Panitch, O. Akkus, Incorporation of a decorin biomimetic enhances the mechanical properties of electrochemically aligned collagen threads, Acta biomaterialia 2011, 7, 2428-2436.

# Chapter 2

# General experimental

**CONTENT**

## 2.1 Introduction

This chapter mainly includes the chemicals, materials, instruments, cells and characterization methods used in this thesis. It mainly deals with protein electrocompaction, functionalization, characterization, human skin cell culture and differentiation. More details can be found in the experimental section of relevant chapters.

## 2.2 List of chemicals and materials

Chemicals and materials used in this research are listed below. They were used as received without further treatment unless indicated otherwise.

**Table 2.1.** List of chemicals and materials used in this thesis.

| **Reagent name** | **Source** | **Category Number** |
|---|---|---|
| Type I bovine collagen | Cheng Du Kele biology technology | Nil |
| Ulvan | Venus Shell Systems Pty Ltd | Nil |
| Elastin from bovine neck ligament | Sigma | E1625 |
| Hyaluronic acid | Xi'an Rongsheng Biotechnology | Nil |
| Collagenase | Sigma | C2674 |

| | | |
|---|---|---|
| N-(3-Dimethylaminopropyl )-N′ -ethylcarbodiimide Hydrochloride (EDC) | Sigma | E1769 |
| *N*-hydroxysuccinimide (NHS) | Sigma | 56485 |
| PBS tablet | Sigma | P3813 |
| Dulbecco's Modified Eagle Medium (DMEM) High Glucose | Sigma | D1152 |
| Penicillin/Streptomycin | Gibco | 15140122 |
| β-mercaptoethanol | Gibco | 21985023 |
| PrestoBlueTM | Invitrogen | A13261 |
| Calcein AM | Invitrogen | C3099 |
| Propidium iodide (PI) | Invitrogen | P3566 |
| Paraformaldehyde (PFA, 3.7% solution in PBS) | Fluka | 76240 |
| Triton X-100 | Sigma | T8532 |
| Donkey serum | Merck | S30 |
| Prolong Diamond antifade | Invitrogen | P36965 |
| Rabbit Anti-collagen I, N-Terminal | Sigma | SAB4500362 |

| | | |
|---|---|---|
| Rabbit-Anti-collagen VII antibody | ABCAM | AB93350 |
| Anti-Fibronectin antibody | ABCAM | AB2413 |
| Anti-mouse/rat Ki-67 (SOlA15) | Life Technologies | 41-5698-82 |
| Rabbit polyclonal to Collagen III | ABCAM | AB7778 |
| Mouse anti-actin, a-Smooth Muscle-Cy3 Antibody | Sigma | C6198 |
| Rabbit polyclonal to cytokeratin 10 | ABCAM | AB111447 |
| Rabbit polyclonal to E-cadherin | ABCAM | AB815148 |
| Rabbit polyclonal to Elastin | ABCAM | AB21610 |
| Rabbit Polyclonal to involucrin | ABCAM | AB53112 |
| Rabbit Polyclonal to Ki67 | ABCAM | AB15580 |
| Rabbit polyclonal to Loricrin | ABCAM | AB85679 |
| Donkey anti-mouse Alexa 488 | Invitrogen | A21202 |
| Donkey anti-mouse Alexa 594 | Invitrogen | A21203 |
| Donkey anti-rabbit Alexa 594 | Invitrogen | A21207 |
| Donkey anti-rabbit Alexa 488 | Invitrogen | A21206 |
| 4, 6-diamidino-2-phenylindole (DAPI) | Invitrogen | D1306 |

| | | |
|---|---|---|
| AurumTM Total RNA 96 Kit | Bio-rad | 7326800 |
| iScript RT Supermix, 100 rxns | Bio-rad | 1708841 |
| SYBR® Select Master Mix | Life Technologies | 4472897 |
| Hydrocortisone | Sigma | H0888 |
| 2-Phospho-L-ascorbic acid trisodium salt | Sigma | 49752 |
| 3,3′,5-Triiodo-L-thyronine sodium salt | Sigma | T6397 |
| Adenine | Sigma | A2786 |
| Cholera toxin from Vibrio cholerae | Sigma | C8052 |
| Transferrin human | Sigma | T8158 |
| Insulin solution human | Sigma | I9278 |
| Granulocyte-macrophage colony-stimulating factor (GMCSF) | Sigma | H5666 |
| Transforming Growth Factor-α human | Sigma | T7924 |
| Ham's nutrient mixture F12 | Sigma | 51651C |
| Keratinocyte Serum-Free Growth Medium for fetal and neonatal cells | Sigma | 131-500 |

## 2.3 General synthesis and preparation

### 2.3.1 Collagen electrocompaction

The electrocompacted collagen sheet was fabricated following previously published methods with slight modifications [1]. Briefly, by applying a potential to the collagen solution, a pH gradient will be generated because of the electrolysis of water. Due to the amphoteric nature of the collagen molecules, collagen molecules will be isoelectrically compacted to form collagen sheets or threads along the isoelectric point (Figure 2.1.A). In this study, an electrocompaction station containing two electrodes and a laser-cut plastic rim (Figure 2.1.B) as a spacer was assembled (Figure 2.1.C). After loading the collagen solution, a voltage was applied and monitored using the CHI electrochemical workstation (Figure 2.1.D). After electrocompaction, the resultant scaffolds were incubated with PBS and crosslinked before using. Detailed experimental parameters could be found in Chapters 3 and 4. Traditional collagen gel was also prepared as control group.

**A**

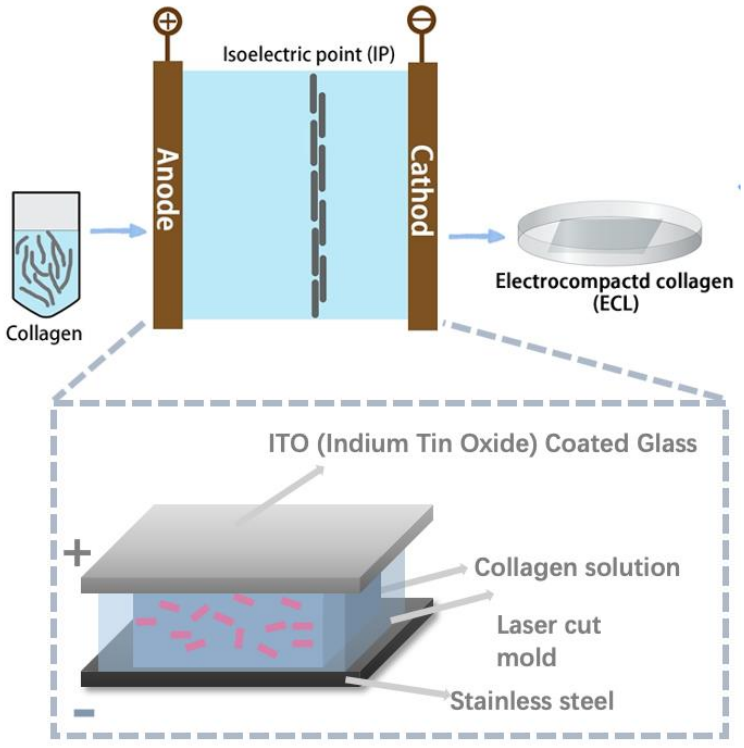

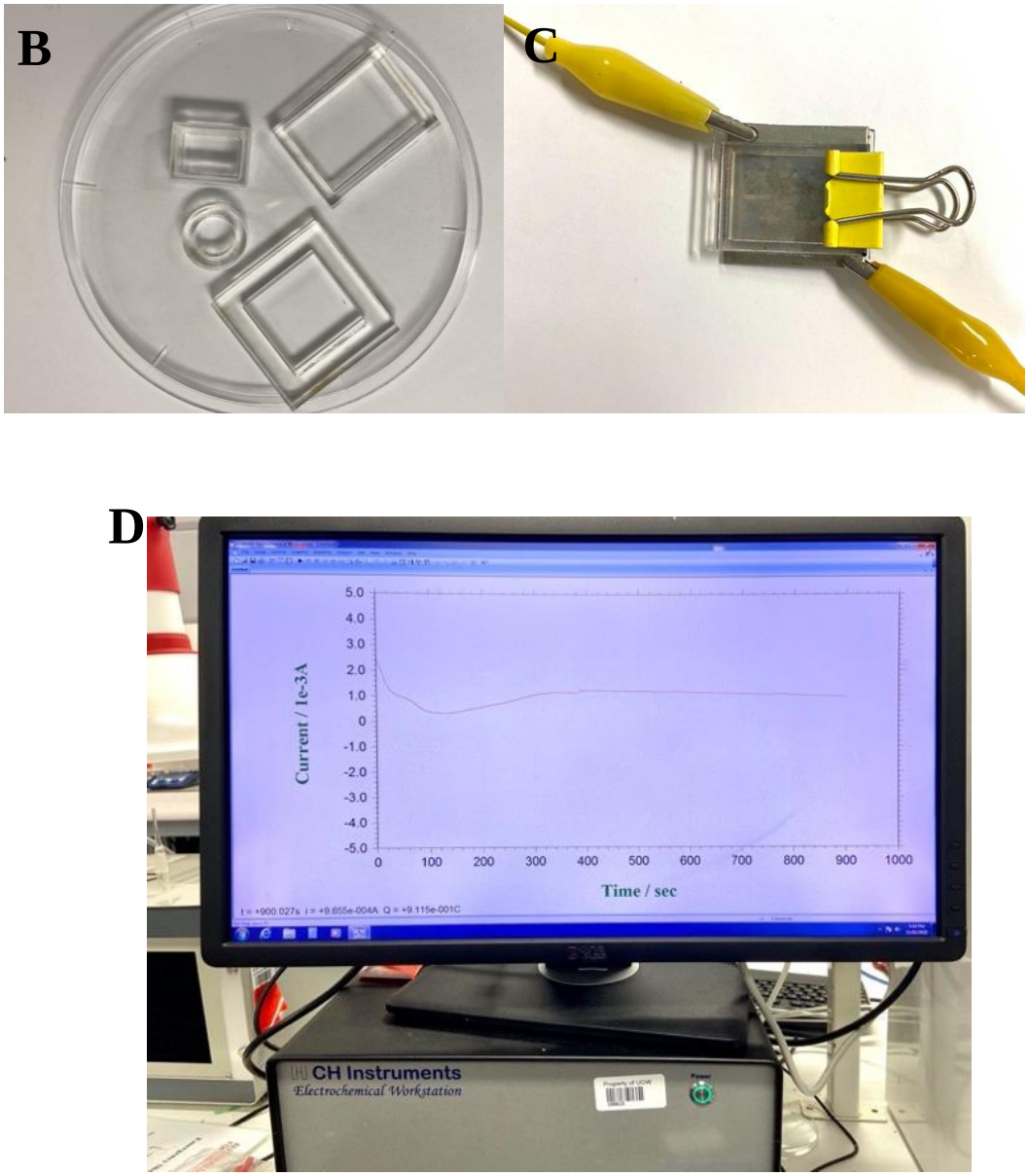


**Figure 2.1.** Devices used for collagen electrocompaction. A) Mechanism of electrocompaction process; B) Laser-cut molds; C) Set up of collagen electrocompaction; D) Electrochemical workstation.

### 2.3.2 Co-electrocompaction of collagen and elastin

In this study, to explore the function of elastin in skin scaffold, insoluble elastin particles were co-electrocompacted to form a collagen/elastin (CE) scaffold. To do this, insoluble

elastin particles were suspended into the collagen solution with a ratio of 7:1 (w/w) to mimic the natural ratio of collagen and elastin in skin tissues. The schematic process was shown in Figure 2.2. Then the mixed solution was electrocompacted and crosslinked following a similar procedure as described below.

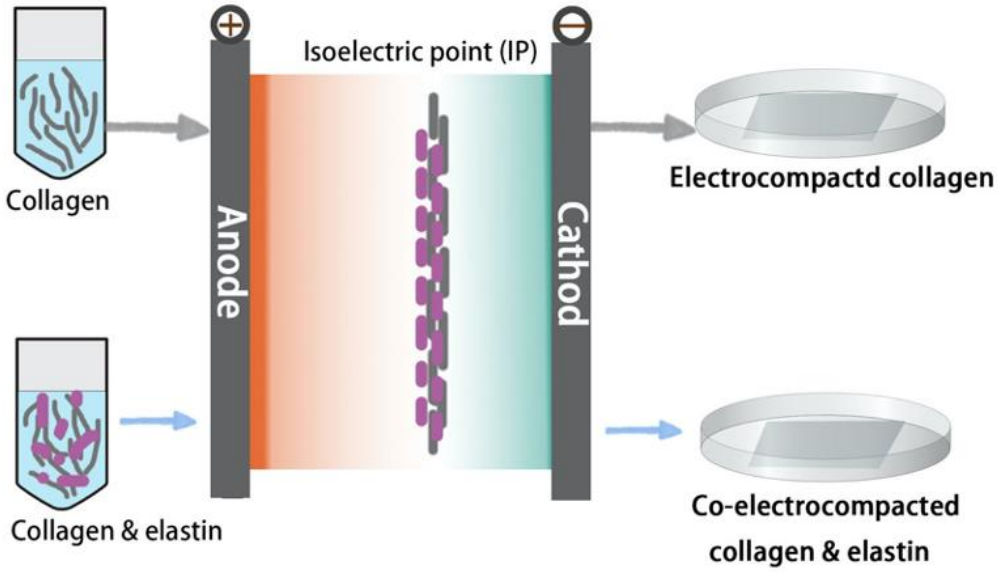


**Figure 2.2.** Illustration of co-electrocompaction of collagen and elastin.

### 2.3.3 EDC/NHS crosslinking between collagen/elastin molecules

1-ethyl-3-(3-dimethylaminopropyl)carbodiimide hydrochloride (EDC) is a popular zero-length crosslinker that can efficiently induce coupling between protein molecules, peptides, or fluorophores [2]. The term zero-length crosslinker means it can mediate crosslinking without EDC becoming part of the final crosslinked molecules. For higher efficiency and more stable couplings, EDC often comes with N-hydroxysuccinimide (NHS) or its water-soluble analog (Sulfo-NHS). EDC, in conjunction with NHS, enables a 2-step coupling of proteins. Firstly, EDC activates carboxyl groups and forms an unstable amine-reactive O-acylisourea ester. Secondly, the NHS group couples with the unstable amine-reactive O-acylisourea ester to form a semi-stable-amine-reactive-NHS ester. This ester further allows

the efficient conjugation to primary amines at physiologic pH. In this research, the EDC/NHS crosslinking method was used in various scenarios to induce crosslinking between collagen or collagen/elastin sheets (Figure 2.3), mediating HA or ulvan incorporation onto the protein scaffolds, and to prepare the fluoresceinamine-labeled ulvan.

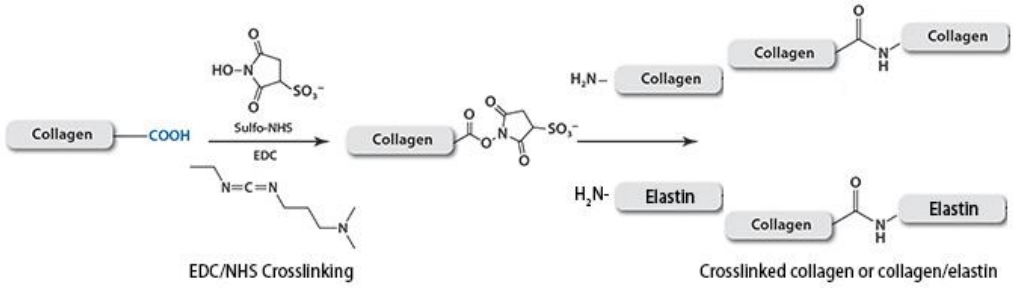


**Figure 2.3.** Crosslinking between collagen/collagen or collagen/elastin using EDC/NHS as crosslinker.

### 2.3.4 GAG coating

In natural skin, apart from collagen, polysaccharides are also crucial native components with functions including hydration, promoting angiogenesis, and binding of effector molecules [3]. To mimic the composition of natural skin matrices and investigate the roles of glycosaminoglycans in wound healing process, naturally occurred polysaccharides such as hyaluronic acid and ulvan from seaweed source [4] were considered in this study (Figure 2.4). To be specific, HA and ulvan were covalently crosslinked to electrocompacted collagen sheets respectively, using EDC/NHS as crosslinker.

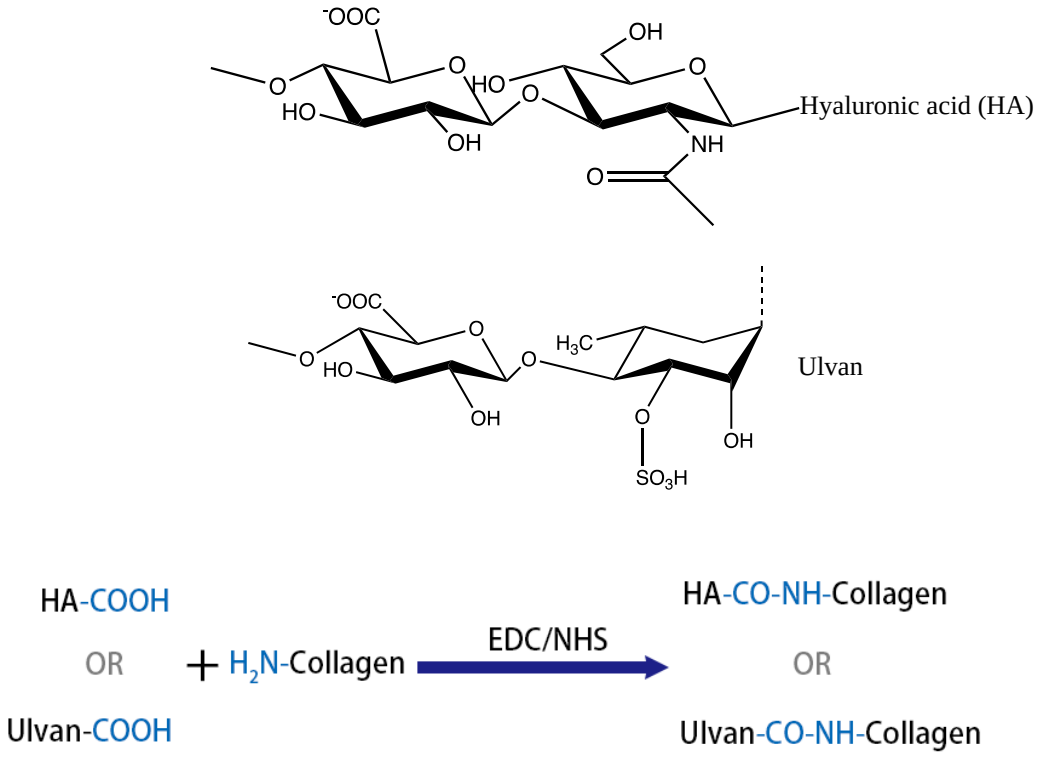


**Figure 2.4.** Molecular structure of Ulvan and HA, and crosslinking between HA or Ulvan with collagen.

### 2.3.5 Fluorophore labeling of ulvan

Fluorescent tagging, or labeling, is a method used to aid in the detection of some biomolecules such as antibodies, amino acid groups, or proteins. A fluorophore, which is a reactive derivative of a fluorescent molecule, is selectively bond to the target molecule, thus enabling detection [5]. In this research, fluoresceinamine (Figure 2.5) labeled ulvan was prepared by crosslinking fluoresceinamine to ulvan molecules using EDC/NHS as crosslinker. The resulted fluoresceinamine labeled ulvan was then being used and confocal inspected to localize the distribution of ulvan.

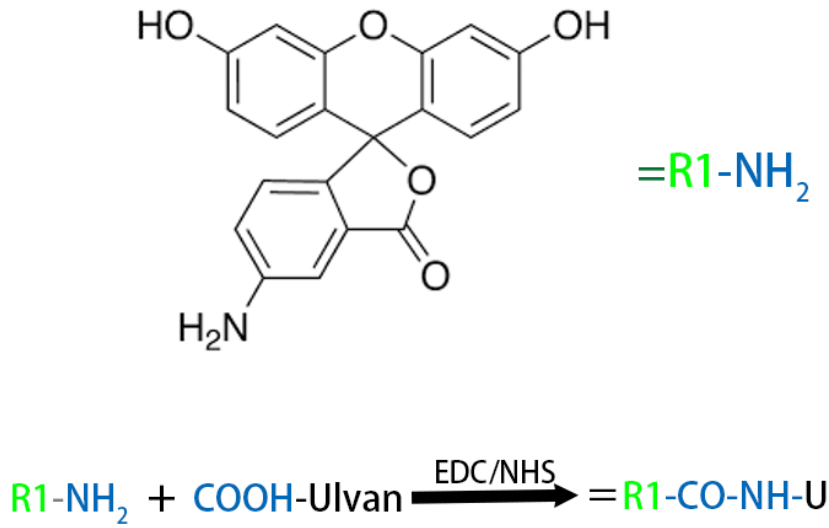


**Figure 2.5.** Chemical structure of fluoresceinamine Isomer 1 (R1-$NH_2$) and fluorophore labeling process of ulvan.

### 2.3.6 CTAB turbidity assay

The cetyltrimethylammonium bromide (CTAB) turbidity assay is a substitute to carbazole assay for HA quantification [6]. Yet, the CTAB assay is easier and faster compared with the carbazole assay. The CTAB assay is determined by the formation of insoluble compounds between cetyltrimethylammonium bromide and hyaluronic acid (Figure 2.6). Upon mixture of hyaluronic acid-containing solution and CTAB, insoluble compounds will be formed. In the reaction system, the degree of turbidity or the insoluble compounds is related to the amount of hyaluronic acid. The turbidity was measured using a plate reader at 600nm. Thus the amount of HA in the system could be calculated based on a standard curve of standard HA concentration vs. turbidity. In this study, the amount of HA immobilized to the collagen-based matrix was quantified using the CTAB turbidity assay. In specific, unreacted HA in the HA-collagen matrix coating system were assessed using the CTAB turbidity assay. Then the amount of HA immobilized to the collagen matrix was

calculated by the subtraction between overall HA amount and unreacted HA amount. Detailed calculation and standard curve were shown in Chapter 4.

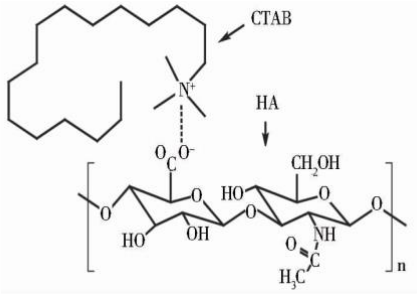


**Figure 2.6.** Mechanism of CTAM turbidity assay.

### 2.3.7 DMMB assay

The dimethylmethylene blue (DMMB, Figure 2.7) assay is widely used to quantify the amount of sulfated GAGs [7], such as chondroitin sulfate, heparin, or ulvan, in target biological samples or solutions. When bound to sulfated GAGs, the dye dimethylmethylene blue undergoes a change in the absorption spectrum due to the induction of metachromasia [8]. This enables rapid detection of sulfated GAGs in solution. A linear calibration curve could be obtained between 0.5-5 μg/mL of GAGs, which further allows the quantification of GAGs in solution. In this research, the DMMB assay was utilized to quantify the amount of ulvan that was incorporated into the collagen matrices. To do this, the target matrices were dissolved in HCL firstly. DMMB solutions were then added to the target solution. Absorbance at 540 nm and 595 nm of the mixture were recorded immediately. And a final concentration of ulvan could be calculated based on the change of absorbance and a standard curve. Detailed calculation was shown in Chapter 3.

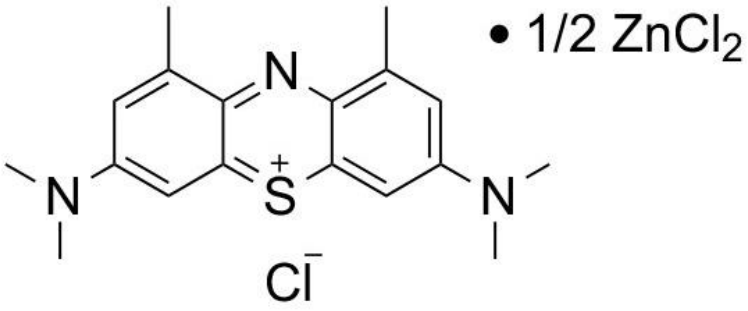


**Figure 2.7.** Structure of the DMMB.

## 2.4 Cell culture

### 2.4.1 Skin cell culture

Human dermal fibroblast cells (HDFs) and human immortalized keratinocytes (HaCaTs) (Figure 2.8) were utilized in this study. HDFs and HaCaTs were obtained from Sigma and maintained at 37°C with 5% $CO_2$ in a humidified incubator in the growth medium of regular Dulbecco's Modified Eagle's Medium (DMEM) (D1152, Sigma) containing 10% fetal bovine serum (FBS) and 1% v/v penicillin/streptomycin (Life Technologies, USA). Cells were routinely maintained in tissue culture plates and passaged at 1:5 split after reaching 70-80% confluency.

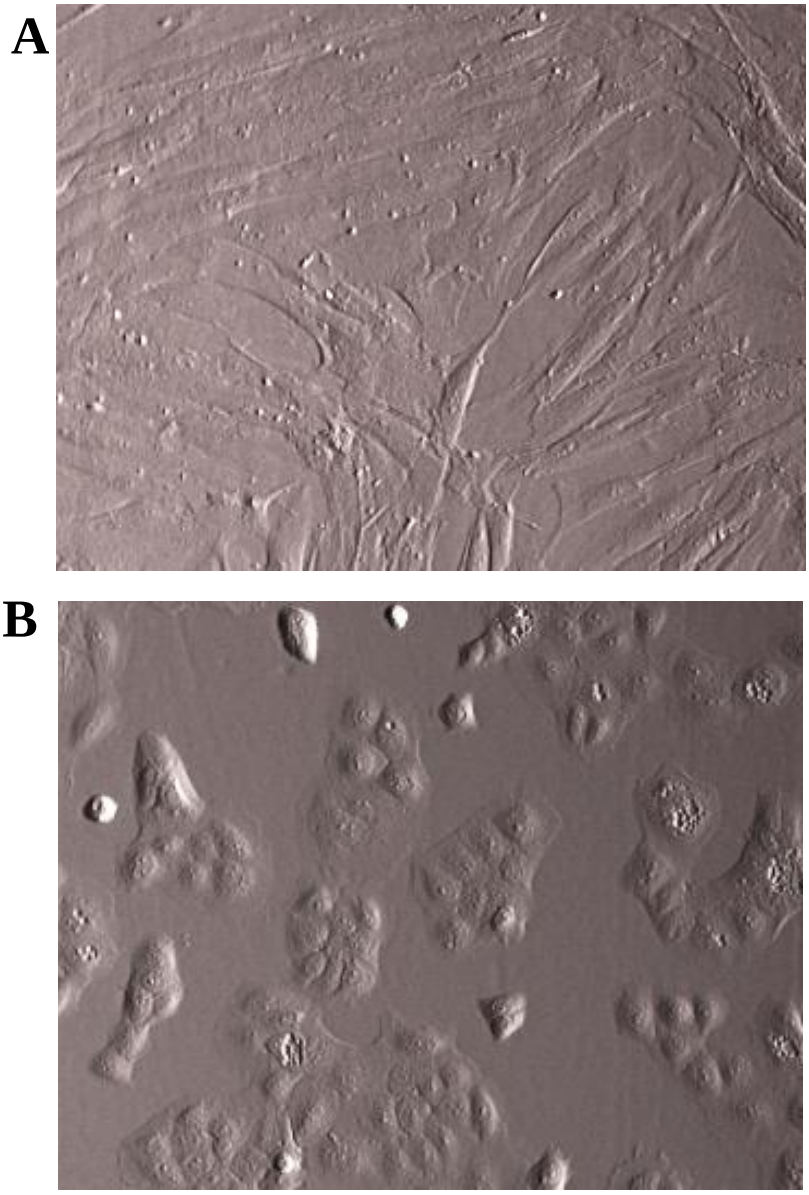


**Figure 2.8.** Skin cells used in this study. A) HDFs ,and B) HaCaTs under optical microscopy.

### 2.4.2 Air-liquid-interface (ALI) cell culture

The method of air-liquid interface cell culture (ALI) is designed to culture the bottom layers of cells in contact with media while keeping the top layers exposed to the air. To do this, cells seeded on a special insert are firstly cultured under normal conditions for the

initial growth. Then cells are lifted to the air-liquid interface and cultured with special medium to induce cell differentiation. It is primarily designed to mimic respiratory tract epithelial in vitro [9]. This is known to support the differentiation of 3D multilayered skin models [10]. In this study (Figure 2.9), HDFs were seeded into compartmentalized culture systems on porous filter supports as the dermal layer followed by keratinocytes cell seeding. After a certain initial period, cells were then lifted, exposing cells of the surficial layer to the surrounding air to induce differentiation. At the same time, nutritive supply to the cells was guaranteed by the basolateral poles in the inserts. Air-liquid interface (Ali) systems allow the establishment of a 3D culture environment more representative of that in vivo than traditional culture-plate systems. Detailed culture protocol and composition of differentiation medium are explained in Chapter 5.

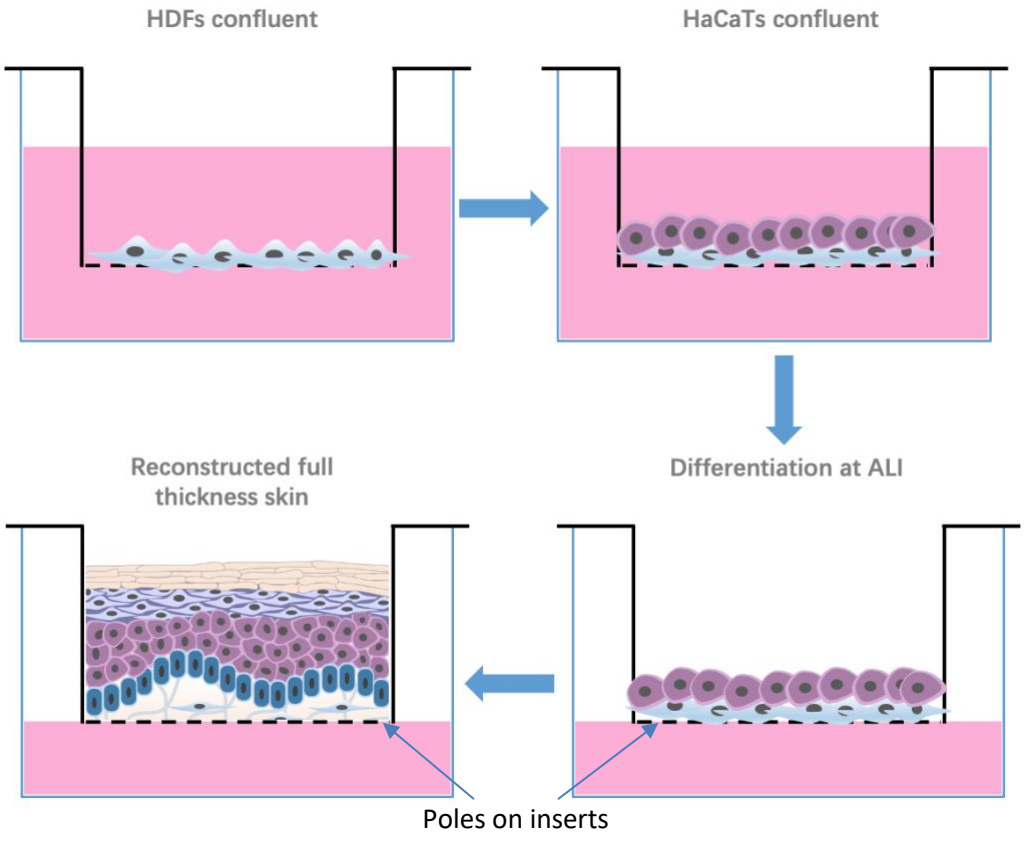


**Figure 2.9.** ALI co-culture of HDFs and HaCaTs.

## 2.5 Physicochemical characterization

### 2.5.1 Scanning electron microscope (SEM)

The SEM uses a focused beam of high-energy electrons to interact with the surface of solid specimens to generate information. This information could reveal the external morphology (texture) and orientation of the microstructure. Before SEM imaging, biological samples need to be pre-processed into conductive samples. Thus, the samples were fixed and dehydrated, followed by gold coating of 20 nm using a sputter coater. Finally, the surface morphology was obtained at various magnification using a JSM-7500FA LV Scanning Electron Microscope (JEOL Ltd, USA). In this study, the micro-morphologies of the collagen gel and electrocompacted collagen were obtained and evaluated.

### 2.5.2 Confocal inspection

Confocal microscopy, or confocal laser scanning microscopy (CLSM), is an optical imaging technique used to obtain high-resolution images. With the advantages of controlled illumination of depth and area of the sample, there has been a growing number of applications in cell biology that rely on imaging both fixed and living tissues [11]. In this study, the confocal laser scanning microscope (CLSM, Leica TCS SP5, Germany) was firstly used to confirm the presence of elastin particles in the collagen/elastin membrane. Under the DAPI (4',6-diamidino-2-phenylindole) set, insoluble elastin particles have autofluorescence. The confocal microscope was also used for immunofluorescent staining in this study to explore the protein expression and distribution in target cells.

### 2.5.3 FTIR

Fourier-transform infrared spectroscopy (FTIR) is a technique to obtain the information of the absorption or emission of an infrared spectrum of a solid, liquid, or gas [12]. In infrared spectroscopy, an infrared (IR) radiation is passed through a sample. Due to the specific intrinsic property of different samples, some of the infrared radiation is passed through (transmitted), and some are absorbed by the sample (absorbed). The resulting spectrum reflects the molecular absorption and transmission, representing a molecular fingerprint of the sample. FTIR can be used to identify unknown materials, determine the consistency or quality of a sample, or used together with other methods to determine the number of components in a mixture. In this research, FTIR technique was used to obtain the spectrum of co-electrocompacted collagen/elastin sheets to demonstrate the successful incorporation of these two proteins. FTIR was also used to verify the amination of HA. Related spectrum were shown in Chapter 4.

**2.5.4 NMR**

NMR is an abbreviation for Nuclear Magnetic Resonance. NMR spectroscopy is a technique used to analyze the molecular structure of a material by measuring the interaction of nuclear spins when placed in a strong magnetic field. The principle behind NMR is that all nuclei are electrically charged, and many of them have spin. When a nucleus is placed in a strong magnetic field, it will begin to process thus has a precession frequency. If the sample placed in a magnetic field is irradiated with radio waves corresponding to the precession frequency, an NMR spectrum can be recorded (Figure 2.10). In this research, the NMR spectrum of the HA before and after amination (shown in Chapter 4) were recorded to evaluate the modification process.

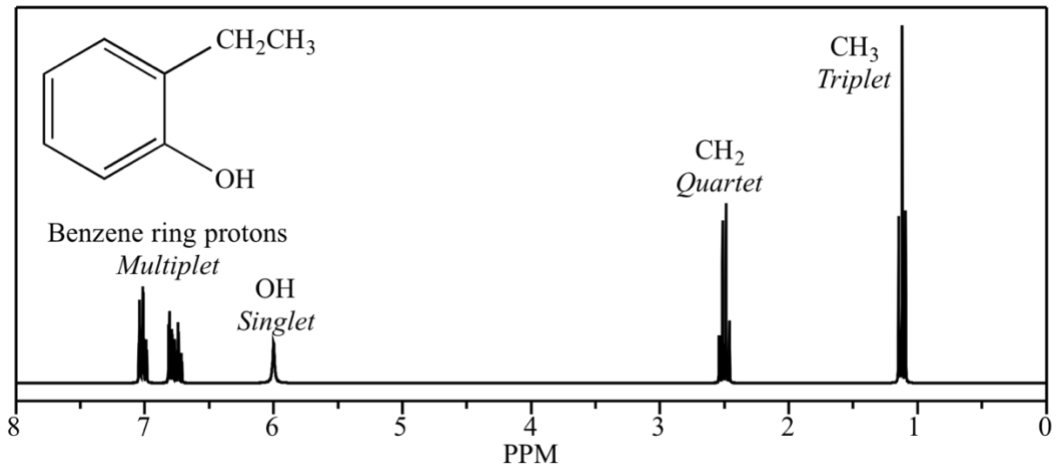


**Figure 2.10.** An example of NMR spectrum.

### 2.5.5 Tensile tester

The young's modulus, elongation to break and elasticity of the scaffold are crucial scaffold properties [13]. With controlled testing parameters, these data could help determine the maximum strength or load that a scaffold can withstand. In this research, the mechanical property of the scaffold was evaluated using an EZ-S mechanical tester (Figure 2.11, Shimadzu, Japan) using procedures as previously described [1]. The samples were cut, and both sides were fixed to each side of a 10 N load cell. The samples were then stressed with a strain rate of 2 mm/min. The Young's modulus was calculated by a linear regression fit of the strain-stress curve between the end of the toe region and the midpoint of the linear elastic region. For each reported value, three different samples were tested, and the results were averaged.


**Figure 2.11.** Photo of EZ-S mechanical tester.

### 2.5.6 Swelling ratio

The swelling ratio or water/solution uptake ability of a hydrogel/scaffold is defined as the fractional increase in the total weight of the hydrogel/scaffold due to water absorption. It is an important factor when evaluating the intrinsic property of a scaffold in interacting with the liquid environment [14]. These scaffolds need to be able to absorb bioactive molecules from neighboring tissue and thus promote cell growth and function [15]. Also, during the wound healing process, the maintenance of moisture near the wound site is a critical aspect of wound management [16]. In this study, the swelling ratio of the GAGs-incorporated scaffolds was evaluated. To do this, the initial dried weight was recorded as $W_d$. Samples were then soaked in PBS for desired time for complete hydration, and the wet weight ($W_w$) was recorded after removing excess water on sample surface using Kimwipe.

The swelling ratio of target matrices was calculated following the equation 2.1 as shown below:

$$Swelling\ ratio\ (\%) = \left(\frac{Ww-Wd}{Wd}\right) \times\ 100\% \qquad (2.1)$$

### 2.5.7 Degradability

The stability of scaffolds over time [17] were determined in this study. To do this, a collagenase solution was prepared to mimic the physiological conditions [18]. In this study, the stability of electrocompacted collagen structure was determined by assessing the resistance of the matrices to collagenase treatment. With the initial dried weight of the target structures known, samples were immersed in the digest solution containing 100 μg/mL (28 units) collagenase (type I, Sigma-Aldrich, Castle Hill, Australia) in PBS (pH 7.4) and incubated for desired time points. The digest solution was replaced every 2 h. At desired time points, the samples were removed from the digest solution and freeze-dried. Then the residual mass at each time point was calculated.

## 2.6 Biological characterization

### 2.6.1 Cell viability assay

Live/Dead Assay, which utilizes calcein AM for the staining of live cells and Propidium iodide (PI) for the staining of dead or dying cells, is a quick and easy two-color assay to determine cell viability (Figure 2.12). In living cells, the cell-permeant calcein AM could penetrate cells and react with the intracellular esterase, thus to be converted into green-fluorescent calcein. In dying or dead cells with compromised plasma membranes, the membrane-impermeant propidium iodide (PI) binds to DNA with high affinity and generates a bright red fluorescence. In this study, samples were treated with calcein AM at room temperature for 10 min, followed by PI for 5 min to distinguish between live and

dead cells. Then, samples are ready for confocal inspection with a Leica TSC confocal microscope, and Image J is used to calculate the cell viability by counting the numbers of the live and dead cells, respectively.

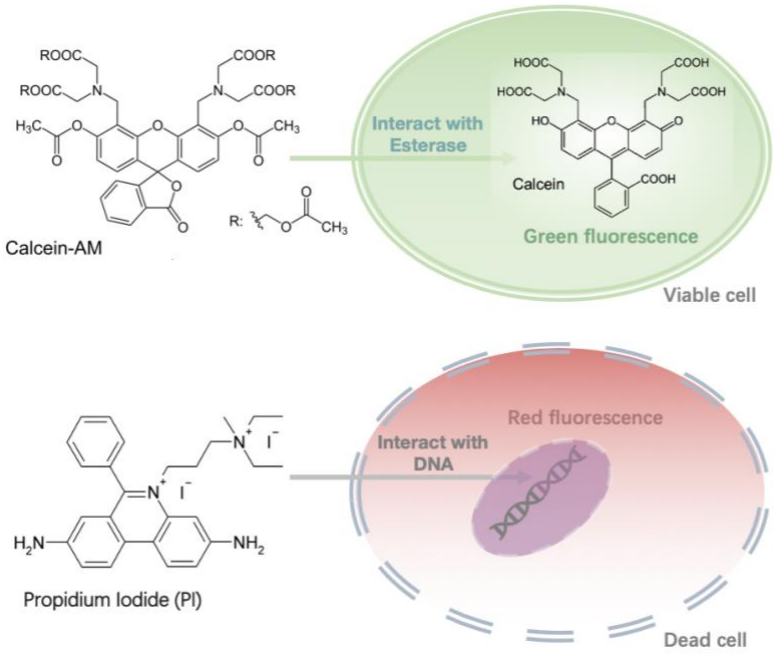


**Figure 2.12.** Mechanism of live/dead assay.

### 2.6.2 Cell proliferation assay

The proliferation behavior of cells is quantified using PrestoBlue®, which contains a cell-permeant compound resazurin that is blue in color and virtually nonfluorescent (Figure 2.16). When incubating with living cells, as shown in Figure 2.13, resazurin-based PrestoBlue® solution will turn red due to the reducing power of living cells, thus to quantitatively measure the proliferation of cells [19]. In this research, the cell-seeded samples were firstly incubated with the reagent in incubators for 30 min, the supernatant was then collected and transferred into a 96-well plate (Greiner bio-one, 655180), and the fluorescent intensity was obtained by using a microplate reader (POLARstar Omega). The scaffolds without cells were used as blank control.

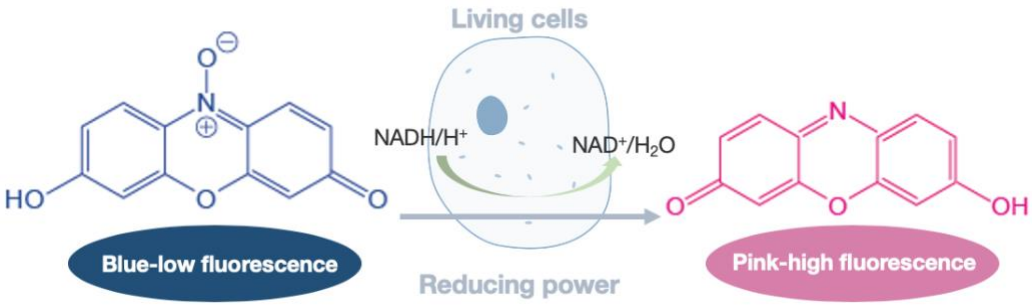


**Figure 2.13.** Mechanism of cell proliferation assay using PrestoBlue.

### 2.6.3 Tissue preparation and procession

Before any staining or microscopic analysis, fresh samples or tissues need to be fixed and processed to prevent decay as well as to preserve tissues as close to the natural states as possible [20]. Also, microscopic analysis of tissues needs to be prepared to the state of thin, high-quality sections mounted on some specific glass slides and properly stained to show those complicated structures. “Tissue processing” requires fixation to maintain a state that is completely infiltrated with a suitable histological wax or paraffin, then prepared for sectioning using a microtome. In this work, tissue processing was conducted using a tissue processor (Figure 2.14, Leica ASP300S). During tissue processing, samples were put into cassettes, and a series of chemicals were applied, including formalin, 70% alcohol, 80% alcohol, 95% alcohol, 100% alcohol, xylene and paraffin. These chemicals were used for fixation, dehydration, cleaning, and embedding of the samples. After tissue processing, samples are ready for sectioning.


**Figure 2.14.** Photo of tissue processor - Leica ASP300S.

### 2.6.4 Tissue embedding

In this work, processed samples were embedded in paraffin using a Leica EG1150 H Heated Paraffin Embedding Module (Figure 2.15.A). During this process, high-quality paraffin was used and melted before embedding to ensure high-quality blocks that are easy to cut. Tissues were then put into properly sized mold (Figure 2.15.B) to hold the melted paraffin. This step should be handled gently to avoid tissue broken. Tissues embedded in paraffin (Figure 2.15.C) were then cooled down on the cold table and preserved.

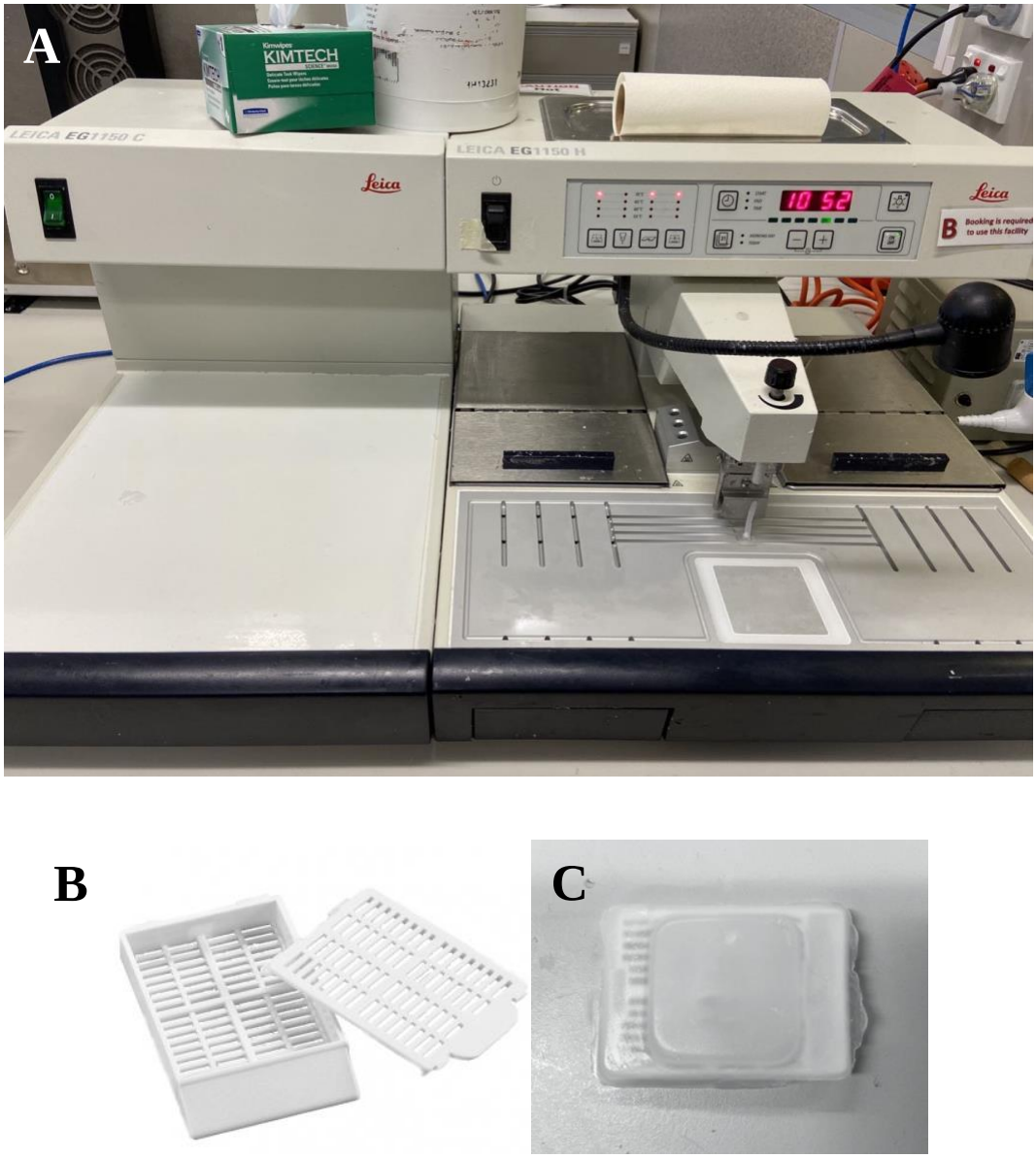


**Figure 2.15.** Equipment and molds used for tissue embedding. A) Leica EG1150 H Heated Paraffin Embedding Module; B) Cassettes used to hold tissues and paraffin; C) Tissue embedded paraffin blocks for sectioning.

### 2.6.5 Tissue sectioning, floating and drying

Tissue embedded paraffin blocks were then cut using a Leica RM2235 Manual Rotary Microtome (Figure 2.16.A). This step aims to produce a series of thin section of uniform thickness for optimal microscopic examination.

In this work, sections of 7 um thickness were collected for later use. Before sectioning, blades and tissues in paraffin were chilled to facilitate smooth and uniform cutting. Sections were then floated using a Leica HI1210 water bath which allows warm water held within to float sections onto slides. To collect those floated sections, Polyline slides (Thermo Scientific, Figure 2.16.B) were used here in this work to prevent sections detection. Another reason for using a water bath here is sections will be slightly crinkled after being cut and the water bath helps to flatten these sections out. The bath was kept at 40 $^{o}$C throughout the mounting stage. Sections mounted on slides were finally dried using a slide drying hotplate (Figure 2.16.C; Thermo Fisher Scientific).


**Figure 2.16.** Equipment and devices used for tissue sectioning, floating, and drying. A) Leica RM2235 Manual Rotary Microtome for sample sectioning and water bath for sample floating; B) Slides used to collected floating sectioned samples; C) Slide drying hotplate.

### 2.6.6 Cell Immunophenotyping

Cell immunophenotyping is a general technique using immunohistochemistry reaction to examine the protein expressed by cells (Figure 2.17) [21]. To do this, samples were usually

fixed using a 3.7 % paraformaldehyde (PFA; Fluka) solution to stabilize proteins and preserves morphology. The samples were then blocked and permeabilized overnight to allow access of antibodies into cells. After that, samples were incubated with primary antibodies overnight, followed by incubation with Alexa Fluor-conjugated secondary antibody. Cell nuclei were then counterstained using DAPI at RT for 10 min. The anti-fade reagent was applied afterward to help preserve the fluorescent signals. Samples were imaged with a Leica TSC confocal microscope.

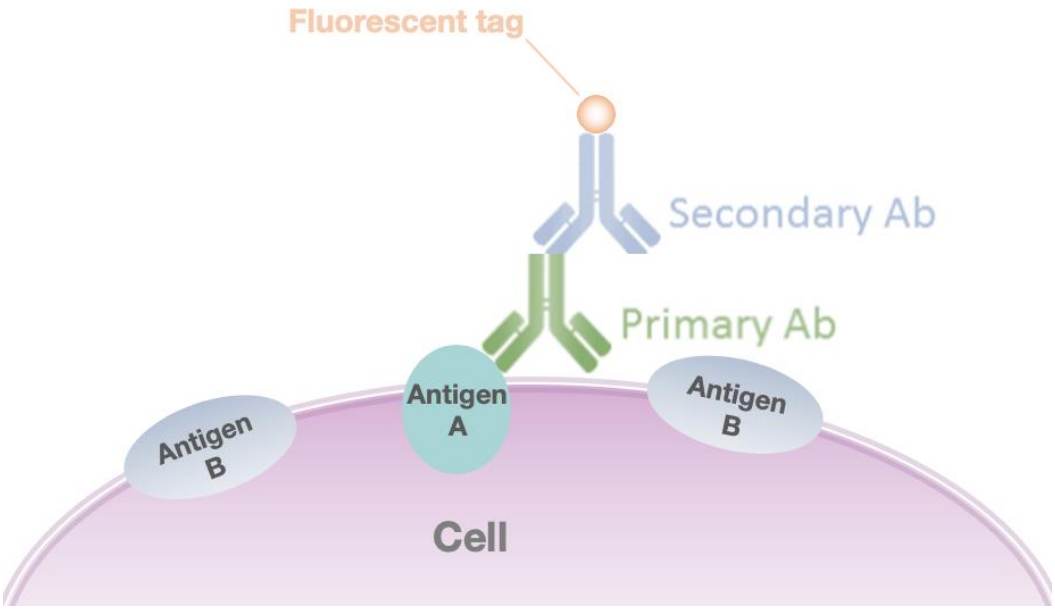


**Figure 2.17.** Mechanism of immunohistochemistry staining.

### 2.6.7 Histological staining

The H&E staining is one of the principal tissue staining methods in histology and medical diagnosis [22]. It can be done quickly, cheaply, and delivers valuable information on target tissues. Before H&E staining, target samples need to be fixed, embedded, and sectioned to a specific thickness. For the sectioned sample, hematoxylin solution is applied firstly to stain the cell nuclei giving it a bluish or dark blue color. Then, eosin is used to stain the

extracellular matrix and cytoplasm pink. With other structures taking on different combinations of these colors, the results can reveal general distribution of cells and extracellular matrix and provides an overview of the sample structure.

In this work, before H&E staining, biological samples were fixed firstly in n 3.7% PFA solution in PBS at room temperature for 2h. The samples were pre-processed and embedded in paraffin blocks. Sections of 7 μm thickness were then cut using a Reichert-Jung 2035 microtome, collected on Polysine slides (Thermo scientific). After dewaxing and rehydration, the section-mounted glass slides were stained using hematoxylin solution (Sigma) for 10 min and then dipped in an eosin Y solution (Sigma Aldrich, WI) for 60s. After washing and dehydration, the samples were sealed with coverslips using Permount Mounting Medium (examples of H7E stained samples shown in Figure 2.18) (Fisher Scientific, MA, USA). Photographs were taken on a Nikon microscope with a Leica DM 750 microscope (Leica Microsystems, Mannheim, Germany).


**Figure 2.18.** Example of H&E stained section.

### 2.6.8 RT-qPCR

Reverse Transcription-quantitative Polymerase Chain Reaction RT-qPCR (RT-qPCR) is a laboratory technique of molecular biology based on the polymerase chain reaction [23]. It

is primarily used to quantify the amount of a specific RNA. RT-PCR is widely used in the analysis of gene expression a cell or tissue and in the diagnosis of genetic diseases. Typically, RT-qPCR was conducted in a two-step manner. In the first step, the mRNA of target samples was extracted and transcripted into complementary DNA (cDNA) using a reverse transcriptase. Secondly, exponential amplification of specific cDNA was achieved using the cDNA as templates through polymerase chain reaction (PCR). In this study, total RNA was firstly isolated using AurumTM Total RNA Mini Kit with the purity defined by NanoDropTM. The iScriptTM Reverse Transcription Supermix Kit (Bio-rad, 1708841) was then used to transcribe the RNA into cDNA. Finally, qPCR was performed with the following set up (Figure 2.19) using a SYBRTM Select Master Mix for CFX (4472942) using a Bio-Rad CFX real-time instrument.

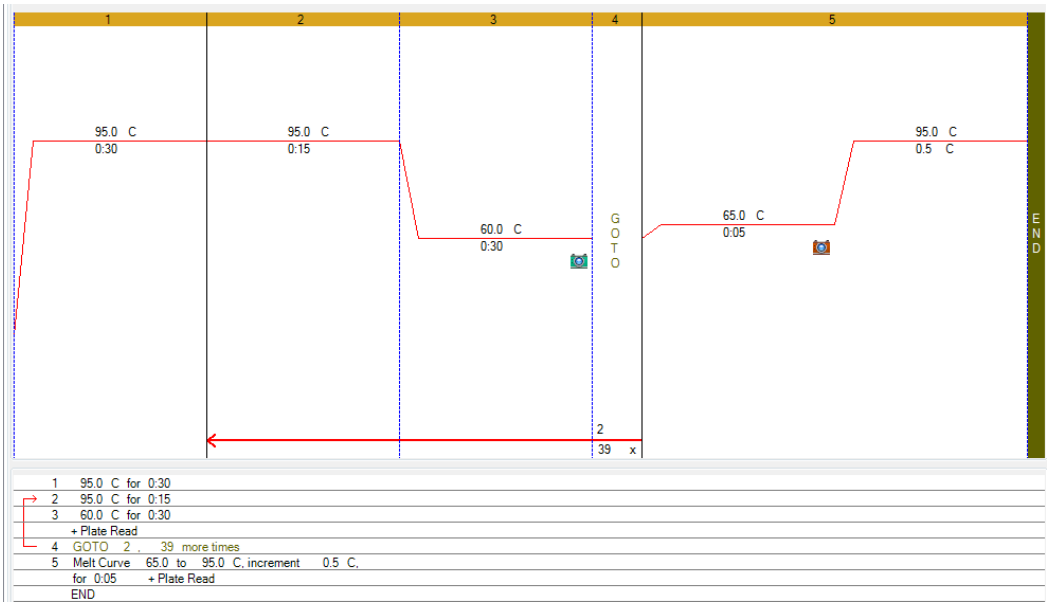


**Figure 2.19.** Program used for RT-qPCR

## 2.7 References


1. L. Kang, X. Liu, Z. Yue, Z. Chen, C. Baker, P.C. Winberg, G.G. Wallace, Fabrication and in vitro characterization of electrochemically compacted collagen/sulfated xylorhamnoglycuronan matrix for wound healing applications, Polymers 2018, 10, 415.

2. J. Lee, H. Edwards, C. Pereira, S. Samii, Crosslinking of tissue-derived biomaterials in 1-ethyl-3-(3-dimethylaminopropyl)-carbodiimide (EDC), Journal of Materials Science: Materials in Medicine 1996, 7, 531-541.

3. S. Ghatak, E.V. Maytin, J.A. Mack, V.C. Hascall, I. Atanelishvili, R. Moreno Rodriguez, R.R. Markwald, S. Misra, Roles of proteoglycans and glycosaminoglycans in wound healing and fibrosis, International journal of cell biology 2015, 2015.

4. M. Lahaye, A. Robic, Structure and functional properties of ulvan, a polysaccharide from green seaweeds, Biomacromolecules 2007, 8, 1765-1774.

5. R. Chen, Z. Yue, M.E. Eccleston, N.K. Slater, Aqueous solution behaviour and membrane disruptive activity of pH-responsive PEGylated pseudo-peptides and their intracellular distribution, Biomaterials 2008, 29, 4333-4340.

6. Y.-H. Chen, Q. Wang, Establishment of CTAB Turbidimetric method to determine hyaluronic acid content in fermentation broth, Carbohydrate polymers 2009, 78, 178-181.

7. V.J. Coulson-Thomas, T.F. Gesteira, Dimethylmethylene blue assay (DMMB), Bio-protocol 2014, 4, e1236.

8. C.B. Whitley, M. Ridnour, K. Draper, C. Dutton, J.P. Neglia, Diagnostic test for mucopolysaccharidosis. I. Direct method for quantifying excessive urinary glycosaminoglycan excretion, Clinical chemistry 1989, 35, 374-379.

9. A.A. Pezzulo, T.D. Starner, T.E. Scheetz, G.L. Traver, A.E. Tilley, B.-G. Harvey, R.G. Crystal, P.B. McCray Jr, J. Zabner, The air-liquid interface and use of primary cell cultures

are important to recapitulate the transcriptional profile of in vivo airway epithelia, American Journal of Physiology-Lung Cellular and Molecular Physiology 2011, 300, L25-L31.

10. T. Sun, D. Norton, J.W. Haycock, A.J. Ryan, S. MacNeil, Development of a closed bioreactor system for culture of tissue-engineered skin at an air–liquid interface, Tissue engineering 2005, 11, 1824-1831.

11. P.J. Caspers, G.W. Lucassen, G.J. Puppels, Combined in vivo confocal Raman spectroscopy and confocal microscopy of human skin, Biophysical journal 2003, 85, 572-580.

12. S.M. Ali, F. Bonnier, H. Lambkin, K. Flynn, V. McDonagh, C. Healy, T. Lee, F. Lyng, H. Byrne, A comparison of Raman, FTIR and ATR-FTIR micro spectroscopy for imaging human skin tissue sections, Analytical Methods 2013, 5, 2281-2291.

13. P.G. Agache, C. Monneur, J.L. Leveque, J. De Rigal, Mechanical properties and Young's modulus of human skin in vivo, Archives of dermatological research 1980, 269, 221-232.

14. C. Chang, B. Duan, J. Cai, L. Zhang, Superabsorbent hydrogels based on cellulose for smart swelling and controllable delivery, European polymer journal 2010, 46, 92-100.

15. R. Xu, H. Xia, W. He, Z. Li, J. Zhao, B. Liu, Y. Wang, Q. Lei, Y. Kong, Y. Bai, Controlled water vapor transmission rate promotes wound-healing via wound re-epithelialization and contraction enhancement, Scientific reports 2016, 6, 24596.

16. J.P. Junker, R.A. Kamel, E. Caterson, E. Eriksson, Clinical impact upon wound healing and inflammation in moist, wet, and dry environments, Advances in wound care 2013, 2, 348-356.

17. F.R. Huss, E. Nyman, C.-J. Gustafson, K. Gisselfält, E. Liljensten, G. Kratz, Characterization of a new degradable polymer scaffold for regeneration of the dermis: in vitro and in vivo human studies, Organogenesis 2008, 4, 195-200.

18. L. Ma, C. Gao, Z. Mao, J. Zhou, J. Shen, X. Hu, C. Han, Collagen/chitosan porous scaffolds with improved biostability for skin tissue engineering, Biomaterials 2003, 24, 4833-4841.

19. M. Boncler, M. Różalski, U. Krajewska, A. Podsędek, C. Watala, Comparison of PrestoBlue and MTT assays of cellular viability in the assessment of anti-proliferative effects of plant extracts on human endothelial cells, Journal of pharmacological and toxicological methods 2014, 69, 9-16.

20. J.D. Bancroft, M. Gamble, Theory and practice of histological techniques, Elsevier health sciences2008.

21. J. Ramos-Vara, M. Miller, When tissue antigens and antibodies get along: revisiting the technical aspects of immunohistochemistry—the red, brown, and blue technique, Veterinary pathology 2014, 51, 42-87.

22. A.H. Fischer, K.A. Jacobson, J. Rose, R. Zeller, Hematoxylin and eosin staining of tissue and cell sections, Cold spring harbor protocols 2008, 2008, pdb. prot4986.

23. A. van der Smissen, V. Hintze, D. Scharnweber, S. Moeller, M. Schnabelrauch, A. Majok, J.C. Simon, U. Anderegg, Growth promoting substrates for human dermal fibroblasts provided by artificial extracellular matrices composed of collagen I and sulfated glycosaminoglycans, Biomaterials 2011, 32, 8938-8946.

# Chapter 3

# Fabrication and characterization of a collagen-ulvan (SXRGlu) dermal scaffold

---

Some parts of this chapter have appeared in the published article "Fabrication and in vitro characterization of electrochemically compacted collagen/sulfated xylorhamnoglycuronan matrix for wound healing application" by Kang, Lingzhi, Xiao Liu, Zhilian Yue, Zhi Chen, Chris Baker, Pia C. Winberg, and Gordon G. Wallace. Polymers 10, no. 4 (2018): 415.

**CONTENT**

## 3.1 Introduction

Skin is the largest organ of the human body and it acts as a physical barrier against the external environment. Compromised wound healing is a major issue in the treatment of massive skin lesions. Currently, widely used strategies to treat skin wounds include wound dressing, skin autografts and allografts [1]. However, these applications are limited by various disadvantages, such as low adhesion to lesions, donor shortage, and immune rejection [1]. Advances in tissue engineering have made the production of artificial skin possible.

Skin tissue engineering alleviates the issue associated with donor shortage and prompts wound management via the use of bioactive cell-material complex scaffolds [2]. Currently, available tissue-engineered skin substitutes include epidermal substitutes, dermal substitutes, and epidermal-dermal substitutes [3]. While skin is the first type of tissue that has been successfully engineered for implementation into the clinical application, tissue-engineered skin still faces a number of challenges, limiting its wider application. These include the inability to mimic the composition and structure of natural skin, poor vascularization, scar formation, missing appendages and pigmentation and high manufacturing costs [4]. Typically, tissue-engineered skin involves the use of biodegradable materials to either induce the ingrowth of surrounding cells or to act as temporary supports for transplanted cells to attach, proliferate and differentiate to enable neo-tissue genesis [5]. Thus, the role of scaffold material is crucial and this material should be carefully selected [6]. Among the wide range of available biocompatible materials, including synthetic polymers and natural polymers, preferences are given to natural polymers such as collagen, elastin, and polysaccharides because of their biocompatibility, biodegradability and presence of bonding sites with cells and bioactive molecules [7].

In skin tissue, collagen is the most abundant component in the extracellular matrix, providing integrity, rigidity and elasticity [8]. Collagen has thus been pursued in wound healing for several decades [3]. In particular, type I collagen is of key importance for cell-material interactions, as it contains crucial integrin-binding sequences including the arginine-glycine-aspartic acid (RGD) and glycine-phenylalanine-hydroxyproline-glycine-glutamic acid-arginine (GFOGER) sequence [9]. However, traditionally fabricated collagen hydrogels mainly contain randomly distributed fiber and cannot adequately emulate the complexity of natural ECM and skin mechanical properties. Collagen electrocompaction, which is a collagen densification method that takes advantage of the amphoteric nature of the collagen molecules to isoelectrically compact collagen molecules into densely packed and highly ordered bundles [10], is a promising method to fabricate collagen sheet that mimics the alignment, density and mechanical properties of collagen in skin tissues.

In natural skin, apart from collagen, polysaccharides are also important native components with functions including maintaining moisture environment, promoting angiogenesis, offering binding sites for drugs or growth factors [7]. Recently, marine biomass has gained increasing attention as an abundant and sustainable source of polysaccharides [11]. Among them, sulfated xylorhamnoglycuronan (SXRGlu), a sulphated polysaccharide extracted from the cell wall of specific green algae, is a promising candidate to explore. SXRGlu shares chemical similarities with natural-skin glycosaminoglycan polymers such as dermatan sulfate and hyaluronic acid [12], and from our previous lab trials with this species-specific extract, has shown a strong binding affinity to fibroblast cells and collagen, as well as organized structure and anti-inflammatory activity. Thus, the incorporation of SXRGlu is a strong candidate ingredient in electrochemically aligned collagen, as it may

serve as a suitable skin scaffold component substitutes for skin regeneration and wound healing.

The aim of this chapter is to fabricate biomimicry dermal scaffolds using electrochemically aligned collagen (ECL) and SXRGlu for wound healing applications. SXRGlu was introduced to the ECL scaffold by chemical crosslinking, using 1-ethyl-3-(3-dimethylaminopropyl) carbodiimide and *N*-hydroxysuccinimide (EDC–NHS) as crosslinker. Physiochemical properties of the fabricated scaffolds including micromorphology, SXRGlu content and distribution, mechanical property, water uptake ability and degradability were evaluated. In addition, HDFs were cultured on the scaffolds to assess the cell viability, proliferation, and morphology.

## 3.2 Materials and Methods

### 3.2.1 Synthesis of Electrocompacted Collagen Scaffolds

The fabrication process of traditional collagen gel (GEL), electrocompacted and crosslinked collagen (ECLC), as well as SXRGlu-conjugated ECLC (ECLCU) scaffold, is illustrated in Figure 3.1. Type-I collagen powder (Kele Biotech Co., Chengdu, China) was dissolved in 0.5 M acetic acid at 6 mg/mL and dialyzed against ultrapure water at 4 °C for 12 h. Then the dialyzed collagen was loaded into a circular rubber washer (diameter = 1.2 cm and thickness = 2 mm) sandwiched between two oppositely charged electrodes. Upon application of an electric field of 6 volts for 15 min, a pH gradient was generated between the two electrodes. As a result of the amphoteric property of the collagen molecules, the collagen molecules would be driven by the electrostatic repulsion from the electrodes and compacted along the isoelectric point thus forms a transparent “wet” collagen sheet (ECL). Then the freshly aligned collagen sheet was incubated in PBS at 37 °C for 4 h for fibril formation.

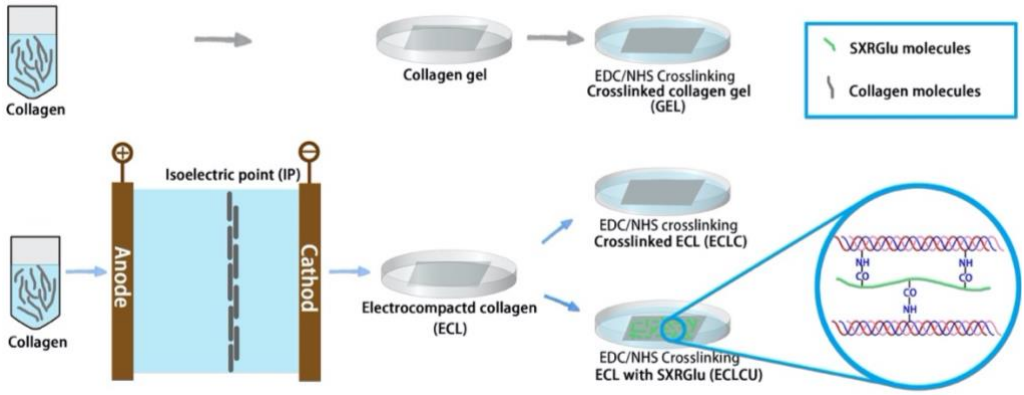


**Figure 3.1.** Schematic illustration of the preparation of electrocompacted collagen matrices (grey and green rods represent collagen and collagen/sulfated xylorhamnoglycuronan (SXRGlu) molecules, respectively). The colorful waves in the magnification represent electrocompacted collagen attached to SXRGlu (green).

To enhance the mechanical property and stability of the collagen scaffolds, the ECL scaffold was crosslinked using 20 mM EDC and 20 mM NHS in 50 mM 2-(*N*-morpholino) ethanesulfonic acid (MES) buffer for 4 h at room temperature [13]. The crosslinked ECL scaffold (ECLC) was washed thoroughly with PBS to remove unreacted chemicals in the crosslinking solution.

Traditionally fabricated collagen gels were prepared as controls by mixing the dialyzed collagen solution (8 parts) with 10 × PBS (1 part) and adjusting the pH to 7.0–7.5 using 0.1 N NaOH (1 part). The mixture was then cast into molds and allowed to gel at 37 °C for 24 h followed by crosslinking using 20 mM EDC and 20 mM NHS in 50 mM MES buffer. Strips or circle membranes were then cut from these gels and processed as mentioned above for subsequent tests. An equal amount of collagen was used for fabrication of both compacted and uncompacted scaffolds.

### 3.2.2 SXRGlu Conjugation to ECL Matrices

To mimic the more complex scaffold structure of skin matrices and investigate the functions of SXRGlu in wound healing applications, an SXRGlu rich extract, obtained from the cell wall of a DNA barcoded green macroalgae (PhycoTrix™, Venus Shell Systems, Bomaderry, Australia), was crosslinked to the ECL scaffold by soaking the freeze-dried ECL matrices in 1% SXRGlu, 20 mM EDC and 20 mM NHS in 50 mM MES buffer for 4 h at room temperature. After that, the SXRGlu conjugated-ECL (ECLCU) was rinsed thoroughly with PBS, freeze dried and stored at 4 °C for further application.

To quantify the amount of SXRGlu in the ECLCU scaffold, the ECLCU scaffold were dissolved in 1 N HCl and incubated at 37 °C for 72 h. The dimethylmethylene blue (DMMB) assay [14] was used to quantify the amount of SXRGlu in the solution which indicated the SXRGlu amount that was crosslinked to ECLCU. To visualize the distribution of SXRGlu through the ECLCU, fluorescent labeling and confocal inspection were conducted. Fluoresceinamine labeled SXRGlu (Fluo-SXRGlu) was prepared by mixing 25 mM EDC, 25 mM sulfo-NHS, 1.25 mM fluoresceinamine (Sigma-Aldrich, Castle Hill, Australia) and 5% (*w*/*v*) SXRGlu into 0.1 M MES buffer (pH 6.0) and incubating under gentle stirring at room temperature for 24 h. Extra dyes were removed by dialyzing against distilled water for 7 days. Then the Fluo-SXRGlu was crosslinked to the ECL using the same procedures mentioned above.

### 3.2.3 SEM Inspection of the Electrocompacted Collagen Matrices

Scanning electron microscopy (SEM, JSM-7500FA Field Emission Scanning Electron Microscope) inspections were conducted on GEL, ECL, ECLC, and ECLCU to investigate the effect of electrocompaction process on the microstructure of collagen. Samples used for SEM imaging were hexamethyldisilane (HMDS, Sigma-Aldrich, Castle Hill, Australia)

dehydrated. The fixing and dehydration process are as following [15]: freshly compacted collagen sample were immersed in PBS for 10 min then transferred to a fixing solution (2.5% glutaraldehyde in 0.2 M PBS, pH 7.0) for 0.5 h followed by washing with distilled water for 10 min. Samples were then immersed in graded ethanol series (50%, 75%, 90%, and 100%) for 10 min at each concentration for dehydration and then in HMDS solution for 30 min and air dried in a fume hood at room temperature. Finally, samples were mounted on the SEM samples stub and coated with platinum (20 nm) using an Edwards sputter coater and then observed using SEM.

### 3.2.4 Mechanical Property

Tensile mechanical properties of the traditional collagen GEL, ECLC, and ECLCU were tested using a Shimadzu EZ-L universal mechanical tester at wet state with a 10 N load cell at a crosshead speed of 10 $mm \cdot min^{-1}$. Before testing, samples were washed with deionized water, dehydrated using a series of ethanol washes, and air dried. The two ends of the dried bundles were glued onto transparency sheets using a UV curable glue (Dymax 425, Dymax Corporation, Torrington, CT, USA) and rehydrated with PBS [10]. The Young's modulus was calculated by a linear regression fit of the strain-stress curve between the end of the toe region and the midpoint of the linear elastic region. For each reported value, three different samples were tested, and the results were averaged.

### 3.2.5 Swelling Ratio

To evaluate the effect of electrocompaction and SXRGlu incorporation on the water uptake behavior of collagen matrices, samples of $0.5 \times 0.5$ $cm^2$ were weighed in the dry state and were recorded as ($W_d$). Following this, samples were soaked in PBS for 24 h for complete hydration and then the wet weight ($W_w$) was recorded after removing excess water on

sample surface using Kimwipe. The swelling ratio of collagen matrices was calculated using equation 3.1 [13]:

$$\text{Swelling ratio}\% = \left(\frac{W_w - W_d}{W_d}\right) \times 100 \qquad (3.1)$$

### 3.2.6 Degradability

The stability of electrocompacted collagen scaffolds was determined by assessing the resistance of the matrices to collagenase treatment. Collagen scaffolds were freeze-dried and the initial weight of the matrices prior to collagenase treatment was recorded ($W_0$). Following this, collagen scaffolds were immersed in the digest solution which contained 100 μg/mL (28 units) collagenase (type I, Sigma-Aldrich, Castle Hill, Australia) in PBS (pH 7.4) and incubated in water bath at 37 °C for desired time points. The digest solution was replaced every 2 h. At t = 2 and 4 h, scaffolds were removed from the digest solution and freeze-dried. Then the residual mass at each time point was calculated.

### 3.2.7 Human Dermal Fibroblast Cell Viability, Proliferation, and Morphology on Electrocompacted Collagen Matrices

Human dermal fibroblast (HDFs, Cell Applications, Inc., San Diego, CA, USA) cells at passage 8 were seeded onto the fabricated collagen scaffolds to assess the influence of electrocompaction and incorporation of SXRGlu on cell proliferation and morphology. The HDFs were cultured in Dulbecco's Modified Eagle's medium (DMEM) with 10% (*v*/*v*) fetal bovine serum, 100 U/mL penicillin, and 100 μg/mL streptomycin under 5% $CO_2$ at 37 °C. Before cell seeding, scaffolds in 24 well plate were sterilized firstly by UV irradiation for 1 h, immersion in 70% ethanol for 3 h and washing for five times with PBS for 12 h. To saturate the scaffold with cell culture medium and facilitate cell attachment onto the

collagen matrices, the sterilized scaffolds were incubated in 1 mL of culture medium at 37 °C overnight before cell seeding.

The HDFs were then seeded at the density of $1.0 \times 10^4$ cells/cm$^2$ on the pre-processed scaffolds. Cell proliferation studies over 7 days were performed using the PrestoBlue™ (Life Technologies, Mulgrave, Australia) assay according to the manufacturer's instruction. Briefly, on day 1, 3, 5, and 7, three HDFs-scaffold constructs were incubated with PrestoBlue™ mix for 1 h at 37 °C. Following this, for each sample, 100 µL aliquots of supernatant were pipetted into a 96-well plate in triplicate and measured using a microplate reader (POLAR star Omega, BMG Labtech, Offenburg, Germany).

Live/dead assays were performed to inspect the HDFs cell viability on the scaffolds. Briefly, at each time point, HDFs-scaffold complexes were incubated with Calcein AM (5 µg/mL, Life Technologies, Mulgrave, Australia) at 37 °C for 10 min. Then, after a media change, propidium iodides (PI, 5 µg/mL, Life Technologies, Mulgrave, Australia) were added into the HDF-scaffold complexes and incubated for 5 min followed by a further media change. Images were acquired using a confocal microscope (Leica TSC SP5 II, Buffalo Grove, IL, USA) and the 3D projection tools in the Leica application suite X (LAS X) software (Leica, Buffalo Grove, IL, USA) were used for depth coding.

Alexa Fluor 488-Phalloidin cell cytoskeleton staining (ThermoFisher Scientific, Waltham, MA, USA) were conducted to assess the cell morphology. To do this, collagen scaffolds with cells at day 7 were washed in PBS and fixed in 3.7% paraformaldehyde in PBS for 10 min at room temperature. Then, samples were washed with PBS and permeabilized with 0.1% Triton-X 100 in PBS at room temperature for 5 min. Samples were subsequently stained with Alexa Flour 488-Phalloidin (1:40 in PBS) at room temperature for 1 h, rinsed with PBS, and then incubated with 10 $\mu g \cdot mL^{-1}$ 4′,6-diamidino-2-phenylindole (DAPI,

ThermoFisher Scientific, Waltham, MA, USA) for 10 min at RT to visualize the nuclei. Finally, samples were washed and imaged using a confocal microscope (Leica TSC SP5 II, Buffalo Grove, IL, USA).

## 3.3 Results and Discussion

### 3.3.1 Collagen electrocompaction

After applying electrical field to the collagen solution, collagen densification was noticed. As shown in figure 3.2, the thickness of the electrocompacted collagen was significantly decreased. This is due to the densification of collagen fibers during the electrocompaction process.

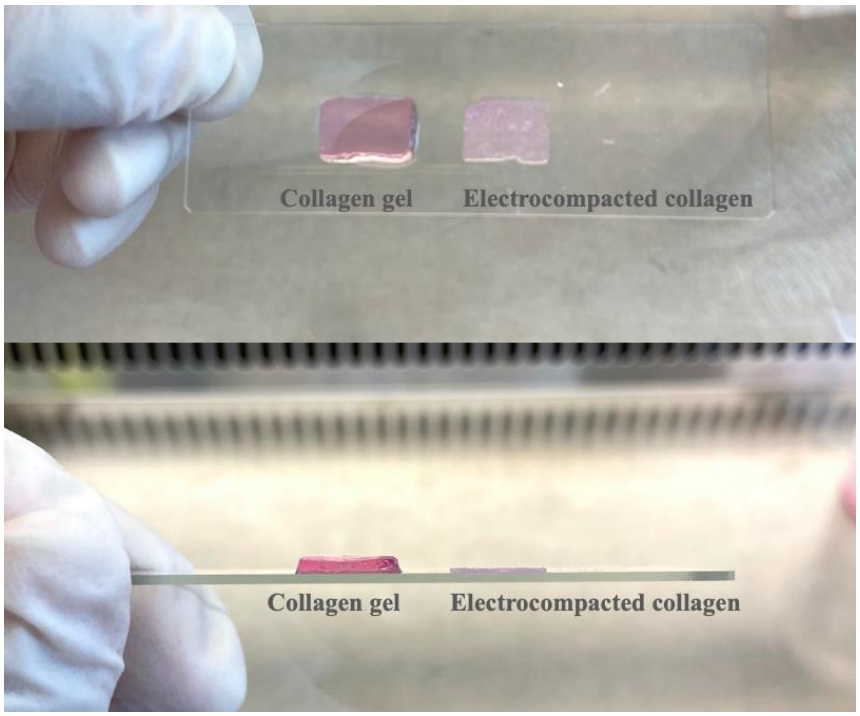


**Figure 3.2.** Thickness change of collagen before and after electrocompaction.

As an ampholytic molecule, during the electrocompaction process, the net charge of collagen molecules near the anode becomes positive, and those near cathodes become

negative [10]. Upon application of the external electric field, charged collagen molecules migrate until having no net charges, which is the isoelectric point. This results in the alignment and densification of collagen molecules along the pI plane. The method of electrocompaction, or isoelectric focusing, has long been used for separation of ampholytic proteins in areas such as biotechnology and chromatography [16]. Until recently, researchers started to explore it for making biomimetic materials.

### 3.3.2 SEM Inspection

SEM images of the electrocompacted collagen (Figure 3.3.A–D) showed uniformly oriented collagen bundle which demonstrated successful electrocompaction, whereas collagen gel without electrocompaction (Figure 3E) showed randomly aligned fibers with loosely packed pattern. Further, as can be seen in Figure 3D the D-banding pattern of collagen fibers are preserved after electrocompaction, which confirmed that the electrocompaction process was not detrimental to the native microstructure of collagen molecules [10]. Besides, after EDC/NHS crosslinking (Figure 3F) and SXRGlu incorporation (Figure 2G), the highly ordered pattern of collagen fibers in ECL was retained. These results are consistent with previously reported works [13] and demonstrated that densely packed and highly ordered collagen matrices were successfully fabricated using the electrocompaction method.

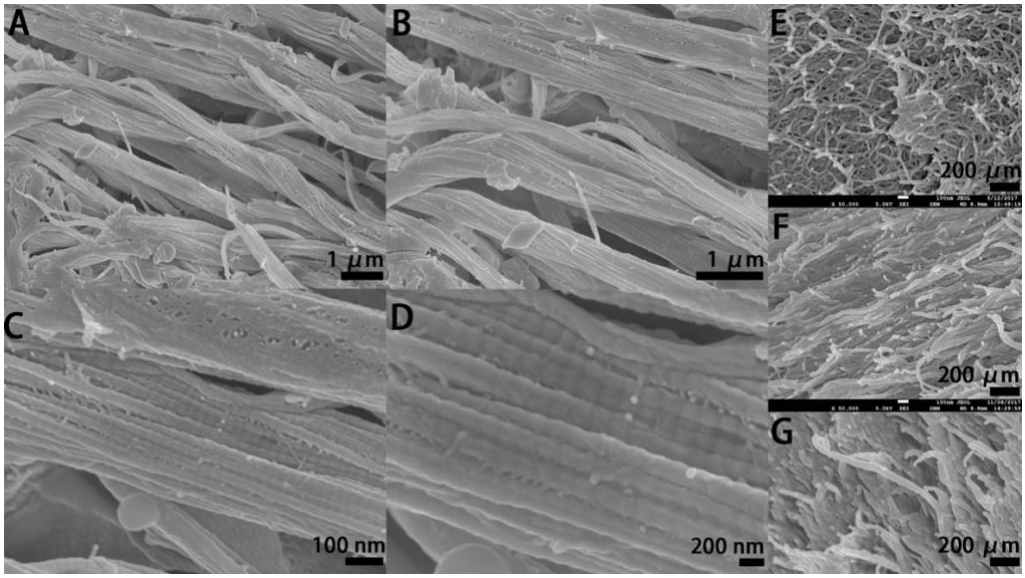


**Figure 3.3.** Representative SEM micrographs of the electrocompacted collagen matrices (ECL) before crosslinking at various magnifications (A–D), and crosslinked traditional collagen gel ((E), GEL), crosslinked ECL ((F), ECLC), crosslinked ECL incorporated with SXRGlu ((G), ECLCU).

Sherman et al. [17] reported the microscopic morphology of collagen fibers in rabbit skin, which showed a well-organized, stacked, and wavy structure of collagen fibers. Besides, rabbit skin exhibited highly orientated order and densely packed pattern of collagen fibrils within each collagen fiber as well as the D-banding pattern in collagen fibrils. Similar orientation, stacking, alignment, and D-banding pattern were observed in our electrocompacted collagen matrices. Thus, the electrocompacted collagen matrices can preliminarily mimic the microstructure of collagen fibers in natural skin. Compared with other popular fabrication methods such as 3D printing [18], electrospinning [19], gas-forming [20], phase separation [21], freeze-drying [22], collagen electrocompaction poses advantages. The whole electrocompaction process takes only 15 min and is comparatively rapid. In addition, this process is simple and highly cost-effective, especially compared with those requiring expensive specialized instruments, such as 3D printing. Furthermore, the whole process is

organic solvent free while in many other methods, such as electrospinning, use of toxic solvents is indispensable.

### 3.3.3 SXRGlu Content Quantification

To mimic the typical scaffold structure of natural skin, SXRGlu was conjugated to the ECL matrices. After SXRGlu conjugation, the final content of SXRGlu confirmed by the calibration curve in the ECLCU was 2.1 ± 0.2%. Confocal images of electrocompacted collagen conjugated with Fluo-labelled SXRGlu (Figure 3.4) confirmed uniform distribution of SXRGlu throughout the plane and depth of collagen. This structure preliminarily mimicked the components of the extracellular matrix in natural skin.

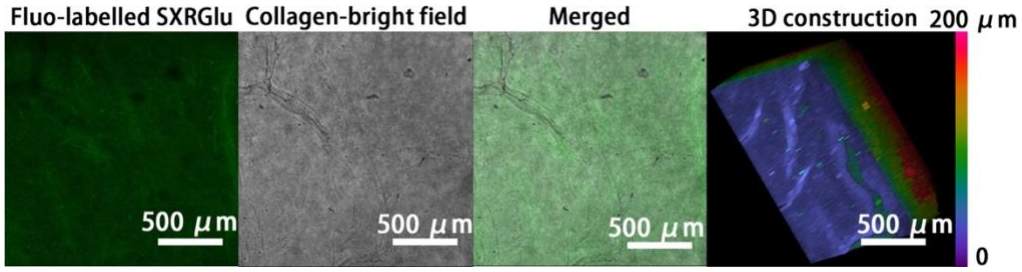


**Figure 3.4.** Confocal images of Fluo-labeled SXRGlu through the ECLCU scaffold, and 3D reconstruction with the pseudo-color scale indicating depth coding of Fluo-labelled SXRGlu along the Z-axis (0–200 μm) (scale bar applied to all figures).

However, with the current EDC/NHS crosslinking method, the amount of SXRGlu that can be introduced into the ECLC scaffold is limited, well below the composition of polysaccharides in native skin, among which collagen and polysaccharides account for 75% and 20% dry weight respectively. An alternative approach to improve SXRGlu loading is to develop SXRGlu derivatives that can carry both positive charge and negative charge, sharing the same isoelectric point with collagen [23]. In this way, SXRGlu and

collagen can be co-electrocompacted at any ratio. Future work will be focused on polysaccharides modification, such as amination, and co-electrocompaction of polysaccharides and collagen to better mimic the ECM structure of natural skin.

### 3.3.4 Mechanical Property

The Young's modulus (Figure 3.5A), ultimate tensile stress (Figure 3.5B), ultimate tensile strain (Figure 3.5C) and strain-stress curves (Figure 3.5D) of the GEL, ECLC and ECLCU were obtained using tensile tests. The Young's modulus of the ECLCU and ECLC was about 0.29 and 0.25 MPa respectively, which was significantly higher than that of collagen gel (0.13 MPa). The ECLCU had a 2-fold greater Young's modulus and 2-fold greater ultimate tensile stress than the traditional collagen gel. In normal skin, the Young's modulus measured from different skin sites is between 0.05 and 0.2 MPa [24]. Thus, the mechanical properties of the ECLC and ECLCU match natural skin very well.

Yet, electrocompaction and crosslinking significantly decreased the extensibility of collagen matrices as shown by the ultimate tensile strain results. This might be due to the crosslinking and SXRGlu incorporation procedure reducing the mobility of collagen chains within the matrices, thus leading to a more rigid molecular structure which finally resulted in weaker elasticity [25]. This could be further improved by the incorporation of elastin component in the collagen scaffold. In skin tissues, fiber forming structural molecules, which include collagen, fibrin, fibronectin, elastin, and fibrillin [26], define the rigidity and elasticity of skin tissue. Typically, the extracellular matrix of dermal skin comprises 70–80% collagen and 3–6% elastin [27]. Elastin fibers are accountable for the recoiling mechanism after deformation or stress [28]. Apart from its mechanical attribute, elastin-derived peptides have also shown to promote cell adhesion and proliferation [16], chemotacticity [29], and enhance protein kinase C activation ability [30] during the wound healing process. In

subsequent studies, elastin will also be incorporated into the ECL system to increase the scaffold elasticity, thus better mimicking the mechanical property of natural skin ECM.

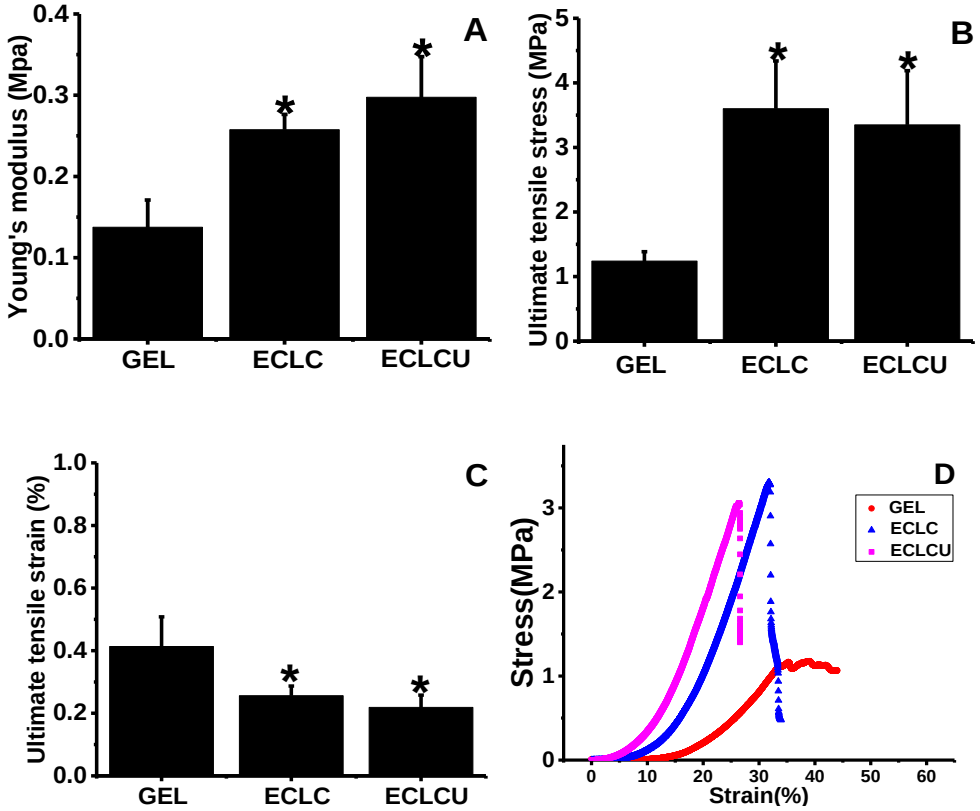


**Figure 3.5.** Tensile properties of GEL, ECLC and ECLCU. (A) Tensile modulus; (B) Ultimate tensile stress; (C) Ultimate tensile strain; (D) Stress-strain curve (* indicates significant difference compared with GEL at $p < 0.05$).

### 3.3.5 Swelling Ratio

The swelling ratio of GEL, ECLC, and ECLCU was compared to evaluate the influence of the electrocompaction process and SXRGlu incorporation on the water uptake behavior of scaffolds. As shown in Figure 3.6, the swelling ratio of GEL was around 1040%, while the electrocompacted collagen matrices (ECLC, ECLCU) exhibited reduced water uptake ability. This could be ascribed to their electrocompacted, densified structure of collagen

fibers, which hindered the penetration of water molecules into the matrices. The incorporation of SXRGlu into the ECLCU matrices counteracted the effect of electrocompaction to a degree and increased the water uptake ability, which could be attributed to the hydrophilic nature of SXRGlu that is abundant in carboxyl, hydroxyl, and sulfate groups.

Apart from fiber-forming structural molecules, components in skin ECM can be divided into "matricellular proteins", and "nonfiber-forming structural molecules" [31]. Matricellular proteins, such as thrombospondin-1 (TSP1), osteonectin, and osteopontin, mainly act as signaling molecules during wound healing stage and do not participate in the structural construction of ECM [32]. Non-fiber forming structural molecules are mainly glycosaminoglycans and proteoglycans such as hyaluronan, chondroitin sulfate, dermatan sulfate, decorin, lumican and versican [33]. They can fill in the gaps of interstitial space and function in buffering, hydration and force dispersion because of their negatively charged and hydrophilic nature. During the wound healing process, the maintenance of moisture near the wound site is a critical aspect of wound management, with demonstrated benefits, including accelerated angiogenesis, pain relief, prevention of tissue dehydration and cell death. Besides, if a scaffold is capable of swelling, it will be able to absorb bioactive molecules from neighboring tissue and thus promotes cell growth and function [34]. Therefore, incorporation of SXRGlu or other kinds of glycosaminoglycans (GAGs) into the collagen matrices can not only increase the water uptake ability but also better mimic the more structured scaffold environment of natural tissue, and as is required for prime cell behavior and functions.

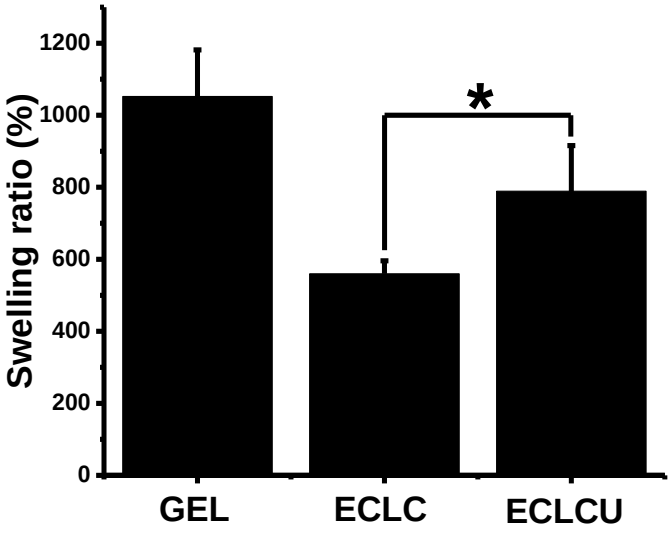


**Figure 3.6.** The swelling ratio of GEL, ECLC, and ECLCU (* indicates significant difference at $p < 0.05$).

### 3.3.6 Degradability

Collagenase treatment to the collagen scaffolds was conducted to evaluate the influence of electrocompaction and SXRGlu inclusion on matrix stability. As shown in Figure 3.7, after 4 h, the residual mass was only 6% for GEL and 17% for ECLC, whereas the SXRGlu incorporated ECLCU remained highest at 36%. These data demonstrated that both the electrocompaction and incorporation of SXRGlu contributed to the improved resistance to collagenase mediated degradation. SXRGlu belongs to a group of algal cell wall extracts that are known for resistance to degradation from human endogenous enzymes [12]. Thus, the incorporation of SXRGlu into the ECL matrices may improve the stability of the collagen matrices in human physiologically relevant conditions.

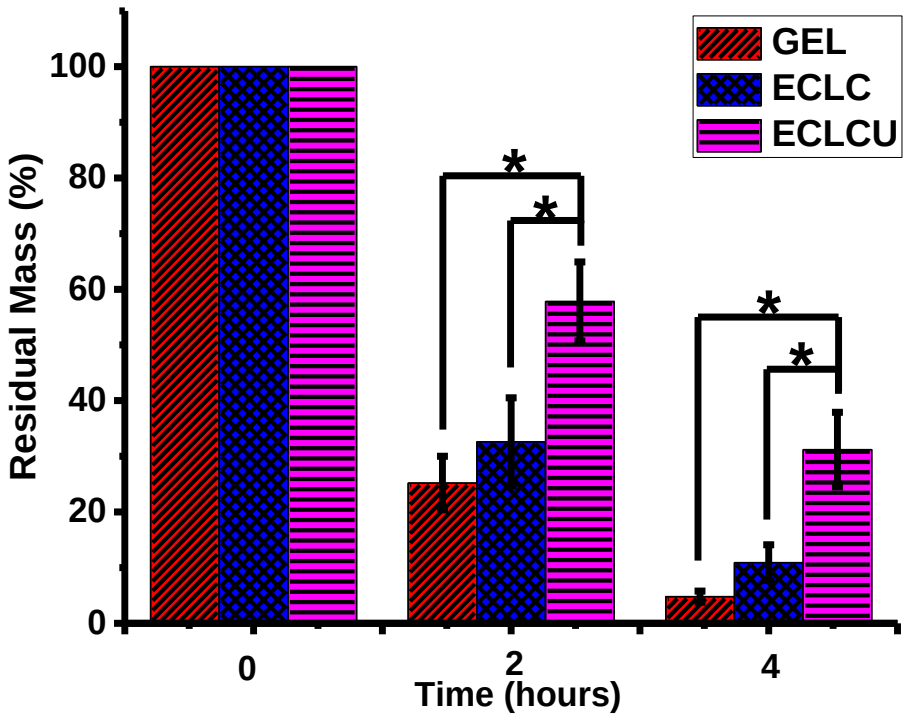


**Figure 3.7.** In vitro degradation of GEL, ECLC, and ECLCU matrices against collagenase (* indicates a significant difference at $p < 0.05$).

### 3.3.7 Human Dermal Fibroblast Cell Viability, Proliferation and Morphology on Electrocompacted Collagen Matrices

Cell studies were conducted to evaluate the viability, proliferation, and cell morphology of HDFs cells cultured on the fabricated collagen matrices. The proliferation of HDFs on collagen scaffolds was assessed using the PrestoBlue assay (Figure 3.8A). Quantitative measurement of cell viability marker PrestoBlue suggested that cell numbers on ECLCU and ECLC were higher than that on GEL on day 5 and day 7, which confirmed that the electrocompacted collagen matrices could promote the proliferation of fibroblasts. This is probably because the electrocompaction process increased the mechanical property of the matrix and this is in accordance with reports that fibroblasts responds to improved matrix stiffness by enhanced proliferation, collagen secretion, and smooth muscle α-actin (αSMA)

stress fibers expression [35]. Especially, the proliferation of fibroblast was reported to be highly dependent on the stiffness of the matrices, and rigid ECM tend to induce the differentiation of fibroblast into contractile myofibroblast [35]. Over the 7-day culture, there is no significant difference in cell numbers between ECLC and ECLCU, which showed that the incorporation of SXRGlu did not inhibit the proliferation of HDFs. Live-dead assay in Figure 3.8B showed that nearly all cells were stained green with very few red cells implying that the HDFs cell viability was maintained on the electrocompacted collagen matrices. Compared to GEL, electrocompacted matrices showed enhanced cell proliferation at day 7, which is consistent with the viability test using PrestoBlue.

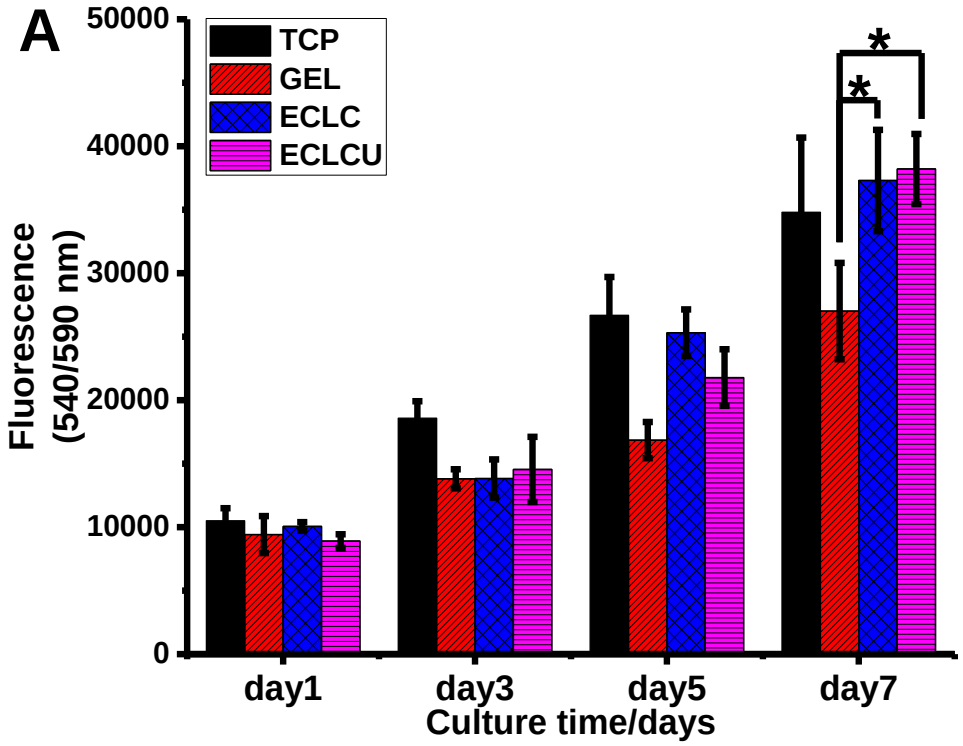

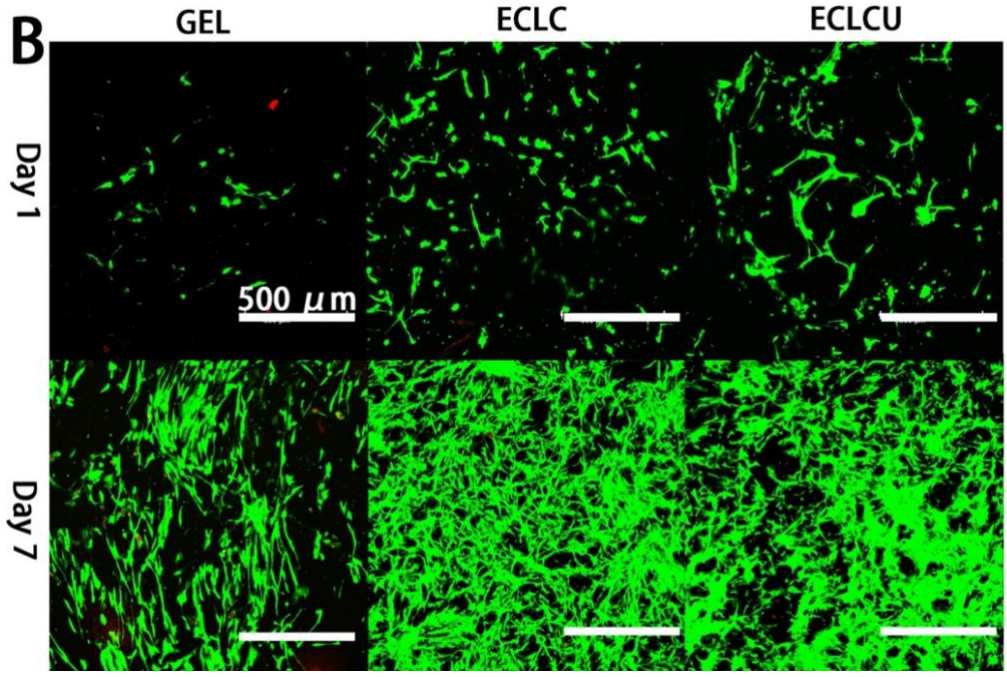


**Figure 3.8.** Survival and proliferation of human dermal fibroblasts (HDFs) on collagen matrix. (A) Proliferation (PrestoBlue™ cell viability indicator) of HDFs on tissue culture plate (TCP), GEL, ECLC and ECLCU matrices (* indicates statistical significance at $p < 0.05$ compared with cell numbers on GEL); (B) Live (stained by Calcein AM in green) and dead (stained by propidium iodide in red) HDFs at day 1 and day 7 (scale bar applied to all figures).

The morphology of HDFs on different matrices and the arrangement of the actin cytoskeleton were visualized by SEM inspection and fluorescent staining of cytoskeletal F-actin filaments after 7 days' cell culture (Figure 3.9). F-actin morphology illustrated a well-visible F-actin filament network on all these matrices suggesting HDFs attach and spread well on the GEL, ECLC, and ECLCU matrices. Mean HDFs cell surface area calculated by Image J on GEL, ECLC, and ECLCU are (960 ± 447), (1400 ± 278) and (2041 ± 214) $\mu m^2$/cell ($n$ = 100) respectively. HDFs on ECLCU resulted in most significantly increased F-actin area, indicative of most enlarged and spread out morphology

of the HDFs. This might because the abundant rhamnose groups in SXRGlu could trigger skin fibroblast recognition and attachment to the ECLCU through the mediation of a unique rhamnose recognizing lectin-site on fibroblasts as receptor [36]. Besides, as shown on the SEM images of overall morphology of cell-material complexes on Figure 8, after supporting the HDFs for 7 days, the GEL matrices maintained the original flat shape while ECLC and ECLCU have shown more pores formed and the ECLCU seemed to exhibit better stability than ECLC. This might be due to cell numbers on the ECLC and ECLCU being significantly higher than on gel at day 5 and day 7 which might result in increased amount secretion of collagenase thus more severe degradation of the scaffold. As cell numbers on ECLC and ECLCU are similar, the less severe extent of degradation on the ECLCU compared with ECLC might be ascribed to the incorporation of SXRGlu. This is in accordance with our previous results that SXRGlu could improve the stability of the collagen matrices against collagenase degradation.

Together, these results demonstrated firstly that electrocompaction of collagen improved the mechanical property of the collagen matrices and promoted HDFs proliferation; secondly, the incorporation of SXRGlu facilitated HDFs spreading and enlargement on the electrocompacted collagen matrices; also, the incorporation of SXRGlu increased the stability of the matrices against collagenase degradation.

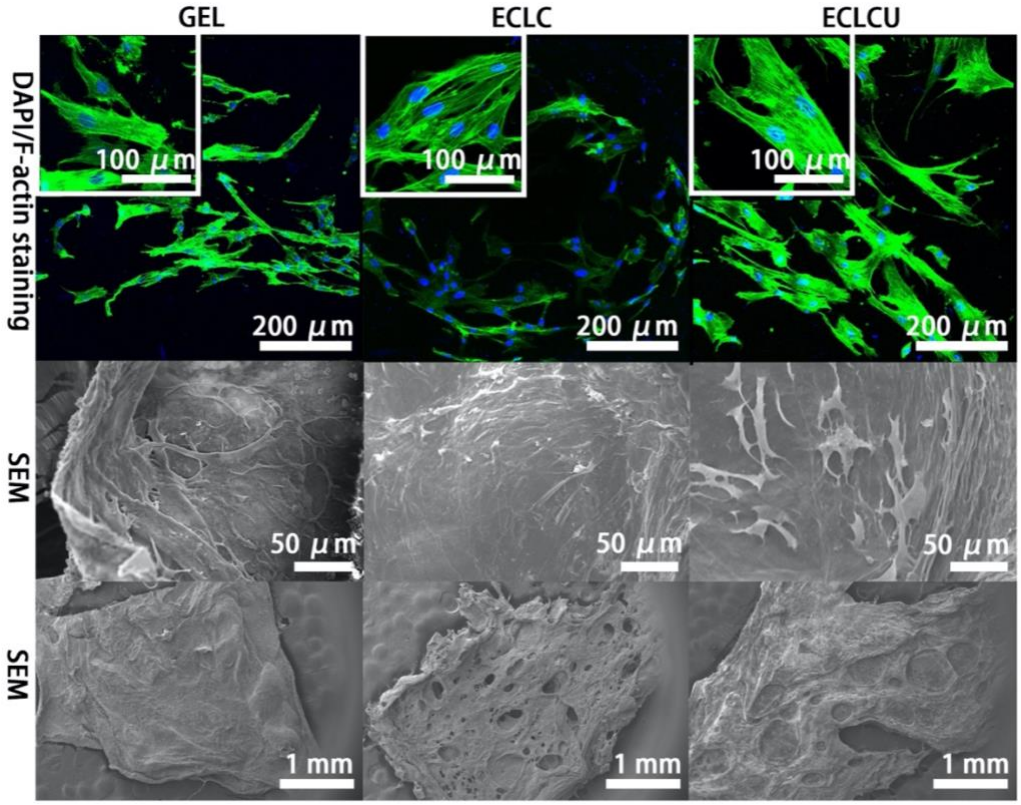


**Figure 3.9.** Representative F-actin filament staining with Alex-488 Phalloidin (staining F-actin in green)/DAPI (staining cell nucleus in blue) staining; SEM images of HDFs cultured on fabricated scaffold for 7 days; overall morphology of cell-material complexes after 7 days' cell culture.

## 3.4 Conclusions

Herein we presented the fabrication and in vitro characterization of a biomimicking skin scaffold using collagen and SXRGlu. Electrocompacted collagen matrices were successfully fabricated. SEM inspection confirmed the presence of highly ordered, densely packed collagen fibers, mimicking the alignment and structure of collagen fibers in natural skin tissue more closely than the non-compacted matrix. Moreover, electrocompacted collagen matrices exhibited increased tensile strength and the mechanical properties of ECLC and ECLCU are comparable to that of natural skin. Incorporation of SXRGlu

significantly improved the water uptake ability and stability of the electrocompacted collagen matrices. Cell proliferation studies showed the electrocompacted collagen matrices promoted the proliferation of HDFs, and SXRGlu facilitated HDFs spreading. Together, these results implied the potential of this SXRGlu incorporated electrocompacted collagen film as a skin scaffold substitute.

In chapter 4 and 5, two more critical components of natural skin ECM, hyaluronic acid and elastin, were incoporated into the electrocompacted-collagen system to fully mimic the components and structure of natural skin ECM. Co-culture of keratinocytes and fibroblasts were performed to do a reconstruction of a full-thickness skin model.

## 3.5 References


1. R.F. Pereira, C.C. Barrias, P.L. Granja, P.J. Bartolo, Advanced biofabrication strategies for skin regeneration and repair, Nanomedicine 2013, 8, 603-21.

2. A.D. Metcalfe, M.W. Ferguson, Tissue engineering of replacement skin: the crossroads of biomaterials, wound healing, embryonic development, stem cells and regeneration, Journal of the Royal Society Interface 2007, 4, 413.

3. W.L. Ng, W.Y. Yeong, M.W. Naing, Cellular approaches to tissue-engineering of skin: A review, Journal of Tissue Science & Engineering 2015, 6, 1.

4. W.L. Ng, S. Wang, W.Y. Yeong, M.W. Naing, Skin bioprinting: impending reality or fantasy?, Trends Biotechnol 2016, 34, 689-699.

5. S.G. Priya, H. Jungvid, A. Kumar, Skin tissue engineering for tissue repair and regeneration, Tissue Engineering Part B: Reviews 2008, 14, 105-118.

6. A.A. Chaudhari, K. Vig, D.R. Baganizi, R. Sahu, S. Dixit, V. Dennis, S.R. Singh, S.R. Pillai, Future prospects for scaffolding methods and biomaterials in skin tissue engineering: a review, International journal of molecular sciences 2016, 17, 1974.

7. L.E. Tracy, R.A. Minasian, E. Caterson, Extracellular matrix and dermal fibroblast function in the healing wound, Adv Wound Care 2016, 5, 119-136.

8. V. Kahan, M. Andersen, J. Tomimori, S. Tufik, Stress, immunity and skin collagen integrity: evidence from animal models and clinical conditions, Brain Behav Immun 2009, 23, 1089-1095.

9. A.M. Wojtowicz, A. Shekaran, M.E. Oest, K.M. Dupont, K.L. Templeman, D.W. Hutmacher, R.E. Guldberg, A.J. García, Coating of biomaterial scaffolds with the collagen-mimetic peptide GFOGER for bone defect repair, Biomaterials 2010, 31, 2574-2582.

10. X. Cheng, U.A. Gurkan, C.J. Dehen, M.P. Tate, H.W. Hillhouse, G.J. Simpson, O. Akkus, An electrochemical fabrication process for the assembly of anisotropically oriented collagen bundles, Biomaterials 2008, 29, 3278-3288.

11. M.F. de Jesus Raposo, A.M.B. De Morais, R.M.S.C. De Morais, Marine polysaccharides from algae with potential biomedical applications, Marine drugs 2015, 13, 2967-3028.

12. F. Chiellini, A. Morelli, Ulvan: a versatile platform of biomaterials from renewable resources, Biomaterials-Physics and Chemistry, InTech2011.

13. V. Kishore, R. Iyer, A. Frandsen, T.-U. Nguyen, In vitro characterization of electrochemically compacted collagen matrices for corneal applications, Biomedical Materials 2016, 11, 055008.

14. M. Younesi, B.O. Donmez, A. Islam, O. Akkus, Heparinized collagen sutures for sustained delivery of PDGF-BB: Delivery profile and effects on tendon-derived cells In-Vitro, Acta biomaterialia 2016, 41, 100-109.

15. J.T.Y. Lee, K.L. Chow, SEM sample preparation for cells on 3D scaffolds by freeze-drying and HMDS, Scanning 2012, 34, 12-25.

16. D. Garfin, S. Ahuja, Handbook of isoelectric focusing and proteomics, Elsevier2005.

17. V.R. Sherman, Y. Tang, S. Zhao, W. Yang, M.A. Meyers, Structural characterization and viscoelastic constitutive modeling of skin, Acta biomaterialia 2017, 53, 460-469 %@ 1742-7061.

18. Q.L. Loh, C. Choong, Three-dimensional scaffolds for tissue engineering applications: role of porosity and pore size, Tissue Engineering Part B: Reviews 2013, 19, 485-502.

19. F.E. Ahmed, B.S. Lalia, R. Hashaikeh, A review on electrospinning for membrane fabrication: challenges and applications, Desalination 2015, 356, 15-30.

20. A.G. Mikos, J.S. Temenoff, Formation of highly porous biodegradable scaffolds for tissue engineering, Electronic Journal of Biotechnology 2000, 3, 23-24 %@ 0717-3458.

21. C. Schugens, V. Maquet, C. Grandfils, R. Jérôme, P. Teyssie, Polylactide macroporous biodegradable implants for cell transplantation. II. Preparation of polylactide foams by liquid-liquid phase separation, Journal of Biomedical Materials Research Part A 1996, 30, 449-461.

22. F.J. O'Brien, B.A. Harley, I.V. Yannas, L. Gibson, Influence of freezing rate on pore structure in freeze-dried collagen-GAG scaffolds, Biomaterials 2004, 25, 1077-1086 %@ 0142-9612.

23. E. Cudjoe, M. Younesi, E. Cudjoe, O. Akkus, S.J. Rowan, Synthesis and Fabrication of Nanocomposite Fibers of Collagen-Cellulose Nanocrystals by Coelectrocompaction, Biomacromolecules 2017, 18, 1259-1267 %@ 1525-7797.

24. X. Liang, S.A. Boppart, Biomechanical properties of in vivo human skin from dynamic optical coherence elastography, IEEE Trans Biomed Eng 2010, 57, 953-959.

25. S. Benavides, R. Villalobos-Carvajal, J.E. Reyes, Physical, mechanical and antibacterial properties of alginate film: Effect of the crosslinking degree and oregano essential oil concentration, Journal of Food Engineering 2012, 110, 232-239 %@ 0260-8774.

26. C. Frantz, K.M. Stewart, V.M. Weaver, The extracellular matrix at a glance, J Cell Sci 2010, 123, 4195-4200.

27. G.D. Weinstein, R.J. Boucek, Collagen and elastin of human dermis, J Invest Dermatol 1960, 35, 227-229.

28. H. Oxlund, J. Manschot, A. Viidik, The role of elastin in the mechanical properties of skin, J Biomech 1988, 21, 213-218.

29. R.M. Senior, G.L. Griffin, R.P. Mecham, D.S. Wrenn, K.U. Prasad, D.W. Urry, Val-Gly-Val-Ala-Pro-Gly, a repeating peptide in elastin, is chemotactic for fibroblasts and monocytes, The Journal of cell biology 1984, 99, 870-874 %@ 0021-9525.

30. S. Tajima, H. Wachi, Y. Uemura, K. Okamoto, Modulation by elastin peptide VGVAPG of cell proliferation and elastin expression in human skin fibroblasts, Archives of dermatological research 1997, 289, 489-492.

31. H. Järveläinen, A. Sainio, M. Koulu, T.N. Wight, R. Penttinen, Extracellular matrix molecules: potential targets in pharmacotherapy, Pharmacol Rev 2009, 61, 198-223.

32. P. Bornstein, E.H. Sage, Matricellular proteins: extracellular modulators of cell function, Curr Opin Cell Biol 2002, 14, 608-616.

33. O. Okamoto, S. Fujiwara, Dermatopontin, a novel player in the biology of the extracellular matrix, Connect Tissue Res 2006, 47, 177-189.

34. R. Xu, H. Xia, W. He, Z. Li, J. Zhao, B. Liu, Y. Wang, Q. Lei, Y. Kong, Y. Bai, Controlled water vapor transmission rate promotes wound-healing via wound re-epithelialization and contraction enhancement, Sci Rep 2016, 6, 24596.

35. F. Liu, J.D. Mih, B.S. Shea, A.T. Kho, A.S. Sharif, A.M. Tager, D.J. Tschumperlin, Feedback amplification of fibrosis through matrix stiffening and COX-2 suppression, The Journal of cell biology 2010, 190, 693-706.

36. E. Andres, J. Molinari, G. Péterszegi, B. Mariko, E. Ruszova, V. Velebny, G. Faury, L. Robert, Pharmacological properties of rhamnose-rich polysaccharides, potential interest in age-dependent alterations of connectives tissues, Pathol Biol (Paris) 2006, 54, 420-425.

# Chapter 4

# Fabrication and physiochemical characterization of an ECM - like skin scaffold

**CONTENT**

## 4.1 Introduction

Skin is the largest organ of the body, protecting the internal organs from the external environment [1]. Advances in tissue engineering have made the production of artificial skin possible. Over the past several decades, remarkable efforts have been made in the development of artificial skin. A variety of approaches have been reported for engineering artificial skin [2] and 3D *in vitro* skin models [3]. ECM components, including collagen, glycan, and polysaccharides, have dominated the compositions of tissue-engineered skin grafts [4]. This is particularly in the case of collagen as it represents the major ECM component in native skin. However, the collagen-based skin scaffolds reported so far generally have a low mechanical strength, which results in fast degradation, severe contraction, and limited lifespan [5]. This could be addressed by several approaches, such as the inclusion of chemical crosslinkers, which might introduce additional cytotoxicity [6], incorporation of synthetic polymers which may reduce the compliance of the resulted grafts[7], or decrease the local pH and results in the inflammatory response [8].

A simple method named electrocompaction for fabrication of collagen matrix with improved mechanical properties was reported in 2008 [9]. During this process, collagen solution was loaded between two oppositely charged electrodes. Upon application of an electric field, an electrochemically induced pH gradient will be formed. Due to the amphoteric nature of the collagen molecules, collagen molecules will be aligned along the isoelectric point (pI) to form densely packed and highly oriented collagen threads or sheets. This method is a simple, economic and versatile process as it can be carried out with minimum equipment at physiological conditions. Besides, varied electrodes sizes and shapes can help to achieve controllable and diverse structures. As such, electrocompacted collagen sheets or threads were applied in variant areas such as tendon regeneration, corneal regeneration, cartilage repair [10], conduits for nerve guidance [11], skin grafts [12],

and orthopedic implants [13]. Also, different components can be incorporated for various applications [12]. For example, Nguyen [14] reported the work of incorporating elastin within alchemically aligned collagen fibers for vascular engineering where elastin incorporation was found to lower the modulus and increase the yield strain. In the work by Kishore et al. [15], decorin was incorporated into the electrocompacted collagen threads to increase the mechanical property for tendon regeneration. To increase the biostability and mechanical property of collagen matrix, Elvis Cudjoe et al. [16] co-electrocompacted carboxylic acid functionalized cellulose nanocrystals (CNCs) with collagen to fabricate aligned micron-sized CNC fibers for repair of load bearing tissues. Younesi et al. [17] reported the achievement of prolonged release of growth factors by incorporating heparin into the aligned collagen threads.

In our previous work [12], marine seaweed sourced polysaccharide (sulphated xylorhamnoglycuronan) was incorporated into the electrocompacted collagen as the first trail of electrocompacted matrix for wound healing application. To better mimic the extracellular matrix (ECM) of native skin, in this chapter, skin ECM components including collagen, elastin, and hyaluronic acid were fabricated together to recreate the compositional features of the native skin (working flow shown in Figure 4.1).

Collagen and elastin are naturally electrocompactable molecules as both of them carry positively charged groups (amino groups) and negatively charged groups (carboxylic acid groups). They also have similar isoelectric point (pI) point that enables them to be co-electrocompacted together [14]. Yet, HA molecules are highly negatively charged molecules and carries no positively charged groups. Thus naturally occurred HA are not electrocompactable unless modified, such as introducing positively charged amino groups into HA molecules. Cudjoe et. al. [16] reported a cellulose modification method to introduce amino groups into the cellulose molecules, making it electrocompactable. Here

in this chapter, to introduce HA molecules into the collagen/elastin sheets, two parallel procedures were tested (working flow shown in Figure 4.1). In the first procedure, HA was aminated following a similar method reported in [16], and then was tried to be co-electrocompacted together with collagen and elastin. In another procedure, collagen and elastin were co-electrocompacted firstly, unmodified HA was then crosslinked into the collagen/elastin sheets by EDC/NHS crosslinking. The second procedure was chosen for later applications due to relatively convenience and simple operating procedures. Physiochemical characterization of these scaffold, including: elastin distribution, hyaluronic acid amount quantification, mechanical property and swelling ratio, were conducted. By integrating the ECM cue, the ECM-like CEH scaffold may serve as a promising candidate for skin regeneration and wound healing application.

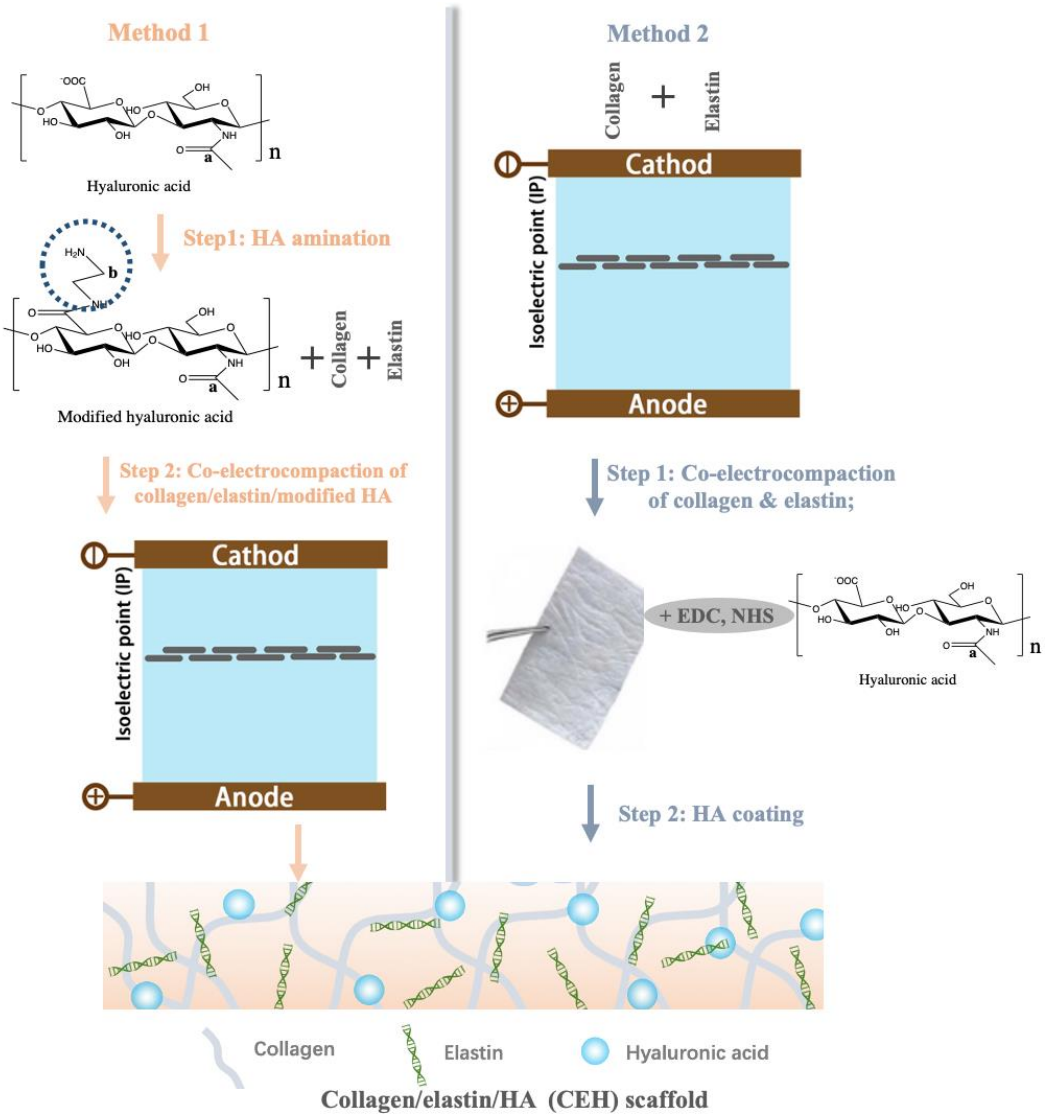


**Figure 4.1.** Working flow of the fabrication of collagen/elastin/HA scaffolds.

Apart from the fabrication and physiochemical characterization of the CEH scaffold, exploration of more versatile scaffolding system based on electrocompacted collagen were conducted. Especially, tubular electrical field was applied to collagen solution surrounding a graphene fiber to fabricate a collagen-coated graphene scaffolding system. Biocompatibility characterization of such a conductive fiber was conducted. A graphene sheet coated with collagen was also fabricated, and possible application of such a conductive soft polymer was analyzed.

## 4.2 Materials and methods

### 4.2.1 HA amination

HA-COOH-$NH_2$ was synthesized following a previously published protocol [16] with slight modification (Figure 4.2). Briefly, HA (0.6 mmol) was dispersed homogeneously in DI water (100 mL) using a sonicator, followed by the addition of EDC (6 mmol) and NHS (6 mmol). After fully dissolving, tert-butyl (2-aminoethyl) carbamate (6 mmol) was added to the solution and stirred at 50 ºC for 2 h. The resultants were precipitated using excess ethyl acetate, filtered and washed extensively with ethyl acetate and DI water. The resulted animated HA were dialyzed in HCL for 1 day to remove the Boc groups, followed by another 3 days dialysis in DI water for further purification. The solids were freeze-dried and kept in the freezer for later use.

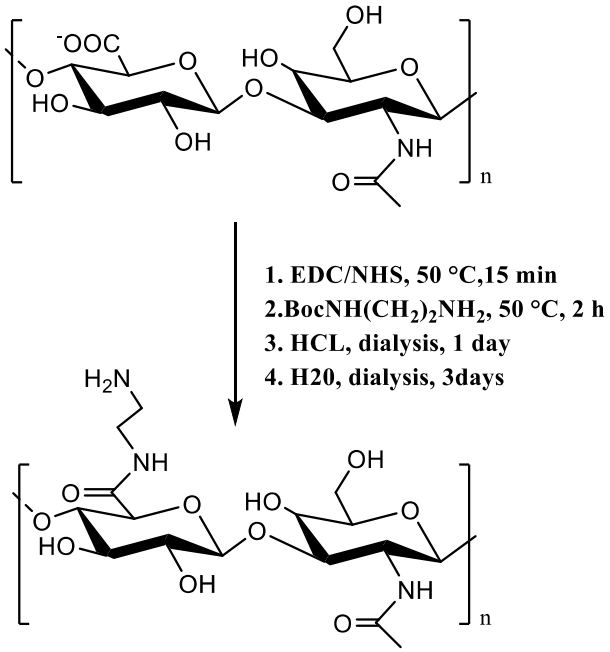


**Figure 4.2.** Schematic illustration of hyaluronic acid modification.

### 4.2.2 FTIR and NMR inspection of animated HA

Structural characterization of HA before and after animation were performed by FTIR and NMR. Prior to these analysis, samples were freeze-dried overnight. FTIR spectra were inspected in the range of 1800–700 $cm^{-1}$ at a resolution of 4 $cm^{-1}$ using an IRPrestige-21 spectrometer (Shimadzu, Japan). 1 H NMR spectroscopy of HA and animated HA were recorded in $D_2O$ at 60 °C using a Bruker Advance III 400 MHz spectrometer (Bruker, Germany). The 1 HNMR spectra between 5 to −2 ppm using a relaxation delay time of 1 s were recorded. Chemical shift values were recorded in parts per million (ppm).

### 4.2.3 Collagen electrocompaction and co-electrocompaction with elastin or aminated HA

The electrocompacted and crosslinked collagen (COL) were fabricated following previously published methods with slight modifications [12]. The working flow is shown in Figure 4.3. Briefly, type-I collagen powder (Kele Biotech Co., Chengdu, China) was dissolved in 0.1 M acetic acid at 6 mg/mL and dialyzed against ultrapure water at 4ºC for 12 h. The dialyzed collagen was then loaded into a rectangular rubber washer (length × width = 1.5 × 2.5 cm and thickness = 5 mm) sandwiched between two oppositely charged stainless steel electrodes. By applying of the electric field of 6 volts for 15 min, a pH gradient between the electrodes was generated. This gradient further resulted in the self-aggregation of collagen molecules at the isoelectric point (pI) to form a densely packed and highly ordered electrocompacted collagen (ECL) sheet [9].

Co-electrocompaction of aminated HA with collagen was performed following a similar protocol reported in [14] with the mixture of aminated HA into the collagen solution at the ratio of collagen : aminated HA = 7: 2. Co-electrocompacted collagen and elastin (CE) sheets were fabricated with the suspension of insoluble elastin particles into the collagen

solution at the ratio of collagen: elastin=7:1. Then the freshly compacted ECL or CE sheets were incubated in PBS at 37 ºC at RT for 4 h for fibril formation. To improve the stiffness of the fabricated matrices, the ECL and CE matrices were crosslinked using 20 mM 1-ethyl-3-(3-dimethylaminopropyl) carbodiimide (EDC, Thermo Fisher Scientific, USA) and 20 mM N-hydroxysuccinimide (NHS, Thermo Fisher Scientific, USA) in PBS at RT for 4 h. The crosslinked ECL and CE matrices were washed thoroughly with PBS and deionized water and freeze-dried.

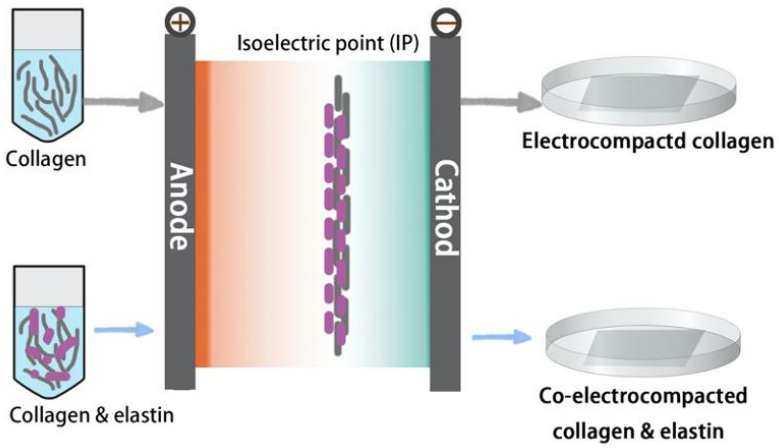


**Figure 4.3.** Working flow of collagen electrocompaction.

### 4.2.4 Confocal and FTIR inspection of elastin distribution

In order to visually confirm the presence and uniform distribution of insoluble elastin particles within the CE matrices, the fibers were imaged using a confocal laser scanning microscope (CLSM, Leica TCS SP5, Germany), as insoluble elastin particles tend to auto fluorescence under the DAPI filter [14]. FTIR inspection were performed on collagen, elastin, and dried co-electrocompacted collagen & elastin sheet following a similar protocol as described in chapter 4.2.2.

### 4.2.5 HA incorporation and quantification

To mimic the composition of natural skin matrices and investigate functions of hyaluronic acid in wound healing applications, hyaluronic acid (molecular weight= 0.9 MDa) was crosslinked to the CE matrices to produce the collagen/elastin/HA (CEH) scaffold. The procedure was shown in Figure 4.5. Briefly, the incorporation of HA was done by soaking the freeze-dried CE matrices in 1% HA, 20 mM EDC and 20 mM NHS in PBS for 4 h at room temperature. The HA conjugated-CE (CEH) was then washed thoroughly with DI water, freeze-dried, and preserved at 4 $^{o}$C for further application.

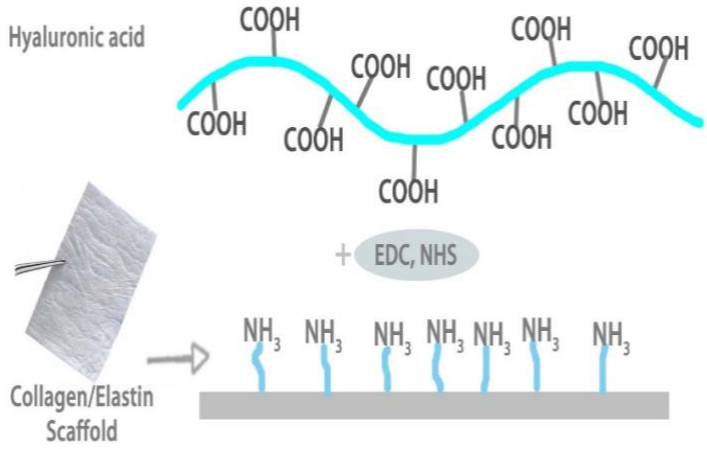


**Figure 4.4.** HA incorporation into the collagen/elastin (CE) scaffolds.

The amount of HA immobilized in a CEH matrix was quantified following a simplified cetyltrimethylammonium bromide (CTAB, Sigma-Aldrich, USA) turbidity assay (Figure 4.5) [4]. To do this, unreacted HA in the HA-CE coating system were assessed firstly, then the amount of HA immobilized in the final CEH matrix was calculated by subtracting the overall HA amount and unreacted HA amount. Briefly, standard solutions were prepared using hyaluronic acid (molecular weight 1,000,000 Da, Sigma-Aldrich, USA) ranging from 0.1 to 1 mg/ml. 50 uL of each hyaluronic acid standard solution was mixed with 50 uL of

0.2 M acetate buffer (0.2 M sodium acetate, 0.15 M sodium chloride, adjusting pH to 6 with acetic acid) in a 96 well plate. To synchronize the reaction temperature, the plate was incubated at 37 ºC for 5 min. Then 100 uL of CTAB in 2% sodium hydroxide was added carefully to the remained reaction solution. After vortexing, to prevent the disappearance of the insoluble compounds, the plate was read within 10 min with a plate reader at a wavelength of 600 nm.

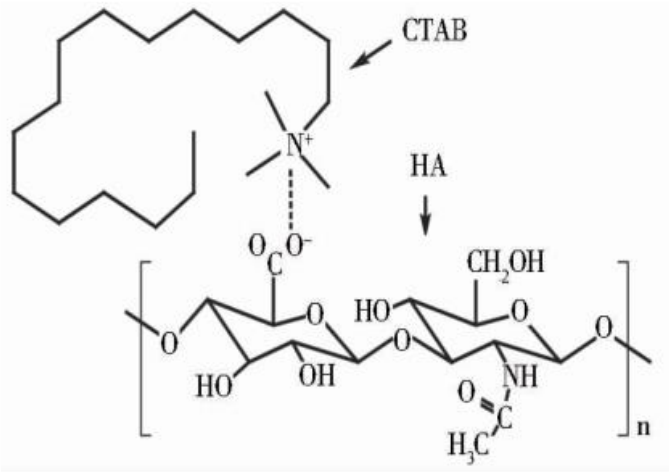


**Figure 4.5.** Mechanism of turbidity reaction between HA and cetyltrimethylammonium bromide (CTAB).

### 4.2.6 Mechanical property

Tensile mechanical properties of the fabricated COL, CE and CEH scaffold were tested following the previously published protocol [9]. Briefly, samples were immersed with deionized water, dehydrated using a series of ethanol washes, and air-dried. The dried bundles were then glued onto transparency sheets of both ends using a UV curable glue (Dymax 425, Dymax Corporation, Torrington, CT, USA) and rehydrated with PBS. A Shimadzu EZ-L universal mechanical tester was used to perform the tensile strength testing with a 10 N load cell at a crosshead speed of 10 mm/min$^{-1}$. The fracture energy was calculated by an integral calculation under the strain-stress curve before failure happens.

### 4.2.7 Swelling ratio

To evaluate the water up take behavior of different scaffolds, samples of 0.5 × 0.5 $cm^2$ were weighed in the dry state and were recorded as *W*d. Samples were then soaked in PBS for 24 h for complete hydration and the wet weight was recorded as *Ww* after removing excess water using Kimwipe. The swelling ratio of scaffolds was calculated following equation 4.1 [18]:

$$Swelling\ ratio\ \% = \left(\frac{Ww - Wd}{Ww}\right) \times 100\% \qquad (4.1)$$

### 4.2.8 Exploration of versatile scaffolding system using electrocompaction

Graphene fibers [19] or sheets were utilized in this chapter to explore the application of collagen electrocompaction in a versatile, robust scaffolding system [20]. To do this, dialyzed collagen solution at 6 mg/mL were prepared firstly. Tubular or cubic electrical potential (shown in figure 4.6) was applied to the collagen solution to fabricate the collagen-coated graphene fiber or sheets. These collagen-coated fibers were then crosslinked using EDC/NHS as crosslinker using the same protocol described in chapter 3. After sterilization using UV radiation and ethanol soaking, HDFs of passage 6 were seeded onto the collagen-coated graphene fiber. Biocompatibility of these fibers were then evaluated using live/dead assay as indicator.

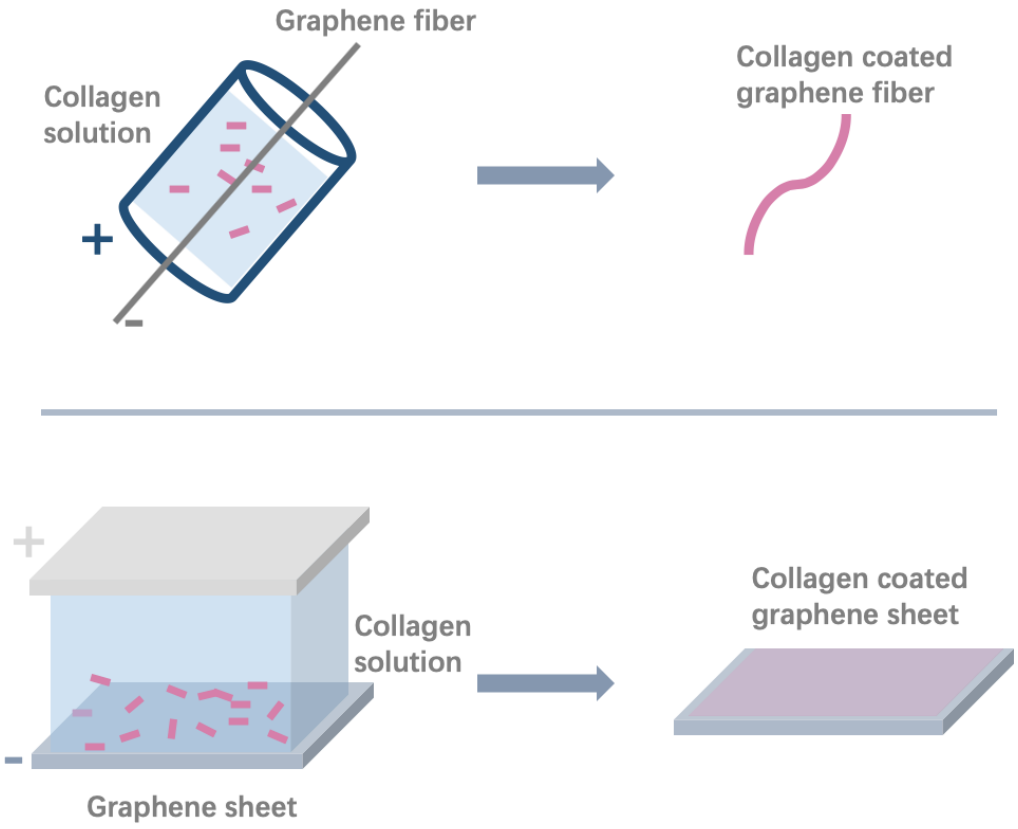


**Figure 4.6.** Collagen electrocompaction on graphene fiber or graphene sheet.

**Statistical analysis:** statistical data were represented as mean ± standard deviation (SD). One-way analysis of variance with ANOVA) tests were used when there are three or more groups to compare. Significance between groups was established for $p < 0.05$.

## 4.3 Results

### 4.3.1 Hyaluronic acid amination

Hyaluronic acid was modified following the procedures illustrated in Figure 4.2 to introduce amino groups to make HA electrocompactable. The reaction mechanism is that carboxyl groups in HA were activated by EDC, then the activated intermediate reacted with an amine to produce hyaluronan amide products. In this way, HA will carry both positively and negatively charged groups, thus make HA electrocompactable.

As described in chapter 1, GAGs are of significant importance in the fabrication of functional skin scaffolding system [21]. Yet, most GAGs are highly negatively charged, thus un-electrocompactable. It will be of huge application if positively charged groups could be introduced into these GAGs to make them electrocompactable. In the works reported by [16], cellulose was modified to introduce amino groups according to the procedure described below in Figure 4.7 to make cellulose electrocompactable. Due to the similarity between the chemical structure of cellulose and HA or ulvan, HA was modified in this work with the aim to make HA electrocompactable and to co-electrocompact collagen with HA.

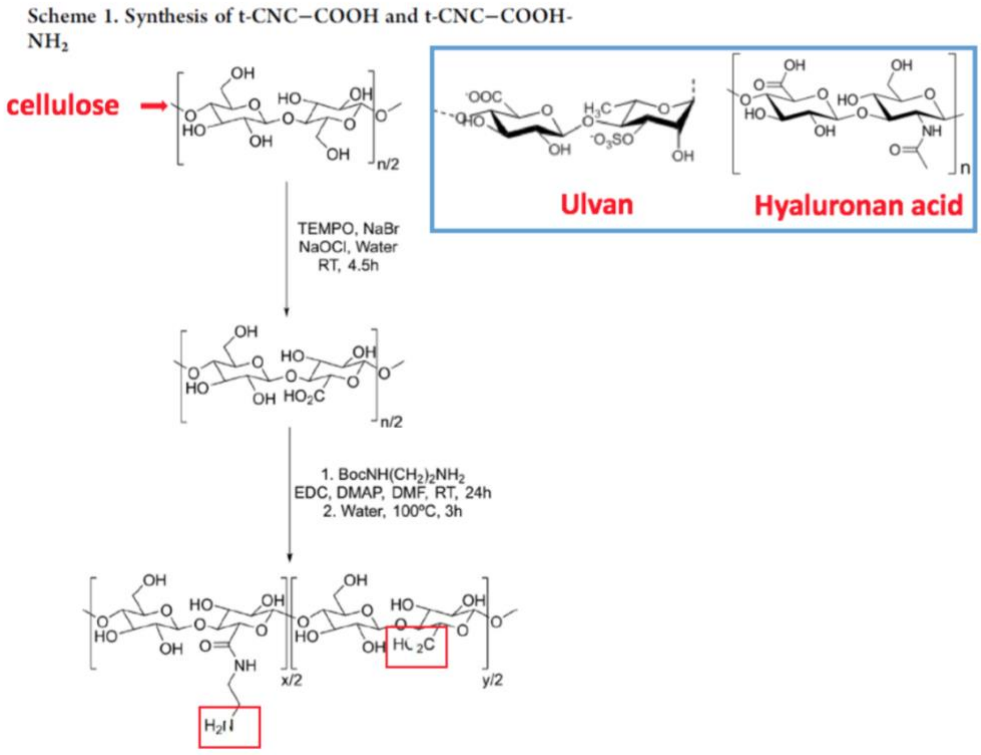


**Figure 4.7.** Modification of cellulose to introduce amino groups.

### 4.3.2 FTIR and NMR of aminated HA

Then FTIR characterization was conducted before and after HA animation to examine the chemical bond changes. As shown in Figure 4.8 A, after modification, a significant difference in the transmittance peaks was noticed near 1625 $cm^{-1}$, which is corresponding to the N-H asymmetric bend in the amino groups [22]. This was assigned to the incorporation of amino groups. This was further confirmed by 1H NMR of HA before and after modification. Among many peaks on 1 H NMR spectra of HA, the broad signal between 3.0 and 3.8 ppm corresponds to the signals of the protons in the sugar rings [23]. The peak at $\delta$ = 1.9 ppm is assigned to the methyl ($-CH_3$) protons of the N-acetyl group of HA. The appearance of a peak at $\delta$ = 2.8 ppm of the modified HA 1H NMR (shown in Figure 4.8 B) corresponds to the newly introduced methylene group in the modified HA. This spectrum change was in accordance with that reported elsewhere [24].

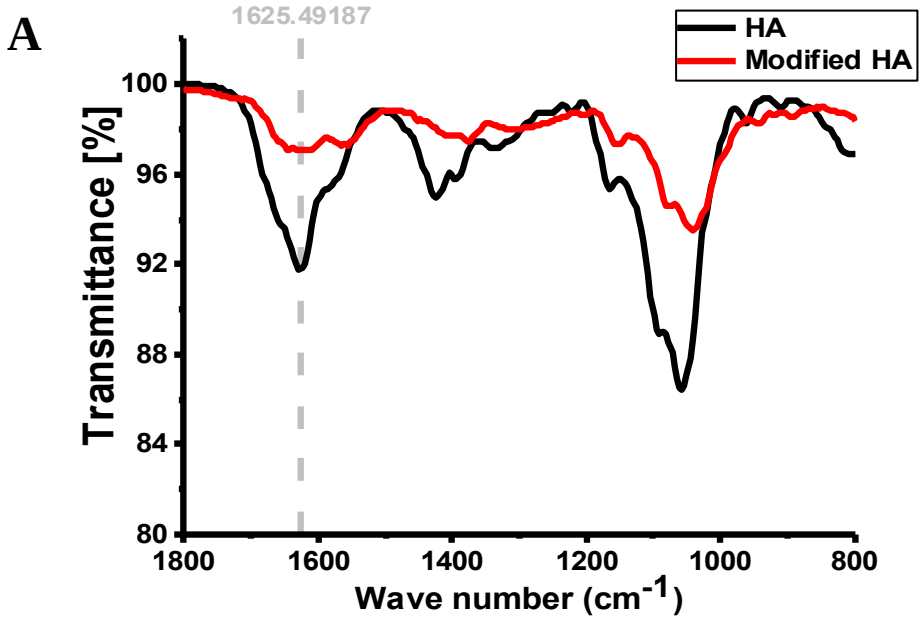


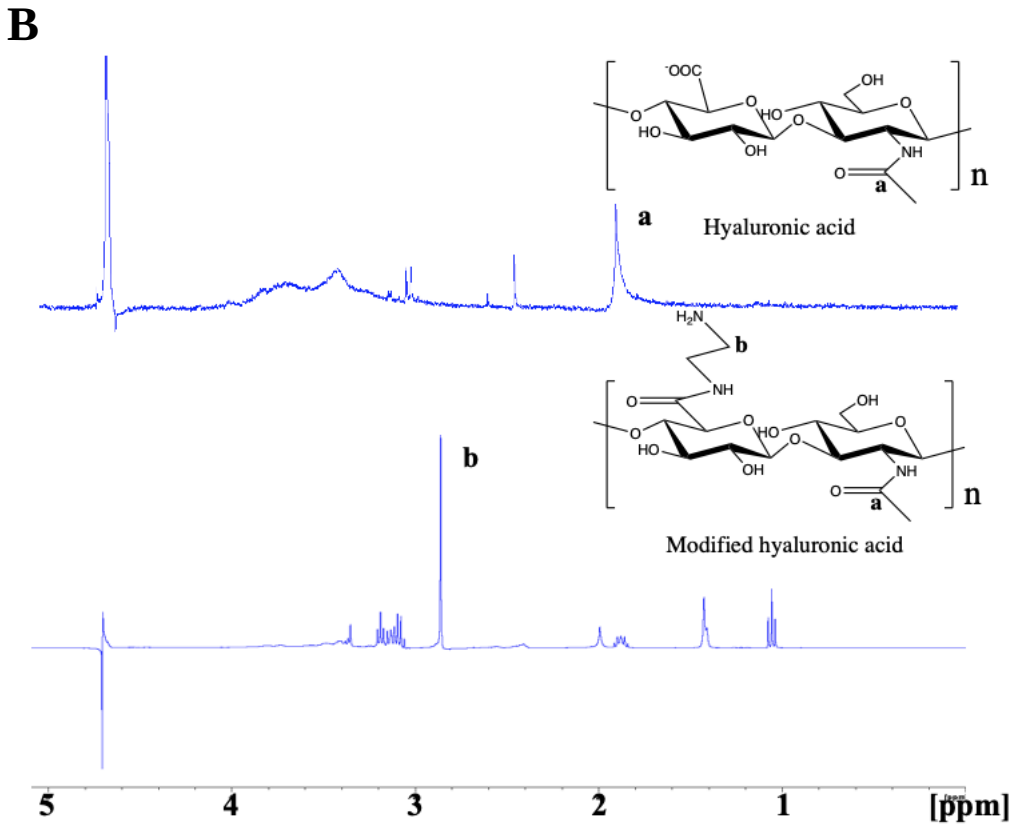

**Figure 4.8.** FTIR and NMR characterization of HA amination. A)FTIR and B)1H NMR spectrum of HA before and after modification confirmed successful amination of HA.

### 4.3.3 Collagen electrocompaction and co-electrocompaction with aminated HA or elastin

Co-electrocompaction of the aminated HA and collagen was tried afterward yet with unsatisfactory results (data not shown). To co-electrocompact HA and collagen, the pI of these two materials should be adjusted to a similar range. As this electrocompaction process is dependent on the net charge of molecules to be processed, where these net charges are further on account of the pH-sensitive groups (carboxylic acid and amines) contained in the molecules. Collagen molecules have + 0.8 coulombs of charge at pH 11 and − 0.8 coulombs of charge at pH 3 [16]. To achieve a similar pI point between collagen and HA, more precise control of the ratio between amino and carboxylic acid groups in the HA molecules need to be obtained. In this research, to introduce HA molecules into the protein system in a cost-effective and convenient manner, the EDC/NHS coupling method was chosen to incoporated HA into protein sheets.

Electrocompaction of collagen and elastin was conducted according to the schematic procedures in Figure 4.3. To test the feasibility of incorporating elastin particles within aligned collagen fibers and to better mimic the components and morphology of natural skin tissue, elastin was mixed with the collagen solution at different weight ratios: collagen only, collagen: elastin at 3:1 and 1:1, and co-electrocompacted. As shown in figure 4.9, collagen and elastin could be successfully co-electrocompacted at the above mentioned ratio range.

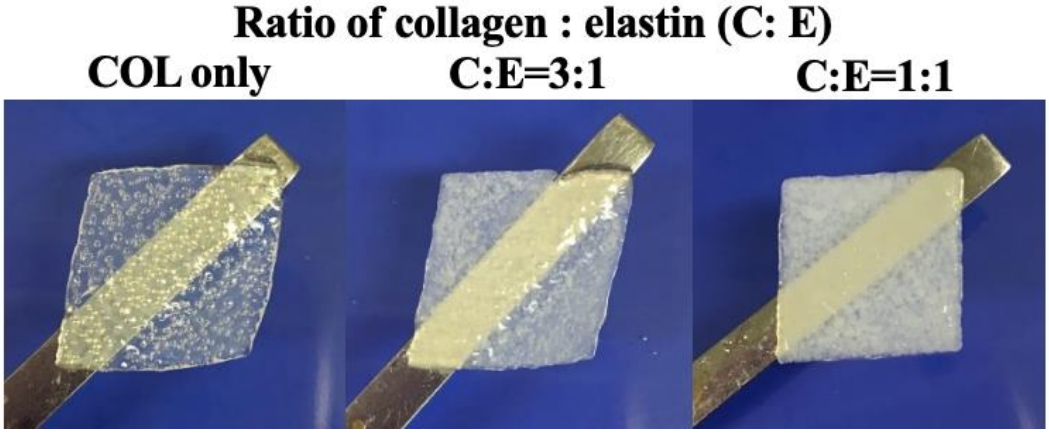


**Figure 4.9.** Co-electrocompaction of collagen and elastin at different ratios.

### 4.3.4 Confocal and FTIR inspection

To investigate the distribution of elastin particles inside the collagen membranes, the resulted CE membrane was inspected by confocal. The fluorescent imaging of CE (Figure 4.10 A) confirmed the successful incorporation and uniform distribution of elastin into the CE membranes as insoluble elastin particles have auto-fluorescent blue color under the DAPI set. This was further confirmed by conformation changes of the amide II peaks in the FTIR spectrum of the elastin, collagen and co-electrocompacted collagen/elastin sheets [22].

**A**

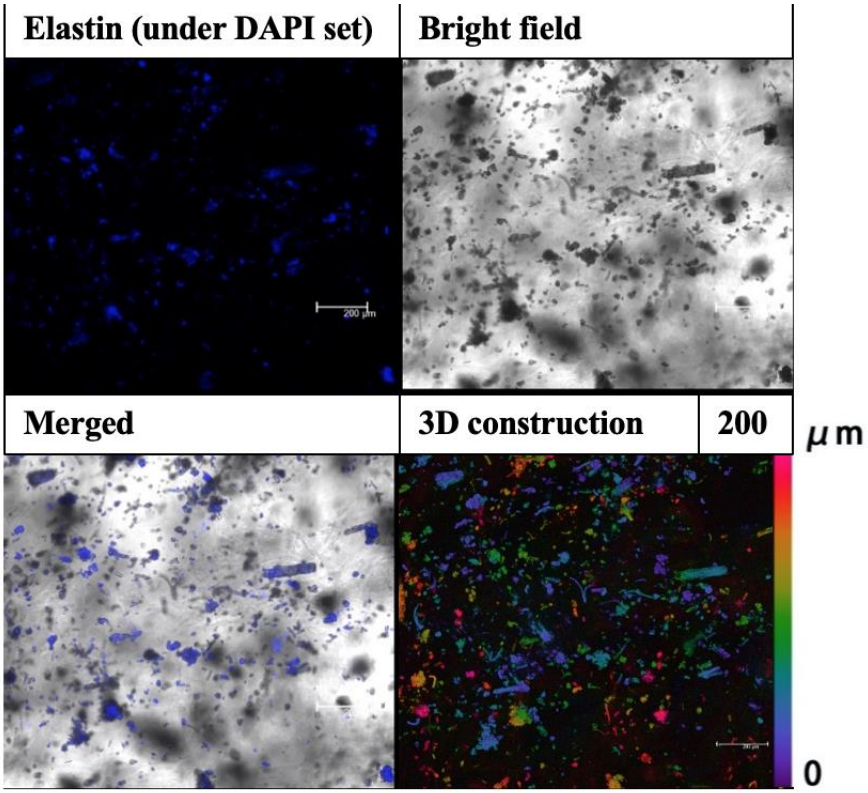


**B**

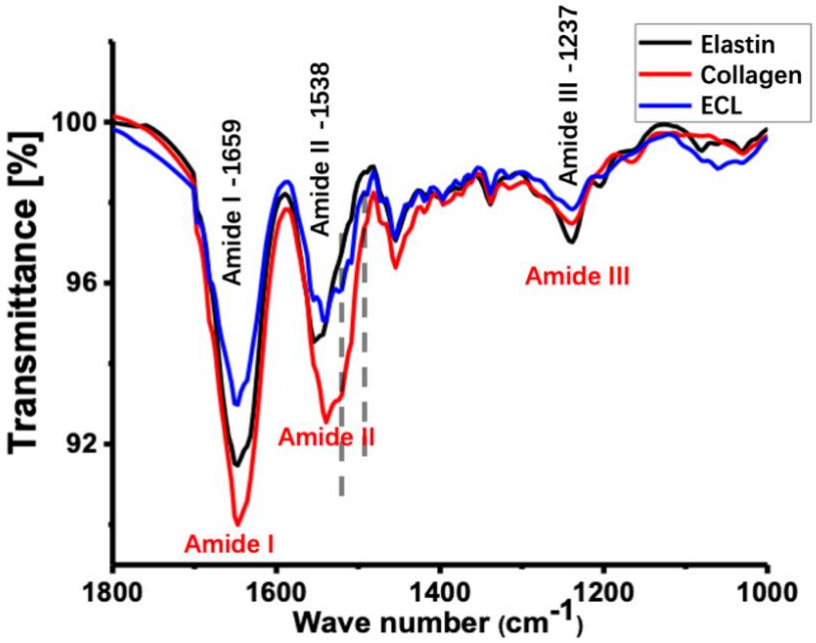

**Figure 4.10.** Characterization of elastin distribution in co-electrocompacted collagen and elastin sheets. A) Confocal, and B) FTIR inspection confirmed successful co-electrocompaction of collagen and elastin.

### 4.3.5 HA incorporation and quantification

To mimic the natural ECM components, HA (MW = 0.9 MDa) was coated onto the co-electrocompacted CE scaffold using EDC/NHS as crosslinker. The quantification of HA content in the CE membrane was performed following the standard CTAB turbidity assay [25]: Insoluble complexes will be formed upon the mixture of hyaluronic acid with CTAB. The amount of insoluble complexes is in proportional to the amount of hyaluronic acid in the testing system (Figure 4.11). The amount of insoluble complexes, which could be reflected by the turbidity, could be measured using a plate reader at the wavelength of 600 nm. By adjusting the amount of HA added, the maximum amount of HA-coated on the CE scaffold was (26.4 ± 3.3) % which is suitable to mimic the ratio of polysaccharides in natural ECM [26] .

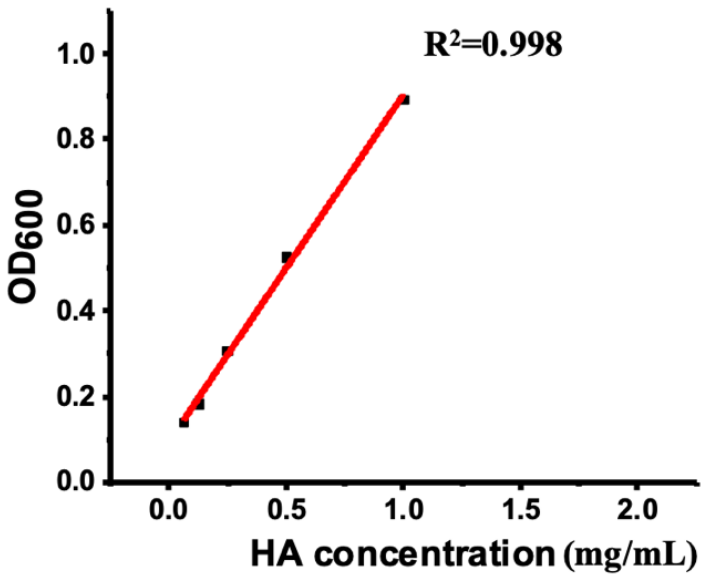


**Figure 4.11.** Standard curve of HA concentration in terms of turbidity.

### 4.3.6 Mechanical property

The young's modulus (Figure 4.12.A) and ultimate tensile strain (Figure 4.12.B) of the COL, CE, and CEH were obtained from tensile tests. The young's modulus of the CE was about 0.17 MPa, which was significantly lower than that of COL (0.25 MPa). This could be ascribed to the incorporation of elastin particles that disturbed the alignment of collagen bundles. This is in accordance with the pervious report [27] that insoluble elastin particles reduce collagen scaffold stiffness in a concentration-dependent manner. After HA incorporation, the CEH (about 0.35 MPa) had a 2-fold greater young's modulus than the CE scaffold. This might due to the enhanced crosslinking between HA and collagen.

The ultimate tensile strain reflected the maximum elongation before a scaffold fail. As shown in Figure 4.12.B, the ultimate tensile strain of the CE scaffold was about 30% and was similar to that of the COL scaffold. The CEH resulted in a significantly higher ultimate tensile strain (about 44%) than the CE scaffold. In normal skin, the reported young's modulus of various skin sites and ages are roughly between 0.05 and 0.2 MPa [28]. The range of ultimate tensile strain of natural skin is 40–70% [29]. Thus, the mechanical properties of the fabricated electrocompacted collagen scaffold lies in a suitable range to be used as a skin scaffold.

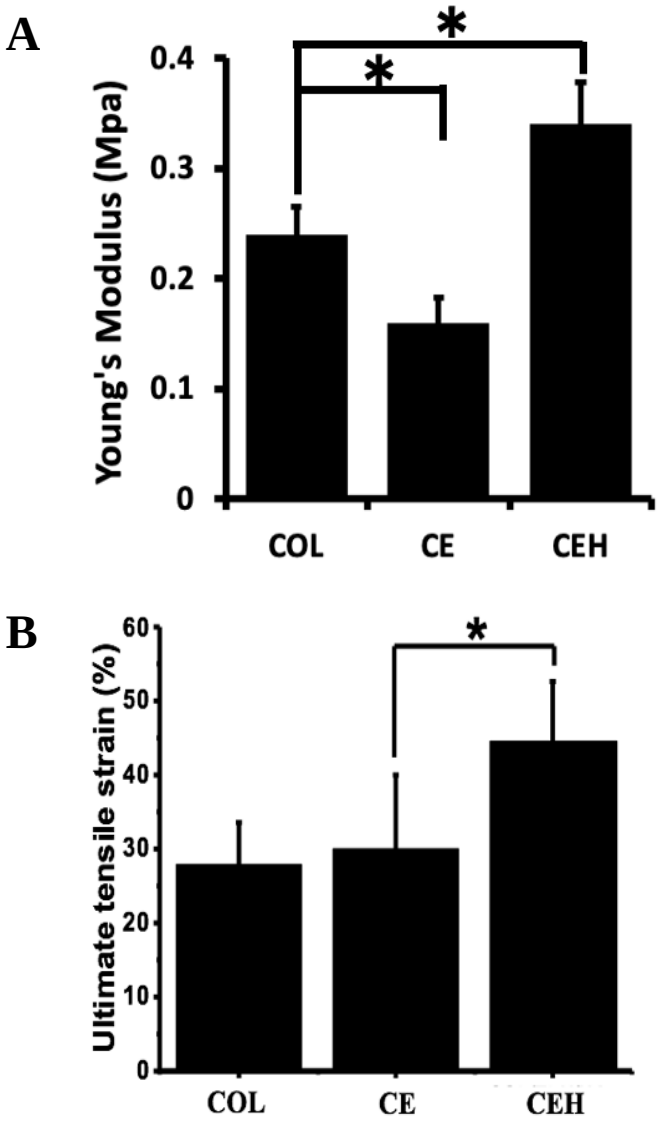


**Figure 4.12.** Mechanical properties of COL, CE, and CEH scaffolds. A) Ultimate tensile strain, and B) Fracture energy of the fabricated COL, CE, and CEH scaffold (* indicates $p < 0.05$).

### 4.3.7 Swelling ratio

The water uptake behavior of COL, CE and CEH scaffold was evaluated. As shown in Figure 4.13, the equilibrium water content of CEH was around 920%, while the electrocompacted collagen matrices without HA exhibited reduced equilibrium water

content. This could be ascribed to the hydrophilic and highly water-absorbing nature of HA that is abundant in carboxyl and hydroxyl groups. The incorporation of elastin into the electrocompacted collagen system did not cause significant change in the equilibrium water content between COL and CE.

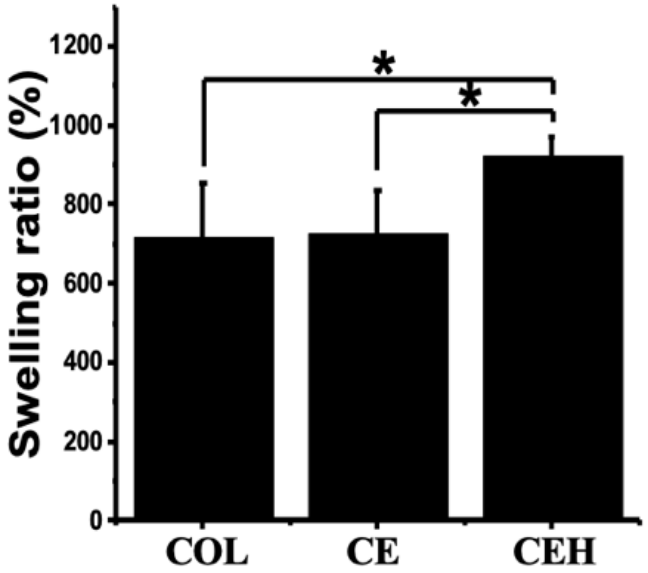


**Figure 4.13.** The swelling ratio of the COL, CE and CEH scaffold.

### 4.3.8 Exploration and examples of versatile application of collagen coated graphene

Collagen coated graphene sheet and fiber were successfully fabricated and shown below in Figure 4.14. During the electrocompaction process, the electrical field pushed the collagen molecules to the pI point, which located near the graphene sheet or fiber. Collagen molecules were thus densely packed and aligned along the graphene to produce this collagen-coated graphene.

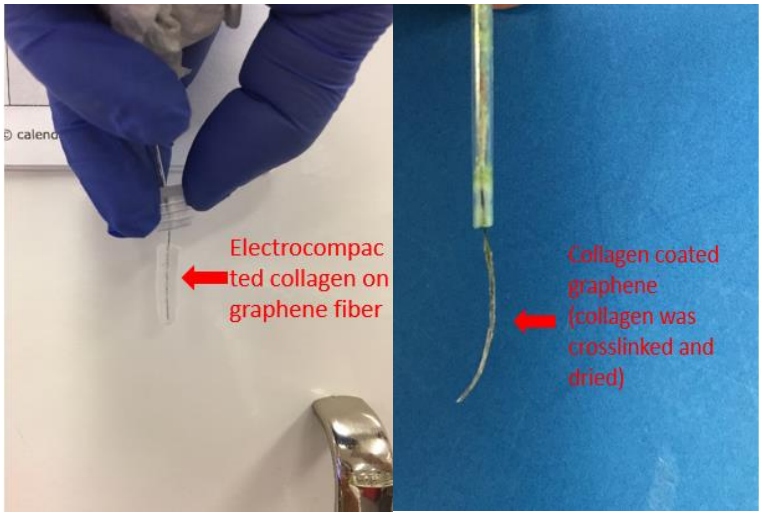


**Figure 4.14.** Collagen electrocompaction on graphene fiber.

To further demonstrate the biocompatibility of the collagen-coated graphene fiber, HDFs were seeded onto the fiber and cultured for 5 days. The live/dead assay result was shown in Figure 4.15.A. The result showed that most of the cells were alive. This implied that this collagen-coated graphene fiber were none toxic and supported HDFs growth.

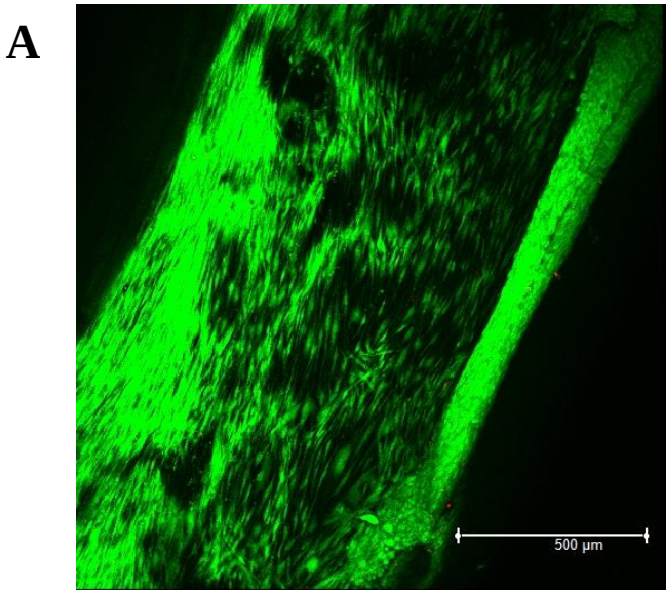

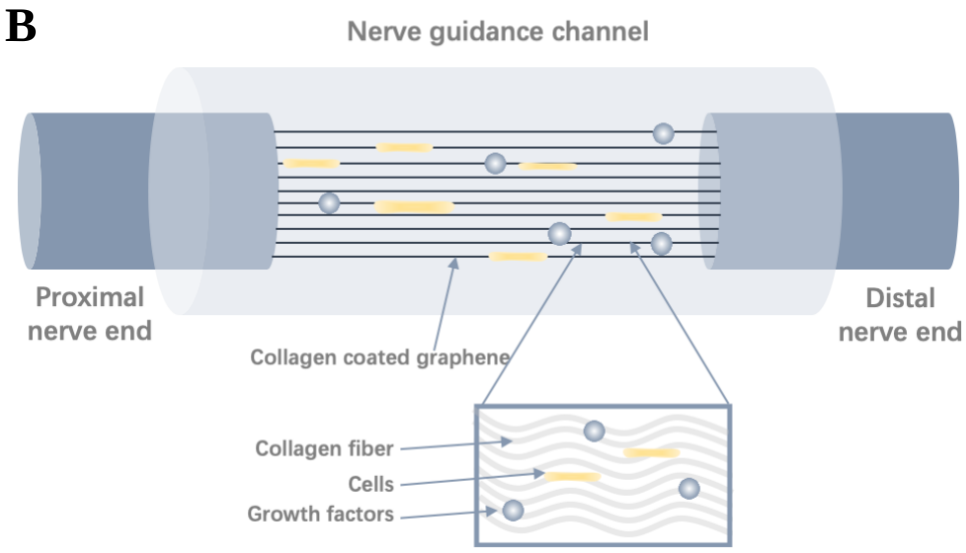


**Figure 4.15.** Biocompatibility of collagen-coated graphene fiber and its possible application as nerve guidance channel. A) Live/Dead assay of HDFs cultured on the collagen-coated graphene fiber, and B) Schematic illustration of nerve guidance channel for nerve regeneration.

One possible application of this collagen coated graphene fiber is nerve guidance channel for nerve regeneration. Previous work showed that electroconductive scaffolds, such as polypyrrole (PPY), can improve peripheral nerve injuries significantly [30]. Polypyrrole (PPY) is an electroconductive polymer with good cell compatibility that has shown great potential as a nerve scaffold [31]. As the collagen-coated graphene fiber showed similar functions, including conductivity and biocompatibility, this collagen-coated graphene could also be applied as grafts for nerve regeneration.

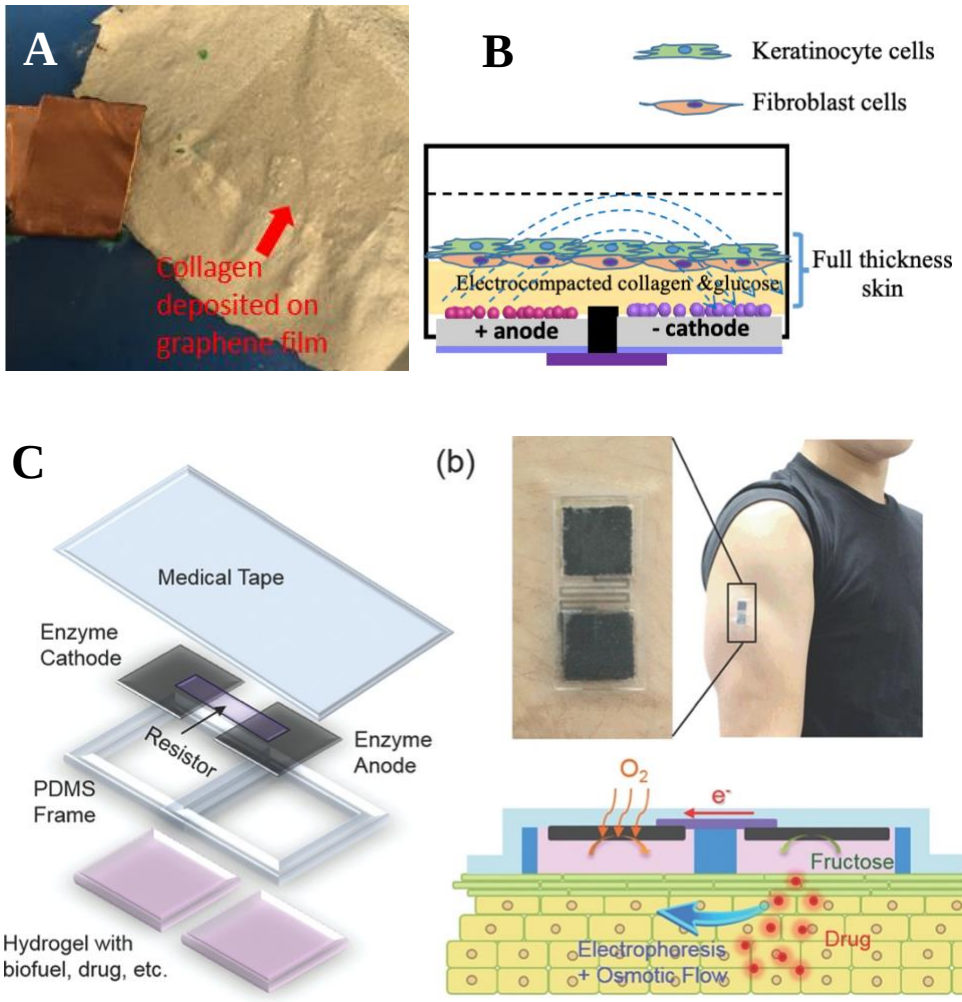


**Figure 4.16.** Collagen coated graphene sheets and its possible application as soft conductive polymer. A) Collagen coated graphene sheet, and B) Schematic illustration of a biofuel transdermal iontophoresis patch based on collagen-coated graphene sheet; C) Example of one possible application of the collagen-coated graphene: An organic transdermal iontophoresis patch for sustained drug release [32].

Collagen coated graphene sheet was also fabricated, as shown in Figure 4.16.A. This collagen-coated graphene sheet could be potentially used as a soft conductive polymer to apply electrical signal to the wound site and stimulate wound healing. Min Zhao [33] reported the cell migration and nerve growth directed by the electric field

generated near the wound site. Y Ogawa et. al. [32] reported the fabrication and application of an organic transdermal built-in biofuel cell with the function of sustained drug release property. For such an application, highly conductive, biocompatible and enzyme coated polymers were needed. This could be achieved by the co-electrocompaction of related enzymes with collagen onto the graphene membrane.

### 4.4 Discussion

The native skin ECM is an active and complex place that can influence cell proliferation, migration and differentiation. Due to their capability to influence the wound healing process, ECM components are valuable building blocks for researching bioactive wound dressings and skin regeneration [34]. Natural skin ECM is mainly made up of collagen, proteoglycans and polysaccharides, and elastin and glycoproteins with the a ratio of roughly 7:2:1 [26]. With collagen provides the structural integrity of the skin tissue, elastin helps to retain mechanical compliance and elasticity of the skin, which makes elastin and ideal protein for dermal skin scaffold design [35]. However, the structural-functional relationship of native elastin is difficult to explore due to the protein's large size and insolubility [27]. Therefore, many researches have focused on elastin derived components, such as hydrolyzed elastin [36], tropoelastin, which is its soluble precursor [37], or elastin-based peptides [38]. While this brings more clues of the molecular basis for elastin's mechanical and biological function, the application of the native insoluble elastin particles provides more advantages for biomimicry tissue engineering. Thus in the current study, insoluble elastin particles (<37 $\mu$m) were incorporated into the collagen scaffold at a weight ratio of collagen: elastin=7:1 to closely mimic the composition of natural skin tissue [26]. During the electrocompaction process, the elastin particles got trapped in between the aligned collagen bundle to form the elastin-incorporated collagen-elastin (CE) membranes.

After the co-electrocompaction of collagen and elastin, HA was incorporated into the scaffold by crosslinking to fabricate the resulted collagen/elastin/HA (CEH) scaffold. HA is a major GAGs in skin ECM and was reported to have significant biological roles in wound healing process by influencing inflammation, granulation, and re-epithelialization [34]. Besides, by incorporating HA into the collagen/elastin scaffold, the swelling ratio of the final scaffold were significantly improved. This is crucial for a successful skin scaffolding system. During the wound healing process, the maintenance of moisture near the wound site is an important aspect of wound management [39]. Besides, a better swelling property can also help the scaffold absorb bioactive molecules from neighboring tissue and thus promote cell function and tissue generation [30]. Therefore, the incorporation of HA or other kinds of glycosaminoglycans (GAGs) into the collagen scaffolds can not only increase the water uptake ability but also better mimic the micro-environment of natural skin tissue.

Often the motivation and most challenging part for collagen fabrication is to recapitulate the aligned and hierarchically organized structure, as well as matching the mechanical property of the fabricated collagen graft with the neighboring tissue. In skin, collagen fibers exist in a densely packed and highly ordered pattern [22]. The method of electrocompaction, which takes advantage of the amphipathic feature of collagen molecules to fabricate densely packed and highly ordered collagen sheets, perfectly meets the requirements of micromorphology as well as mechanical property.

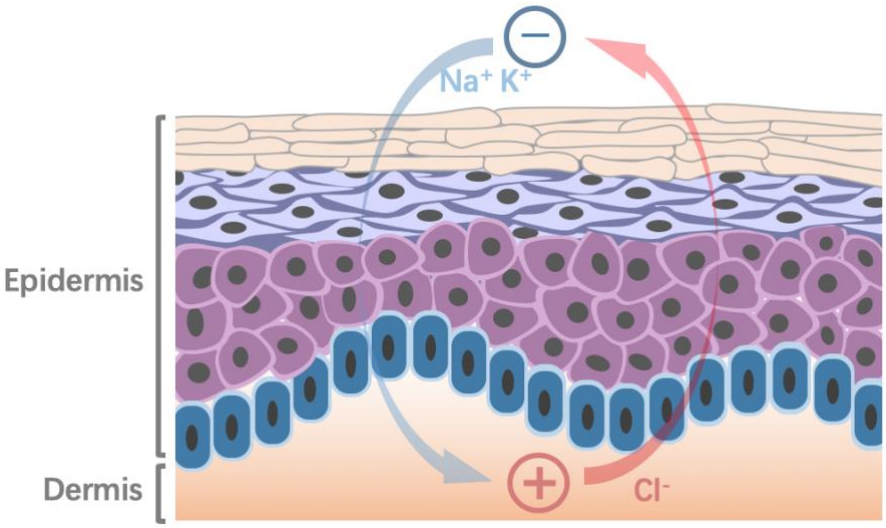


**Figure 4.17.** Endogenous electrical field in health skin.

Besides, using electrical signal to fabricate biomimicry skin graft is more intrinsic. Across the skin tissue, asymmetric ionic flows created transepithelial electric potential where the ECM exists naturally (Figure 4.17) [40]. Thus, the method of applying electric field onto ECM protein molecules (collagen and elastin) mimicked the natural way how collagen fibers are deposited and aligned. Also, electrical signals are especially convenient for fabrication as they can be controllably imposed to promote the electrophoresis, alignment, self-assembly and functionalization of macromolecules to generate hierarchically organized material systems [41].

Before exclusively characterize the biological function of the fabricated ECM components-based skin scaffold, more possible applications of the collagen electrocompaction method were explored. Even though various applications of the collagen electrocompaction were reported as reviewed in Chapter 1, few of these applications integrated the electrical field.

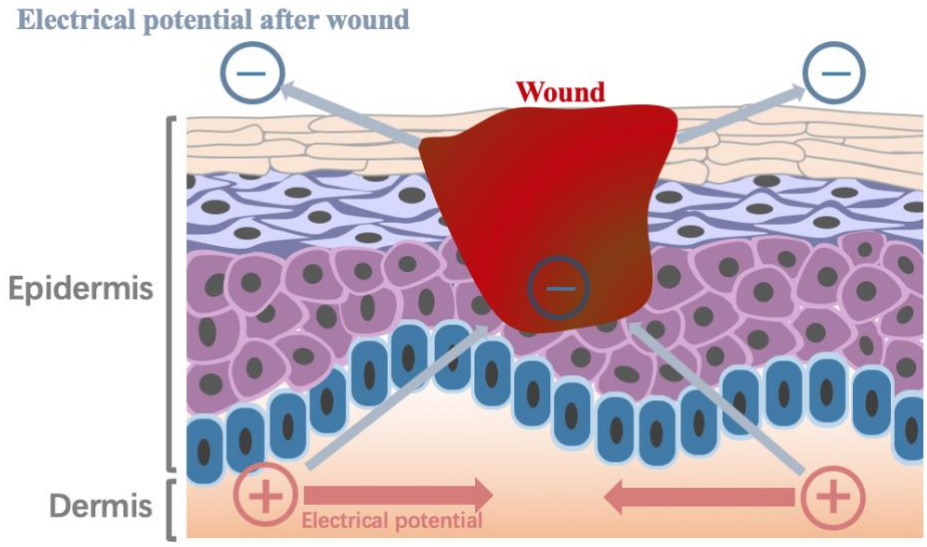


**Figure 4.18.** Electrical potential on skin after wound.

Electricity in animals was detected in the eighteenth century [33]. Naturally occurring electric fields are known to be crucial cues directing tissue growth and healing [40]. In skin, endogenous electrical will be generated instantaneously upon skin injury. Such an electrical field were reported to be fundamental signals directing cell migration during the wound healing process (Figure 4.18) [33]. Even though, exploration of how electrical field affects wound healing in  is not the focus of this thesis, it's worth noting that electrical cues are crucial signals in tissue growth and regeneration. It is highly meaningful and desirable to develop practical and reliable techniques for tissue engineering techniques exploiting electrical signals. The combination of collagen electrocompaction with graphene, as explained in this chapter, could be one cue for such technique.

## 4.5 Conclusion

Development of biomimetic structures with integrated extracellular matrix (ECM) components represents a promising approach for biomaterial fabrication. In this chapter, we reported an artificial ECM comprising the structural protein collagen I (COL) and

elastin (ELN), and glycosaminoglycans (GAGs) hyaluronan (HA). Specifically, collagen and elastin were electrochemically aligned to mimic the morphological and mechanical characteristics of dermal matrix. For HA incorporation, HA amination and co-electrocompaction with collagen was tried yet with unsatisfactory results. Alternatively , HA was finally incorporated into the electrocompacted collagen-elastin (CE) matrices via adsorption and chemical immobilization, to give a final composition of collagen/elastin/HA of 7:2:1. This produced a final collagen/elastin/hyaluronic acid scaffold (CEH) that recapitulated the structural and compositional features of the native skin ECM. Physiochemical characterizations demonstrated its superior properties in components distribution, mechanical properties, and water uptake behavior. In chapter 5, in vitro biological characterization of this ECM-like scaffold, including biocompatibility, ability in supporting dermis, epidermis and full-thickness skin regeneration, will be conducted.

## 4.6 Reference


1. J. Bouwstra, The skin barrier, a well-organized membrane, Colloids and Surfaces A: Physicochemical and Engineering Aspects 1997, 123, 403-413.

2. R.V. Shevchenko, S.L. James, S.E. James, A review of tissue-engineered skin bioconstructs available for skin reconstruction, Journal of the royal Society Interface 2009, 7, 229-258.

3. F. Netzlaff, M. Kaca, U. Bock, E. Haltner-Ukomadu, P. Meiers, C.-M. Lehr, U.F. Schaefer, Permeability of the reconstructed human epidermis model Episkin® in comparison to various human skin preparations, European Journal of Pharmaceutics and Biopharmaceutics 2007, 66, 127-134.

4. P. Olczyk, ł. Mencner, K. Komosinska-Vassev, The role of the extracellular matrix components in cutaneous wound healing, BioMed research international 2014, 2014.

5. W.L. Ng, S. Wang, W.Y. Yeong, M.W. Naing, Skin bioprinting: impending reality or fantasy?, Trends in biotechnology 2016, 34, 689-699.

6. M.-k. Yeh, Y.-m. Liang, K.-m. Cheng, N.-T. Dai, C.-c. Liu, J.-j. Young, A novel cell support membrane for skin tissue engineering: Gelatin film cross-linked with 2-chloro-1-methylpyridinium iodide, Polymer 2011, 52, 996-1003.

7. A. Tiwari, H.J. Salacinski, G. Punshon, G. Hamilton, A.M. Seifalian, Development of a hybrid cardiovascular graft using a tissue engineering approach, The FASEB journal 2002, 16, 791-796.

8. K.A. Athanasiou, G.G. Niederauer, C.M. Agrawal, Sterilization, toxicity, biocompatibility and clinical applications of polylactic acid/polyglycolic acid copolymers, Biomaterials 1996, 17, 93-102.

9. X. Cheng, U.A. Gurkan, C.J. Dehen, M.P. Tate, H.W. Hillhouse, G.J. Simpson, O. Akkus, An electrochemical fabrication process for the assembly of anisotropically oriented collagen bundles, Biomaterials 2008, 29, 3278-3288.

10. M. Younesi, V.M. Goldberg, O. Akkus, A micro-architecturally biomimetic collagen template for mesenchymal condensation based cartilage regeneration, Acta biomaterialia 2016, 30, 212-221.

11. M.T. Abu-Rub, K.L. Billiar, M.H. Van Es, A. Knight, B.J. Rodriguez, D.I. Zeugolis, S. McMahon, A.J. Windebank, A. Pandit, Nano-textured self-assembled aligned collagen hydrogels promote directional neurite guidance and overcome inhibition by myelin associated glycoprotein, Soft Matter 2011, 7, 2770-2781.

12. L. Kang, X. Liu, Z. Yue, Z. Chen, C. Baker, P. Winberg, G. Wallace, Fabrication and in vitro characterization of electrochemically compacted collagen/sulfated xylorhamnoglycuronan matrix for wound healing applications, Polymers 2018, 10, 415.

13. T. Ling, J. Lin, J. Tu, S. Liu, W. Weng, K. Cheng, H. Wang, P. Du, G. Han, Mineralized collagen coatings formed by electrochemical deposition, Journal of Materials Science: Materials in Medicine 2013, 24, 2709-2718.

14. T.-U. Nguyen, C.A. Bashur, V. Kishore, Impact of elastin incorporation into electrochemically aligned collagen fibers on mechanical properties and smooth muscle cell phenotype, Biomedical Materials 2016, 11, 025008.

15. V. Kishore, J.E. Paderi, A. Akkus, K.M. Smith, D. Balachandran, S. Beaudoin, A. Panitch, O. Akkus, Incorporation of a decorin biomimetic enhances the mechanical properties of electrochemically aligned collagen threads, Acta biomaterialia 2011, 7, 2428-2436.

16. E. Cudjoe, M. Younesi, E. Cudjoe, O. Akkus, S.J. Rowan, Synthesis and fabrication of nanocomposite fibers of collagen-cellulose nanocrystals by coelectrocompaction, Biomacromolecules 2017, 18, 1259-1267.

17. M. Younesi, B.O. Donmez, A. Islam, O. Akkus, Heparinized collagen sutures for sustained delivery of PDGF-BB: delivery profile and effects on tendon-derived cells in-vitro, Acta biomaterialia 2016, 41, 100-109.

18. V. Kishore, R. Iyer, A. Frandsen, T.-U. Nguyen, In vitro characterization of electrochemically compacted collagen matrices for corneal applications, Biomedical Materials 2016, 11, 055008.

19. K. Wang, C.L. Frewin, D. Esrafilzadeh, C. Yu, C. Wang, J.J. Pancrazio, M. Romero-Ortega, R. Jalili, G. Wallace, High-Performance Graphene-Fiber-Based Neural Recording Microelectrodes, Advanced Materials 2019, 31, 1805867.

20. M. Younesi, A. Islam, V. Kishore, S. Panit, O. Akkus, Fabrication of compositionally and topographically complex robust tissue forms by 3D-electrochemical compaction of collagen, Biofabrication 2015, 7, 035001.

21. K.R. Kirker, Y. Luo, J.H. Nielson, J. Shelby, G.D. Prestwich, Glycosaminoglycan hydrogel films as bio-interactive dressings for wound healing, Biomaterials 2002, 23, 3661-3671.

22. A. Vasconcelos, A.C. Gomes, A. Cavaco-Paulo, Novel silk fibroin/elastin wound dressings, Acta Biomaterialia 2012, 8, 3049-3060.

23. I. Youm, V. Agrahari, J.B. Murowchick, B.-B.C. Youan, Uptake and cytotoxicity of docetaxel-loaded hyaluronic acid-grafted oily core nanocapsules in MDA-MB 231 cancer cells, Pharmaceutical research 2014, 31, 2439-2452.

24. E.J. Goh, K.S. Kim, Y.R. Kim, H.S. Jung, S. Beack, W.H. Kong, G. Scarcelli, S.H. Yun, S.K. Hahn, Bioimaging of hyaluronic acid derivatives using nanosized carbon dots, Biomacromolecules 2012, 13, 2554-2561.

25. J.-M. Song, J.-H. Im, J.-H. Kang, D.-J. Kang, A simple method for hyaluronic acid quantification in culture broth, Carbohydrate polymers 2009, 78, 633-634.

26. J.B. Park, S. Roderic, Lakes, Biomaterials: An Introduction, Plenum Press, New York, 1992.

27. A.J. Ryan, F.J. O'Brien, Insoluble elastin reduces collagen scaffold stiffness, improves viscoelastic properties, and induces a contractile phenotype in smooth muscle cells, Biomaterials 2015, 73, 296-307.

28. X. Liang, S.A. Boppart, Biomechanical properties of in vivo human skin from dynamic optical coherence elastography, IEEE Transactions on Biomedical Engineering 2009, 57, 953-959.

29. A. Sadeghi-Avalshahr, S. Nokhasteh, A.M. Molavi, M. Khorsand-Ghayeni, M. Mahdavi-Shahri, Synthesis and characterization of collagen/PLGA biodegradable skin scaffold fibers, Regenerative biomaterials 2017, 4, 309-314.

30. M.B. Runge, M. Dadsetan, J. Baltrusaitis, A.M. Knight, T. Ruesink, E.A. Lazcano, L. Lu, A.J. Windebank, M.J. Yaszemski, The development of electrically conductive polycaprolactone fumarate–polypyrrole composite materials for nerve regeneration, Biomaterials 2010, 31, 5916-5926.

31. M.C. Dodla, M. Alvarado-Velez, V.J. Mukhatyar, R.V. Bellamkonda, Peripheral nerve regeneration, Principles of Regenerative medicine, Elsevier2019, pp. 1223-1236.

32. Y. Ogawa, K. Kato, T. Miyake, K. Nagamine, T. Ofuji, S. Yoshino, M. Nishizawa, Organic transdermal iontophoresis patch with built-in biofuel cell, Advanced healthcare materials 2015, 4, 506-510.

33. M. Zhao, Electrical fields in wound healing—an overriding signal that directs cell migration, Seminars in cell & developmental biology, Elsevier, 2009, pp. 674-682.

34. L.E. Tracy, R.A. Minasian, E. Caterson, Extracellular matrix and dermal fibroblast function in the healing wound, Advances in wound care 2016, 5, 119-136.

35. S.M. Mithieux, A.S. Weiss, Elastin, Advances in protein chemistry, Elsevier2005, pp. 437-461.

36. J.B. Leach, J.B. Wolinsky, P.J. Stone, J.Y. Wong, Crosslinked α-elastin biomaterials: towards a processable elastin mimetic scaffold, Acta biomaterialia 2005, 1, 155-164.

37. S.M. Mithieux, J.E. Rasko, A.S. Weiss, Synthetic elastin hydrogels derived from massive elastic assemblies of self-organized human protein monomers, Biomaterials 2004, 25, 4921-4927.

38. D.W. Lim, D.L. Nettles, L.A. Setton, A. Chilkoti, In situ cross-linking of elastin-like polypeptide block copolymers for tissue repair, Biomacromolecules 2007, 9, 222-230.

39. J.P. Junker, R.A. Kamel, E. Caterson, E. Eriksson, Clinical impact upon wound healing and inflammation in moist, wet, and dry environments, Advances in wound care 2013, 2, 348-356.

40. G. Tai, M. Tai, M. Zhao, Electrically stimulated cell migration and its contribution to wound healing, Burns & trauma 2018, 6.

41. J. Li, S. Wu, E. Kim, K. Yan, H. Liu, C. Liu, H. Dong, X. Qu, X. Shi, J. Shen, Electrobiofabrication: electrically based fabrication with biologically derived materials, Biofabrication 2019, 11, 032002.

# Chapter 5

## Biological characterization of the ECM-like skin scaffold

**CONTENT**

## 5.1 Introduction

Skin is the largest organ of the body protecting the internal organs from the external environment [1]. Wounds, originating from physical or chemical trauma, can significantly compromise the skin barrier and impair its physiological functions. In the instances of extensive or deep wounds, it is essential to replace the impaired skin using (bioengineered) skin grafts to prevent water loss and opportunistic pathogens, and to facilitate the wound healing process to restore the barrier structure and functions [2]**.** Beyond wound healing applications, at the early stage of drug discovery or cosmetic formulation development, tissue-engineered skin can serve as an *in vitro* platform to assess the properties of a pharmaceutical or cosmetic agent, such as permeability and the adverse inflammatory responses**.** Tissue-engineered skin models can also be useful tools for elucidating the pathophysiological mechanisms of skin diseases *in vitro* [3]**.** Further, the ban on animal testing for cosmetic industries since 2013 has increased the need for development of *in vitro* skin models that best mimic the native skin [4]**.**

In chapter 4, an ECM-like skin scaffold, including collagen, elastin, and hyaluronic acid, were fabricated and evaluated in terms of its compositional information, mechanical property, and water uptake ability. In this chapter, biological characterizations of this scaffold were conducted. The hypotheses of the function of this ECM-like scaffold include, (1) the CEH scaffold could support dermal skin cell growth and ECM production; (2) the CEH scaffold could support epidermal skin cell growth and stratification; (3) the CEH scaffold could support the organotypic co-culture of human skin fibroblast cells and keratinocyte cells for the formation of the two-layered stratified skin tissue structure. To test these hypotheses (working flow is shown in Figure 5.1), scaffolds with different combinations of ECM components including collagen, elastin, and hyaluronic acid, were synthesized. Human dermal fibroblast cell line: HDFs and human epidermal keratinocyte

cell line: HaCaTs were used in this work to evaluate the influence of the fabricated scaffold on skin cells. Finally, the organotypic co-culture of HDFs and HaCaTs were conducted to evaluate the ability of this CEH scaffold in supporting two-layered skin tissue reconstruction.

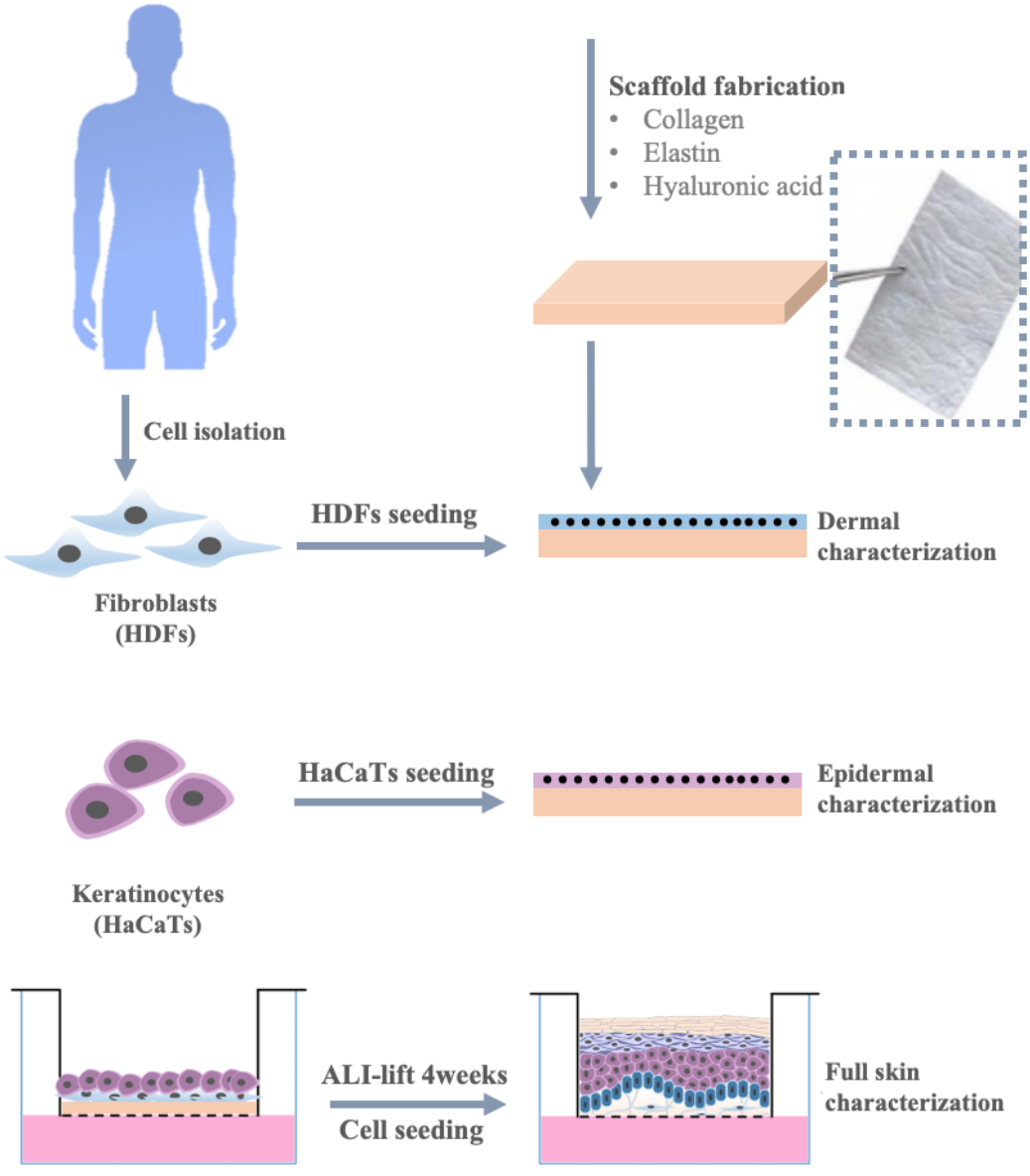


**Figure 5.1.** Schematic illustration of working flow in chapter 5.

## 5.2 Materials and methods

### 5.2.1 HDFs cell viability and proliferation on the COL, CE, and CEH scaffolds

To evaluate the ability of these ECM-like scaffolds in supporting HDFs growth and dermal layer formation, HDFs cell behavior on the COL, CE, and CEH scaffolds, including cell proliferation, cell viability, protein expression, and new ECM deposition, were assessed. To be specific, HDFs at passage six were seeded on the sterilized scaffolds at a cell density of $5 \times 10^4$ cells⁄$cm^2$. The cell-seeded scaffolds were then cultured in the growth medium containing regular Dulbecco's Modified Eagle's Medium (DMEM, Sigma) containing 10% fetal bovine serum (FBS) and 1% v/v penicillin/streptomycin (Life Technologies, USA). Cells were then maintained in a 24 well plate in 5% $CO_2$ at 37°C.

Cell proliferation over 14 days was assessed using the PrestoBlue™ (Life Technologies, Australia) assay. Briefly, on day 1, 4, 7, and 14, three HDFs seeded scaffolds were incubated with PrestoBlue mix for 1 h at 37 ºC. After this, for each sample, 100 µL aliquots of supernatant were transferred into each well of a 96-well plate in triplicate and read using a microplate reader (POLAR star Omega, Germany).

To examine the cell viability on scaffolds, the live/dead assay of cells cultured on scaffolds were conducted. Briefly, after culturing for 7 days, the cell culture medium was replaced by calcein AM (5 µg/mL, Life Technologies, Australia) and incubated at 37 ºC in dark for 10 min. After washing in PBS for 3 times, propidium iodides (PI, 5 µg/mL, Life Technologies, Australia) were added into the cell-scaffold complexes and incubated for 5 minutes in dark at 37 ◦C. Photographs were taken using a confocal microscope (Leica TSC SP5 II, USA).

### 5.2.2 RT-qPCR

To analyze the influence of matrix composition on HDFs gene expression, the mRNA levels of collagen type I (*COL1*), collagen type III (*COL3*), elastin (*ELN*), fibronectin (*FN*), CD44, hyaluronan synthase 2 (*HAS2*), α-smooth muscle actin (*α-SMA*), and glyceraldehyde-3-phosphate dehydrogenase (*GAPDH*, housekeeping gene) were evaluated. To do this, HDFs were cultured on the COL, CE, or CEH scaffolds for 14 days. Total mRNA was then isolated using the Aurum Total RNA Mini kit (Bio-Rad, USA). The concentrations of mRNA were determined using a Nanodrop spectrometer (Thermo Fisher Scientific, USA). Complementary DNA (cDNA) was synthesized, and specific primers for target gene (Table 1) were designed based on the gene sequence database of NCBI. Forward and backward primers were purchased from Sigma. RT-qPCR was run with SYBR® Green Master Mix (Bio-Rad, USA) using a 7500 Real-Time PCR system (Thermo Fisher Scientific, USA). The gene expression levels were normalized with GAPDH, and the data were finally analyzed according to the $2^{-\Delta\Delta C_T}$ method.

### 5.2.3 Immunohistochemistry staining of HDFs differentiation and new ECM secretion

Immunohistochemistry staining was performed to evaluate the influence of three types of scaffolds on HDFs differentiation with α-SMA as maker. New ECM deposition by the HDFs cultured on the CEH scaffold were also evaluated. To perform this, samples were fixed with 3.7% PFA in PBS at RT for 30 min, rinsed in PBS, blocked and permeabilized with 5% (v/v) donkey serum in PBS containing 0.3% (v/v) Triton X-100 (Sigma) at 37 oC overnight. Samples were then incubated with fluorescence conjugated antibodies mouse anti-α-smooth muscle-actin-Cy3 (α-SMA, 1:100, Sigma), or unconjugated primary antibodies collagen I (COL1, Abcam), collagen III (COLIII, Abcam), fibronectin (FN,

Abcam), and elastin (ELN, Abcam) from rabbit at 1:100 dilution at 4 ºC overnight. On the second day, samples were rinsed with 0.1% Triton X-100 in PBS three times. Samples with unconjugated primary antibody were then treated with Alexa Fluor 488 or 596-conjugated secondary antibody (5:1000; Invitrogen) and incubated for 2 h in dark at 37 ºC. After 3 times wash with PBS, cell nuclei were counterstained with 4, 6-diamidino-2-phenylindole (DAPI, 5 µg mL-1) for 10 min in dark at room temperature. Samples were mounted onto glass coverslips with Aquamount (ThermoScientific). Visualization of samples was performed using a confocal laser scanning microscope (Leica TSC SP5 II) applying Leica Application Suite AF (LAS AF) software (Leica).

### 5.2.4 HaCaT cell culture and differentiation

The CEH scaffold was employed for the culture of keratinocytes. HaCaT cells (source) were routinely cultured in 5% $CO^2$ at 37°C in DMEM supplemented with 10% FBS. The scaffolds were placed into 12 well transwell with inserts of polycarbonate membrane (12 mm diameter and 3 µm pore size, Corning Inc., USA). Then HaCaT cells (passage 9) were seeded at a density of $0.2 \times 10^6$ cells $cm^{-2}$. Each cell-seeded scaffold was cultured in 1.5 mL growth medium under submerged condition in 5% $CO^2$ at 37°C for 24 h for the formation of confluent monolayers. The cell culture medium was replaced with 600 µL differentiation medium to expose HaCaT cells to the air-liquid interface for 7-14 days to induce differentiation and stratification. The differentiation medium was prepared as described in [21] with slight modification. Briefly, DMEM/F12 (3:1, v/v) were supplemented with 10% FBS, 1% penicillin/ streptomycin, 1.8 mmol $L^{-1}$ $Ca^{2+}$, 5 µg $mL^{-1}$ insulin, 0.4 µg $mL^{-1}$ hydrocortisone, 0.02 nM triiodothyronine, 0.18 mmol $L^{-1}$ adenine, 5 µg $mL^{-1}$ transferrin, and 2 ng $mL^{-1}$ transforming growth factor α (TGF-α). The differentiation medium was changed on a daily basis. After culturing for 7 days, HaCaT cell viability were evaluated using the live/dead assay as described above.

### 5.2.5 Histology analysis

To observe the stratified multilayer of the resultant epidermis, samples (cultured at air-liquid-interface (ALI) for 1 and 2 weeks) were fixed in 3.7% PFA solution in PBS at room temperature for 2 h and rinsed in PBS. The samples were pre-processed and embedded in paraffin block for routine hematoxylin and eosin (H&E) histology and immunofluorescence staining. Sections of 7 μm thickness were cut using a Reichert-Jung 2035 microtome, collected on Superfrost microscope slides (Fisher Scientific, USA). After dewaxing and rehydration, the section-mounted glass slides were immersed into a hematoxylin solution (Sigma-Aldrich, USA) for 10 min, washed with warm running water for 15 min, and then dipped in an eosin Y solution (Sigma-Aldrich, USA) for 60s. After washing with tap water for 1 min, the sectioned samples were dehydrated by immersing sequentially in 95% ethanol, 100% ethanol, and xylene, twice and 2 min each. The labeled samples were sealed with coverslips using Permount Mounting Medium (Fisher Scientific, USA). Photographs were taken on a Nikon microscope with a Leica DM 750 microscope (Leica Microsystems, Mannheim, Germany). Tissue thickness of the sectioned epidermis was measured on histological sections using the ImageJ software (NIH). Immunohistochemistry staining was conducted on the samples after ALI culture for 14 days, to assess the differentiation and stratification of HaCaT cells cultured on the CEH scaffold. Samples were harvested and sectioned using the same procedure as mentioned in chapter 2.3.2. The sectioned samples were stained against markers including Ki-67 (a proliferation marker), E-cadherin (a cell-cell adhesion marker), involucrin and loricrin (terminal differentiation marker of keratinocytes). Confocal images were collected using (Leica TSC SP5 II) applying Leica Application Suite AF (LAS AF) software (Leica).

### 5.2.6 Organotypic co-culture of HDFs and HaCaTs on the CEH scaffold

To reconstruct double-layered epidermal-dermal like structure, HDF cells (passage 6) were seeded on top of the CEH scaffold at a density of $2\times10^5$ $cm^2$ and cultured in the growth medium for 48 h. Then HaCaT (passage nine) cells were seeded on top of the construct at a density of $1\times10^6/cm^2$ and co-cultured under submerged condition in the growth medium for 24 h, following by the ALI culture for 14 days according to the procedure described in 2.3.1. To view the resulted doubled-layered epidermal/dermal structure, the co-cultured samples following the ALI culture for 14 days were harvested and sectioned. H&E staining was then performed to visualize the resulted stratified epidermal-dermal structure. To further demonstrate the formation of two-layered skin structure, immunohistochemistry staining of epidermis markers (E-cadherin, Involucrin, and Loricrin), dermis marker (collagen I), and cell nuclei were also applied.

**Statistical Analysis:** statistical data were represented as mean ± standard deviation (SD). One-way analysis of variance with ANOVA) tests were used when there are three or more groups to compare. Significance between groups was established for $p < 0.05$.

## 5.3 Results

### 5.3.1 HDFs cell viability and proliferation on the COL, CE, and CEH scaffold

To examine the ability of the COL, CE, and CEH scaffold in supporting fibroblasts growth, HDFs cell viability and proliferation on these scaffolds were evaluated. Figure 5.2.A showed the live/dead assay of cultured HDFs on three types of scaffolds for 14 days. On day 1, HDFs cell attachment were noticed on all three types of scaffold. On day 14, confluent HDF cell layers on all scaffolds were observed. This suggested the HDFs could survive and proliferate well on all these collagen scaffolds for at least 14 days.

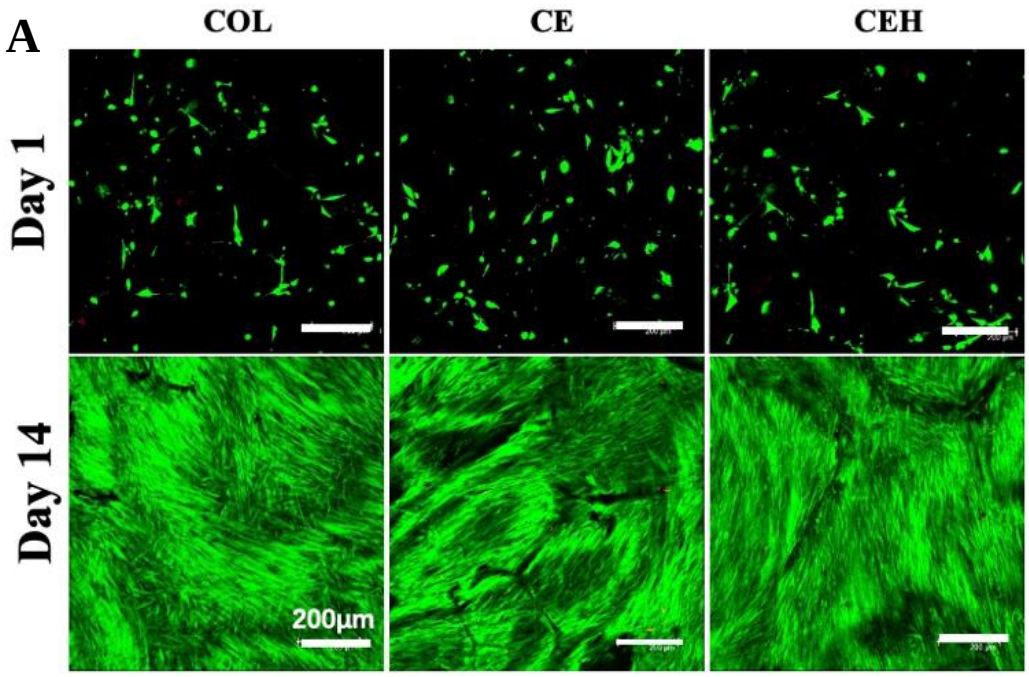

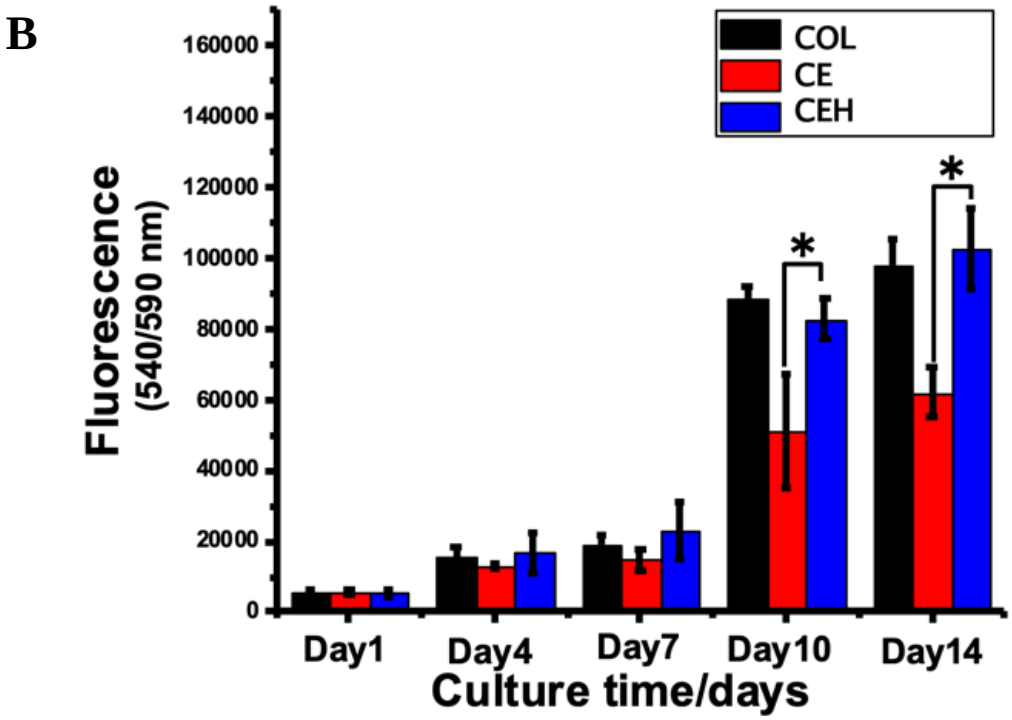


**Figure 5.2.** Survival and proliferation of human dermal fibroblasts (HDFs) on the fabricated scaffold. A) Live (stained by Calcein AM in green) and dead (stained by propidium iodide in red) HDFs at day 1 and day 14; B) Proliferation of HDFs on the COL, CE, and CEH scaffold.

The proliferation behavior shown in Figure 5.2.B demonstrated again that all these scaffolds supported cell growth and proliferation. Especially, cell number on CE at day 10 and day 14 were significantly less than that on COL. This is probably ascribed to the reduced mechanical properties of the CE scaffold as a result of elastin inclusion that comprises the alignment of collagen fiber [16]. The inclusion of HA seemed to be able to counteract this reduction in the CE scaffold as cell numbers on the CEH scaffold were significantly higher than that on the CE scaffold and similar to that on COL. This might be because, firstly, GAGs, including HA, were reported to be able to sequester and concentrate growth factors or nutrients from the neighboring environment, therefore, induce a superior condition for cell function [27]. Secondly, the incorporation and crosslinking of HA into the CEH scaffold resulted in increased mechanical property. This rigid scaffold tends to

stimulate HDFs proliferation [28], and this is in accordance with the tensile mechanical results in Figure 1.D.

However, it was interesting to note that, while the CEH scaffold was stiffer than the COL, the increased stiffness did not result in higher cell proliferation on the CEH scaffold. This might be because not all biologically derived polymers are suitable substrates for cell growth. Even though collagen itself is highly cell adhesive and cell growth supportive, elastin and HA are not as friendly in terms of supporting cell attachment. Elastin was reported to discourage cell attachment and growth unless otherwise modified [29]. To fully explain the influence of elastin and HA incorporation on initial cell attachment on the scaffold, more detailed work was planned for the future work.

### 5.3.2 RT-qPCR

To study the influences of the COL, CE and CEH scaffold on HDFs gene expression, mRNA levels of HDFs cultured on different scaffolds for 14 days were examined. Selected genes are those related to fibroblast ECM deposition, including collagen type I (COL1), collagen type III (COL3), vimentin (VIM), fibronectin (FN), elastin (ELN), and cell function, including CD44 (cell attachment and migration), hyaluronan synthase 2 (HAS2, hyaluronic acid synthesis), and α -smooth muscle actin (α -SMA, maker of myofibroblast cells, promote wound contraction) (Table 5.1).

**Table 5.1.** RT-qPCR primer sequences.

| Primer | Sequence (5'→3') | Sequence (3' →5') |
|---|---|---|
| *GAPDH* | ATGGAAATCCCATCACCATCTT | CGCCCCACTTGATTTTGG |
| *COL1* | GGGAACGCGTGTCAATCC | CAGTTACACAAGGAACAGAACAGTCTCT |
| *COL3* | TGGTCAGTCCTATGCGGATAGA | CGGATCCTGAGTCACAGACACA |
| *VIM* | AATGACCGCTTCGCCAACT | ATCTTATTCTGCTGCTCCAGGAA |
| *FN* | TCGCCATCAGTAGAAGGTAGCA | TGTTATACTGAACACCAGGTTGCAA |
| *KGF-1* | CTTCTGTCGAACACAGTGGTACCT | TCATCTCTTGGGTCCCTTTTACTT |
| *HAS* | AGAGCACTGGGACGAAGTGT | ATGCACTGAACACACCCAAA |
| *ELN* | CTAAATACGGTGCTGCTGGC | CATGGGATGGGGTTACAAAG |
| *α-SMA* | AGACCCTGTTCCAGCCATC | TGCTAGGGCCGTGATCTC |
| *CD44* | GAAAGGAGCAGCACTTCAGG | CACTTGGCTTTCTGTCCTCC |
| *MMP-1* | CAGATGTGGACCATGCCATTGAG | CATCAATGTCATCCTGAGCTAGC |

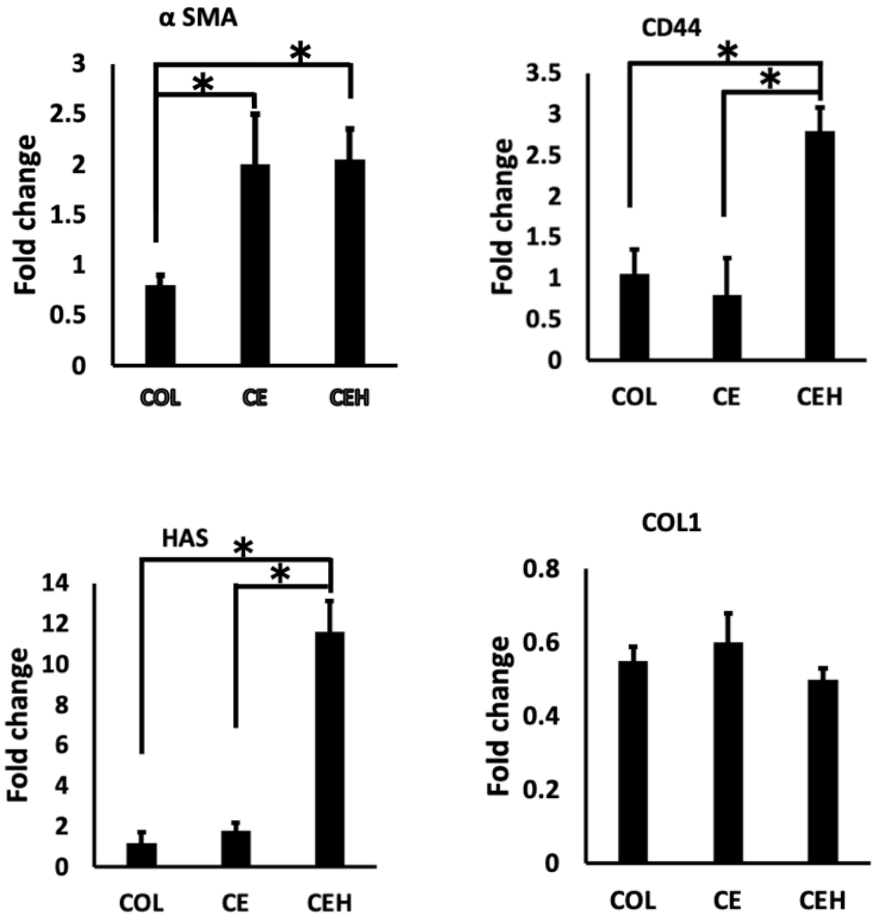

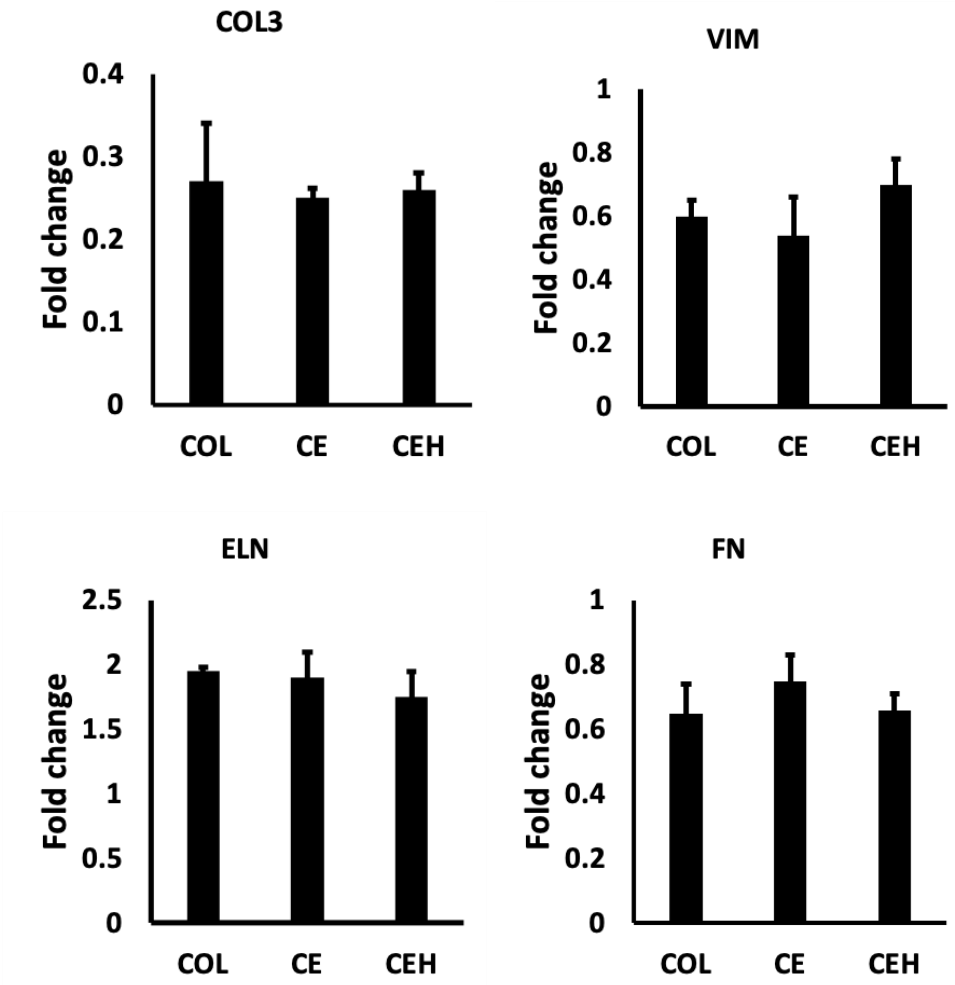


**Figure 5.3.** Comparative RT-qPCR analyses of HDFs gene expression after culturing on different scaffolds for 14 days.

Firstly, as shown in Figure 5.3, the incorporation of elastin and hyaluronic acid did not cause any significant difference in COL1, COL3, VIM, ELN, and FN gene expression compared with COL. The ratio between COL1 and COL3 expressed by HDFs on the COL, CE, and CEH scaffold were 2.03 ± 0.14, 2.17 ± 0.18, and 1.98 ± 0.1, respectively. Incorporation of elastin resulted in significant up-regulation of αSMA of the HDFs cultured on CE or CEH scaffold, compared to COL. HDFs cultured on the CEH scaffold showed

significant upregulation of CD44 and HAS2, compared to COL and CE, attributable to the inclusion of hyaluronic acid.

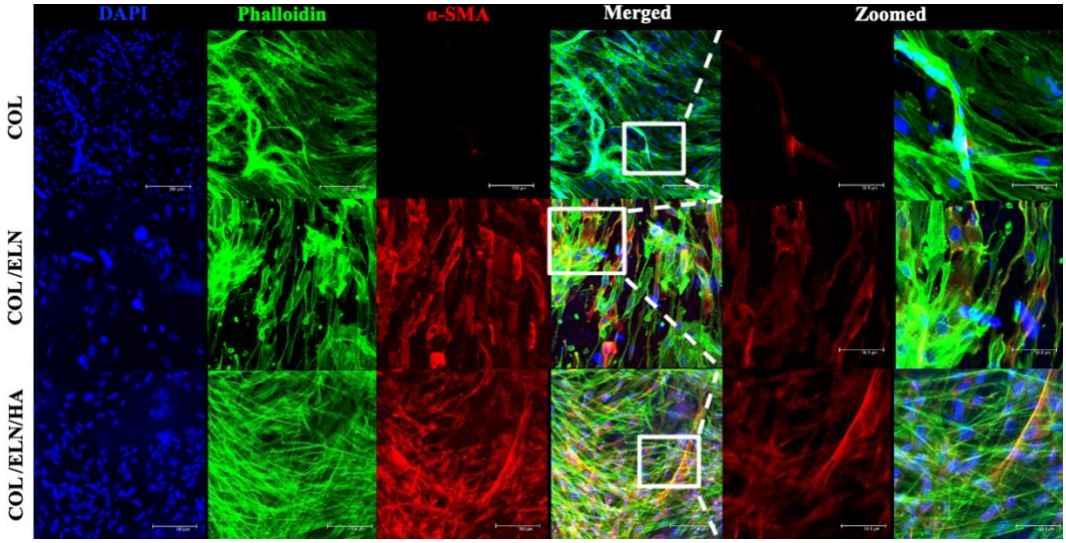


**Figure 5.4.** Immunofluorescent staining of αSMA produced by HDFs cultured on COL, CE, and CEH scaffolds for 14 days. Cell nuclei were stained with DAPI in blue. Cytoskeletons were stained with Alex-488 Phalloidin in green. α-Smooth muscle actins were stained with anti-α-Smooth muscle actin antibody (red).

αSMA staining was conducted on the COL, CE, and CEH scaffold. As shown in Figure 5.4, αSMA expression was noticed on all samples. Especially, more αSMA expression on the CE and CEH scaffold than the COL group were noticed. The overall averaged (n=3) αSMA fluorescence intensity on the CE or CEH was similar. This is in accordance with the RT-PCR results. αSMA is commonly used as a marker of myofibroblasts formation. Myofibroblasts can contract by their smooth muscle type actin-myosin complex [28].

### 5.3.3 Immunohistochemistry staining of HDFs differentiation and new ECM secretion

By far, previously described results confirmed the superiority of the CEH scaffold in terms of mechanical property, water uptake ability, and the highest expression of αSMA, CD44, HAS. From now on, the CEH scaffold was selected for further characterization. As such, the cell-laden CEH constructs were selected for IHC study of new ECM production, including collagen I, collagen III, fibronectin, and elastin. The cytoskeletons of cultured HDFs were stained using Alexa-488 to show the relationship of orientation between ECM fibers and HDFs. The staining results (Figure 5.5) confirmed abundant collagen I&III, fibronectin, and elastin secretion by the HDFs cultured on the CEH scaffold.

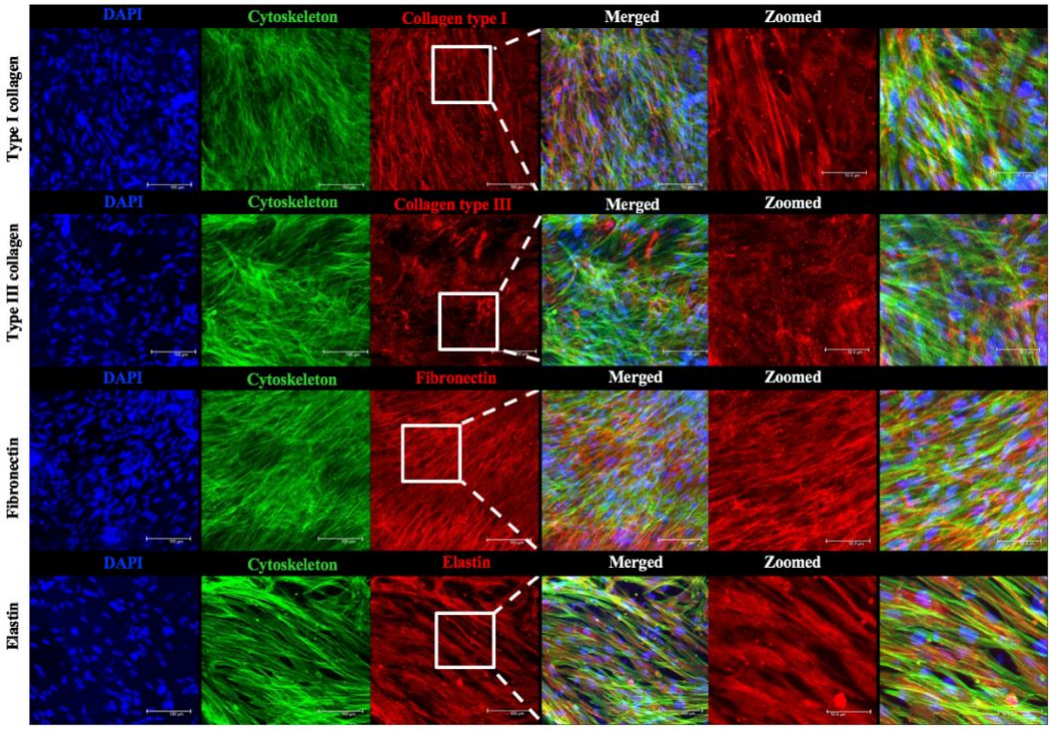


**Figure 5.5.** Immunofluorescent staining of new ECM secretion by HDFs cultured on the CEH scaffold (day 14). Cell nuclei, cytoskeleton, and newly secreted ECM were stained with DAPI (blue), Alex-488 Phalloidin (green),

and antibodies (red) against human type I, III collagen, fibronectin, and elastin, respectively.

### 5.3.4 HaCaT cell culture and differentiation

Immortalized human keratinocytes (HaCaTs) were used in this study to evaluate the ability of the CEH scaffold in supporting epidermis regeneration. HaCaT cell viability and proliferation behavior were evaluated using live/dead assay and immunofluorescent staining of Ki67, a nuclear proliferation marker (Figure 5.6). After culturing on the CEH scaffold for 7 days, the HaCaTs cells were alive, indicating good cell viability and the inherent biocompatibility of the CEH scaffold. The expression of Ki67 by the HaCaTs also confirmed the ability of this CEH scaffold in supporting keratinocytes proliferation.

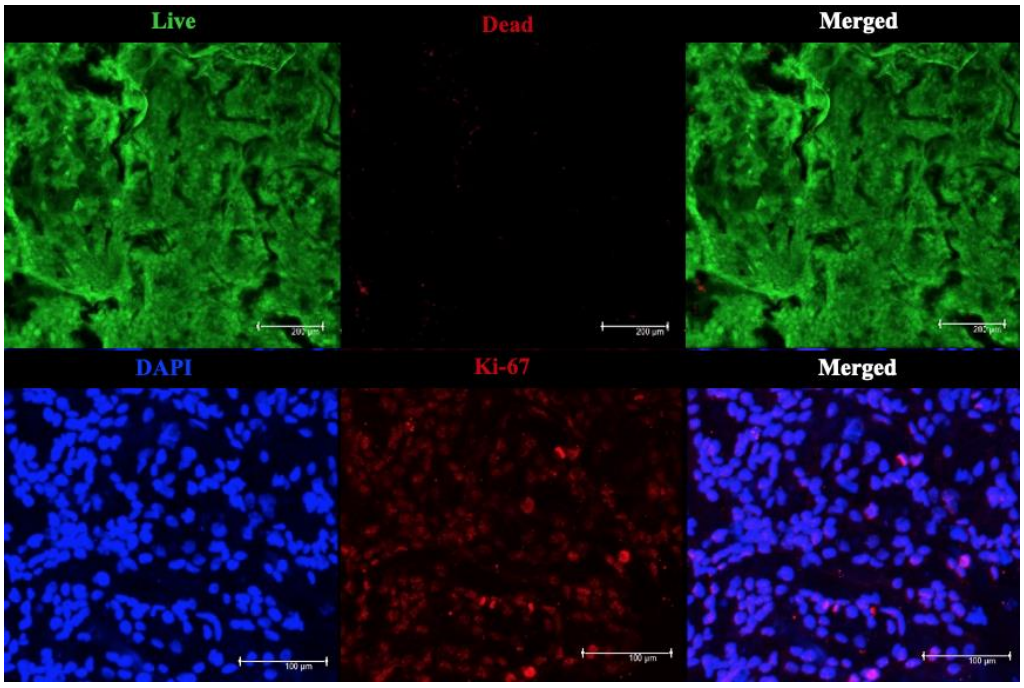


**Figure 5.6.** Viability and proliferation of HaCaT cells cultured on the surface of the CEH scafold after 7 days. Representative live/dead fluorescence images of HaCaT cells on CEH surface with green and red fluorescent

indicate alive and dead cells respectively, HaCaT cells expressed cell proliferation marker Ki67.

To assess the differentiation of HaCaT cells on the CEH scaffold, HaCaTs of passage 9 were seeded on the scaffold and cultured at the air-liquid-interface (ALI) for up to 14 days. The resulted epidermis (Figure 5.7) thickness of day 3, day 7 and day 14 were 9.4 ± 2.8 μm, 36.5 ± 4.3 μm and 78.4 ± 6.3 μm (n = 3), respectively. The thickness of day 14 was significantly better than elsewhere reported regenerated epidermis which was about 20 um [21]. The H & E stained micrographs (Figure 5.7 day14) clearly showed the stratification and flattening of the HaCaT cells cultivated on the CEH scaffold following ALI culture for 2 weeks. The keratinocytes on top of the reconstructed epidermis demonstrated flattened morphology, whereas the bellowing basal keratinocytes exhibited columnar morphology.

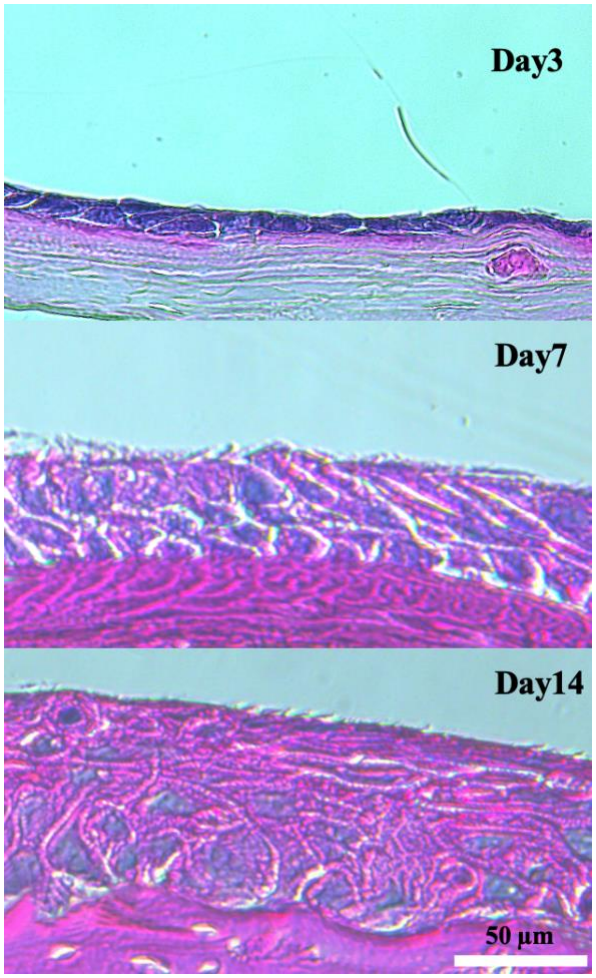


**Figure 5.7.** Representative images of H&E stained sections of reconstructed epidermis on the CEH scaffold after 3, 7, and 14 days culture at the air-liquid interface (ALI). Stratification and flattening of HaCaT cells in the reconstructed epidermis on the CEH scaffold after 14 days culture can be seen clearly.

The expression of differentiation and proliferation markers by the HaCaTs after 7 or 14 days' culture were demonstrated in Figure 5.8, including Ki67 (cell proliferation marker), keratin 10 (K10, an early differentiation marker), involucrin and loricrin (terminal differentiation markers), and E-cadherin (a cell-junction protein). This suggested that the

CEH scaffold were able to support keratinocytes differentiation and epidermal reconstruction.

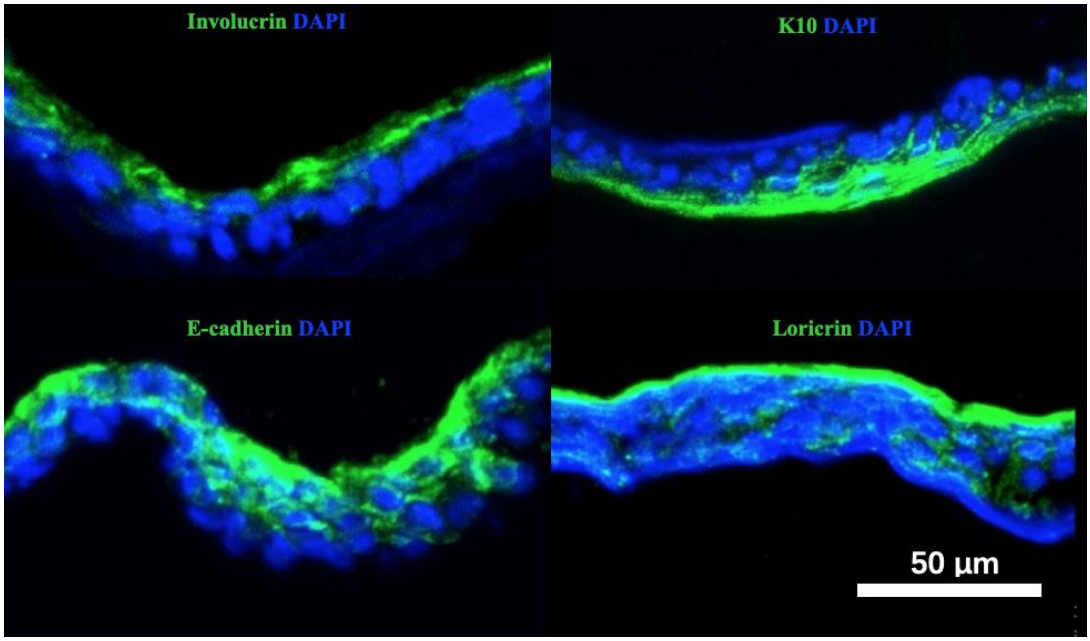


**Figure 5.8.** Expression of proteins of reconstructed epidermis on the CEH scaffold: involucrin & loricrin (green, late differentiation marker), K10 (green, early differentiation marker), E-cadherin (a cell-junction protein), Ki-67 (red, proliferation marker), and DAPI (blue, nuclei) stained sections of the reconstructed epidermis.

### 5.3.5 Organotypic co-culture of HDFs and HaCaTs on the CEH scaffold

In the final stage of this work, the co-culture of HDFs and HaCaTs was performed. After 4 weeks' culture at the ALI, as shown in Figure 5.9, the H&E staining results clearly showed the formation of stratified epidermal and dermal layers. In our observation, the stratified epidermal/dermal skin tissue was stabilized for at least 4 weeks with minimal shrinkage which demonstrated its superior stability.

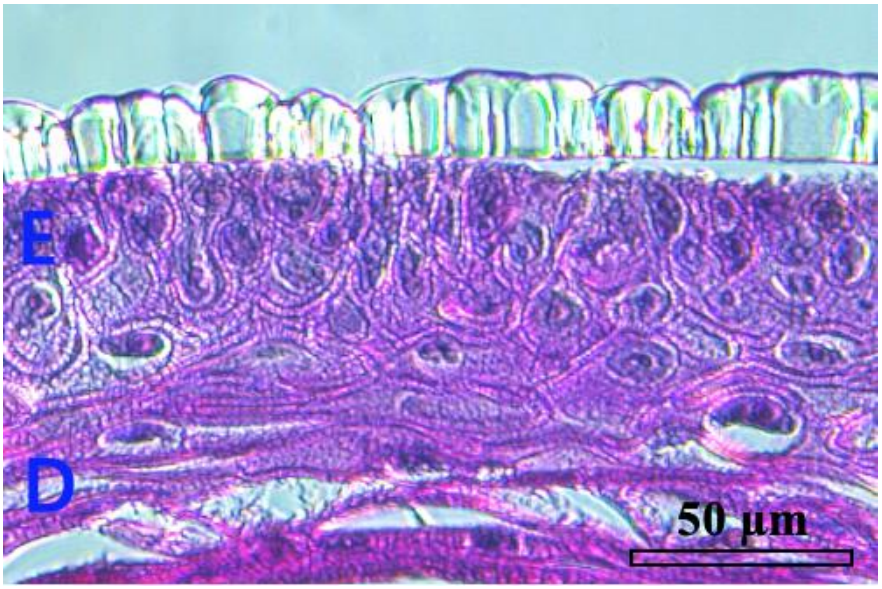


**Figure 5.9.** H&E staining of co-cultured HDFs and HaCaTs after 4 weeks.

The capability of the dermal layer fibroblasts to produce type I collagen in the reconstructed full skin was also evaluated on day 28 (Figure 5.10). The immunofluorescent staining results of collagen I (green) that can only be produced by HDFs in the dermis in this system, and all cell nuclei (blue), indicate that the CEH scaffold could lead to dermal ECM secretion. Cell-cell adherent marker E-cadherin, and epidermis terminal differentiation markers (involucrin and loricrin) were all noticed on the reconstructed epidermal/dermal skin tissue. This further demonstrated the formation of the structured epidermal layer on top of the dermal layer.

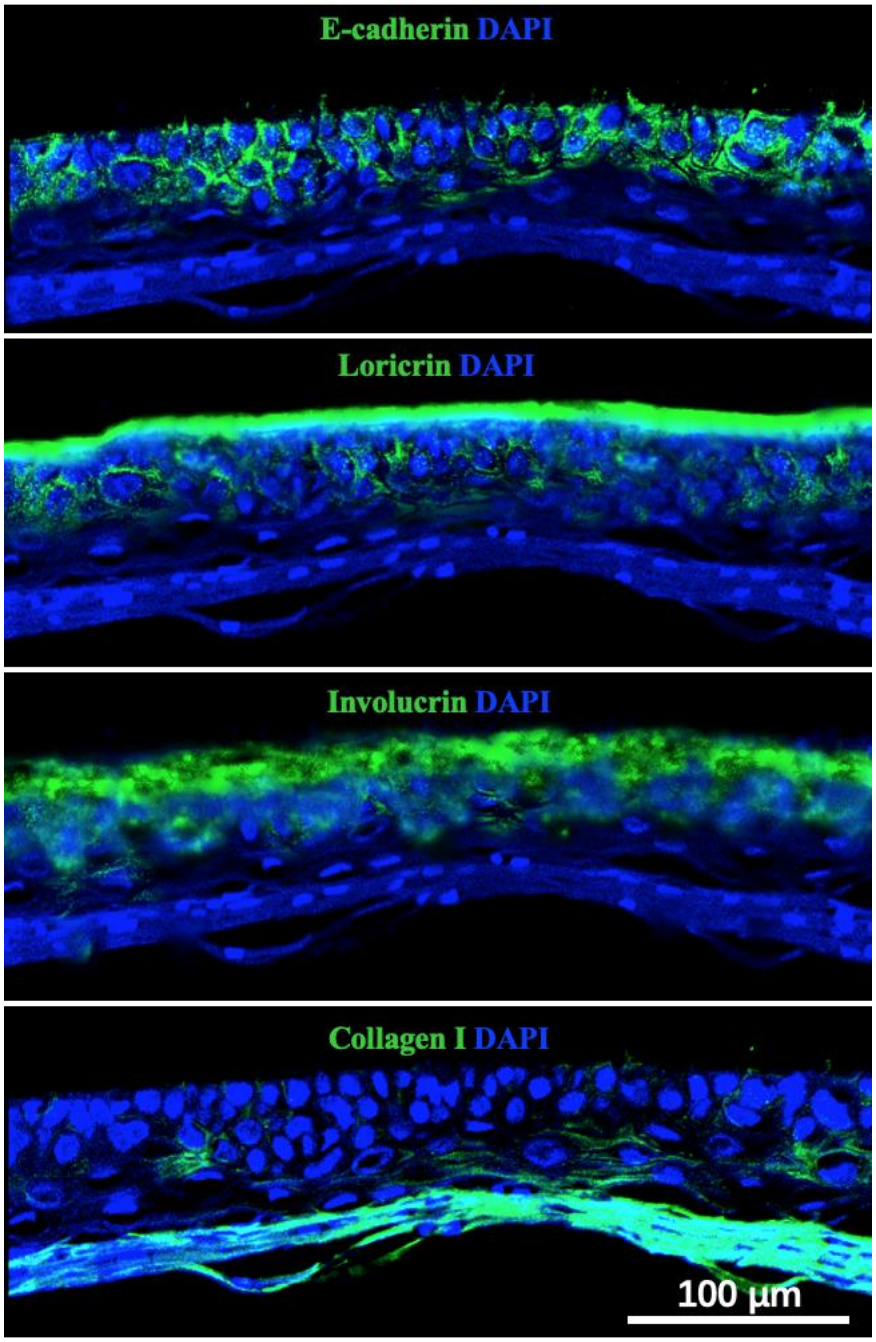


**Figure 5.10.** Immunostaining of E-cadherin, collagen I, loricrin, involucrin and cell nuclei (DAPI) in co-cultured HDFs and HaCaTs after 4 weeks.

## 5.4 Discussion

Fibroblasts play a vital role in normal wound healing. The behavior of fibroblasts, including viability, morphology, proliferation, protein secretion, and gene expression, are of critical importance for successful tissue regeneration [28]. In this research, the gene expression level of HDFs seeded on different scaffolds were evaluated. The results showed firstly that the incorporation of elastin or hyaluronic acid into the collagen scaffold did not cause any significant change in new ECM deposition. However, it is worth noting that the ratio of collagen I : III on all these scaffolds were roughly 2:1, which implied the cultured tissue in this research are more like healthy skin tissues, rather than scar tissues.

In dermis skin, most of the fibrils are made up of type I and type III collagens. Type I collagen is densely packed fibrils that determine the stiffness of the skin. Whereas, type III collagen forms randomly dispersed thin collagen fibrils associated with the flexibility and plasticity of tissues . [33]. The ratio and crosslinking level between collagen I and collagen III determine the strength and stability of both healthy skin tissue and the scar tissue. In normal skin, the ratio between collagen I and III ranging from 2:1 to 4:1 according to different ages or stages of wound healing [33, 34]. Studies of dynamic wound healing process have shown that early granulation tissue has a rather low collagen I : III ratio [35], yet in mature scar tissues, the collagen I:III ratio are quite high [33]. For example, the collagen I: III ratio in normal scar, hypertrophic scar and keloid scar are 6:1, 6:1, and 17:1 [36], respectively. In this research, the collagen I: III ratio by HDFs cultured on three different collagen-based scaffolds were roughly 2:1. This implied the intrinsic biomimicry and skin growth supporting property of these electrocompacted collagen-based scaffolds.

Besides, the HDFs cultured on the CEH scaffold showed upregulated expression of αSMA, CD44, and HAS2 compared to those cultured on COL or CE. The upregulation of αSMA

might be ascribed to the incorporation of elastin. Incorporating elastin into collagen bundles was reported to induce contractile phenotype in smooth muscle cells [24, 27]. Our result is also consistent with previous reports that elastin is involved in preserving a contractile phenotype both in vitro [37] and in vivo [38]. Normal wound healing is composed of three phases: inflammation, proliferation, and remodeling [39]. Both fibroblasts and myofibroblasts play a pivotal role in wound healing. Phenotypically, myofibroblasts are an intermediate cell type between fibroblasts and smooth muscle cells (SMCs) [39]. When skin tissue is damaged, fibroblasts will be activated and differentiate into myofibroblasts. Myofibroblasts then become active during the proliferation phase of wound healing, and gradually disappear in the remodeling stage [39]. Myofibroblasts could generate large contractile forces and actively produce extracellular matrix (ECM) proteins to promote wound closure. Nevertheless, excessive force and over-production of ECM, however, are also the major cause of scar formation. Thus, the issue of how to maintain a balance between fibroblasts and myofibroblasts remains a challenge for further investigation.

Another possible contributing factor for the up-regulation of αSMA might be the incorporation of HA and the matrix mechanical properties. The transformation and maintenance of the myofibroblast phenotype are mediated by HA through a TGF-β1–dependent steps [40]. Recent work has revealed that the rigidity of the ECM has significant effects in fibroblast function [41], including apoptosis signaling, differentiation into myofibroblasts [42], and matrix metalloproteinase (MMP) activity [43].

Inclusion of HA also resulted in the upregulation of CD44 and HAS2 in the HDFs cultured on the CEH scaffold, compared to the COL and CE scaffold. CD44 is the predominant cell surface receptor for HA binding [44]. HA and CD44 are abundant in the extracellular spaces between keratinocytes throughout the epidermis. CD44 receptors were reported to

be responsible for regulating keratinocyte proliferation in response to extracellular stimuli [45]. Also, many of the functions of HA in wound healing are performed in conjunction with or while HA is bound to CD44 [44]. In the final re-epitheliazation stage of wound healing, the complex composed of HA and CD44 regulates keratinocyte migration and proliferation, and maintains local HA homeostasis [46].

By far, we have demonstrated the superiority of the CEH scaffold, including the mechanical property, swelling ratio, stimulating HDFs proliferation, inducing αSMA, CD44, and HAS2 expression, in comparison with the COL and CE scaffold. We further demonstrated the ability of this CEH scaffold in supporting new ECM deposition, including collagen I, collagen III, fibronectin, and elastin. In skin tissues, collagen, elastin and fibronectin are the main components of ECM. With collagen acting as the most prevalent fiber-forming protein and comprising about 70% of the dry weight of human skin, elastin helps define the skin tissue rigidity and elasticity, and fibronectin is one of the key mediators in hemostasis and cell migration in the wound healing [28]. Especially in the proliferative phase of wound healing, fibroblasts are attracted to the wound site to synthesize granulation tissue to fill the wound site and allow ingrowth of new blood vessels [36]. The invasion of fibroblasts into the granulation tissue is dependent on the complex formed by HA and fibronectin [47]. Thus, the fact that HDFs could produce these important ECM components highlight the potential of CEH as dermal scaffolds.

Then, the ability of the CEH scaffold in supporting HaCaTs cell function and epidermis regeneration were further demonstrated. Especially, on the regenerated dermis, important HaCaTs differentiation markers were noticed, including K10 (early differentiation marker), E-cadherin, and involucrin, and loricrin. E-cadherin is one of the most abundant molecules in cell-cell adhesion in epithelial tissues[48]. The presence of cell-cell junction protein E-cadherin, demonstrated the formation of a confluent cell monolayer after being

cultured at ALI for 7 days. The formation of this confluent monolayer is of significant importance for subsequent homogeneous epidermal stratification and retain of the properties of intact epidermis [21]. As uneven keratinocyte patchy formation may result in immature keratinocyte differentiation. A non-uniform stratified epidermal layer might easily peel off [21].

Involucrin and loricrin are terminal differentiation markers expressed by keratinocytes [49]. The involucrin appears earlier than loricrin, and both of them are precursors of the cornified cell envelope. Involucrin, loricrin, together with keratin, filaggrin, and small proline rich proteins (SPRs), form a specialized cornified cell envelope structure [50]. This structure, together with the functional tight junctions and stratified architecture of confluent keratinocyte, help rebuild the mechanical and permeability barrier of epidermis [51].

Therefore, the expression of early differentiation marker K10, terminal differentiation makers including involucrin and loricrin, and adherens junctions' marker E-cadherin, confirmed the superior ability of this CEH scaffold in supporting epidermis differentiation and stratification. Furthermore, in the organotypic co-culture of HDFs and HaCaTs, the formation of a double-layered high stratified skin structure further highlighted the potential of this CEH scaffold in supporting full-thickness skin regeneration.

Further detailed in vitro and in vivo studies will be required to better elucidate the matrix-cell interactions and improve the performance of the biomimicry scaffolds in skin repair and regeneration. The double-layered cellular constructs could be employed as a model to investigate vascularization and nerve innervation. This could be done through co-culture with relevant cell types, such as human umbilical vein endothelial cells and neural stem cells, for example, in combination of related growth factors that can be co-electrocompacted into this collagen based system to achieve a sustained release profile.

## 5.5 Conclusion

In this study, an ECM-like dermal scaffold composed of collagen, elastin, and hyaluronic acid were fabricated to support epidermis/ dermis skin tissue regeneration. The current work demonstrated that incorporation of elastin into the COL membrane induced the contractile phenotype in myofibroblasts. HA incorporation promoted upregulation of HAS2 and CD44, which is vital for new ECM synthesis and fibroblast function. Further, the ECM components-specific microenvironment provided by our ECM-like CEH scaffold encouraged dermal-like ECM secretions, epidermis differentiation, and formation of stratified epidermal-dermal structure. Overall, the outcome of this study provided significant insight into the selection of dermal scaffold components or bio-ink towards advanced skin tissue reconstruction.

## 5.6 Reference


1. J. Bouwstra, The skin barrier, a well-organized membrane, Colloids and Surfaces A: Physicochemical and Engineering Aspects 1997, 123, 403-413.

2. P. Karande, A. Arora, T.K. Pham, D. Stevens, A. Wojicki, S. Mitragotri, Transcutaneous immunization using common chemicals, Journal of Controlled Release 2009, 138, 134-140.

3. H. Aloor, C. Peredo, H. Hofland, S. Smith, J. Therrien, J. Cote-Sierra, A new model for evaluating topical treatments for th17 mediated diseases using ex vivo human skin, JOURNAL OF INVESTIGATIVE DERMATOLOGY, NATURE PUBLISHING GROUP 75 VARICK ST, 9TH FLR, NEW YORK, NY 10013-1917 USA, 2013, pp. S3-S3.

4. W.L. Ng, S. Wang, W.Y. Yeong, M.W. Naing, Skin bioprinting: impending reality or fantasy?, Trends in biotechnology 2016, 34, 689-699.

5. R.V. Shevchenko, S.L. James, S.E. James, A review of tissue-engineered skin bioconstructs available for skin reconstruction, Journal of the royal Society Interface 2009, 7, 229-258.

6. F. Netzlaff, M. Kaca, U. Bock, E. Haltner-Ukomadu, P. Meiers, C.-M. Lehr, U.F. Schaefer, Permeability of the reconstructed human epidermis model Episkin® in comparison to various human skin preparations, European Journal of Pharmaceutics and Biopharmaceutics 2007, 66, 127-134.

7. M.-k. Yeh, Y.-m. Liang, K.-m. Cheng, N.-T. Dai, C.-c. Liu, J.-j. Young, A novel cell support membrane for skin tissue engineering: Gelatin film cross-linked with 2-chloro-1-methylpyridinium iodide, Polymer 2011, 52, 996-1003.

8. A. Tiwari, H.J. Salacinski, G. Punshon, G. Hamilton, A.M. Seifalian, Development of a hybrid cardiovascular graft using a tissue engineering approach, The FASEB journal 2002, 16, 791-796.

9. K.A. Athanasiou, G.G. Niederauer, C.M. Agrawal, Sterilization, toxicity, biocompatibility and clinical applications of polylactic acid/polyglycolic acid copolymers, Biomaterials 1996, 17, 93-102.

10. X. Cheng, U.A. Gurkan, C.J. Dehen, M.P. Tate, H.W. Hillhouse, G.J. Simpson, O. Akkus, An electrochemical fabrication process for the assembly of anisotropically oriented collagen bundles, Biomaterials 2008, 29, 3278-3288.

11. M. Younesi, A. Islam, V. Kishore, S. Panit, O. Akkus, Fabrication of compositionally and topographically complex robust tissue forms by 3D-electrochemical compaction of collagen, Biofabrication 2015, 7, 035001.

12. M. Younesi, V.M. Goldberg, O. Akkus, A micro-architecturally biomimetic collagen template for mesenchymal condensation based cartilage regeneration, Acta biomaterialia 2016, 30, 212-221.

13. M.T. Abu-Rub, K.L. Billiar, M.H. Van Es, A. Knight, B.J. Rodriguez, D.I. Zeugolis, S. McMahon, A.J. Windebank, A. Pandit, Nano-textured self-assembled aligned collagen hydrogels promote directional neurite guidance and overcome inhibition by myelin associated glycoprotein, Soft Matter 2011, 7, 2770-2781.

14. T. Ling, J. Lin, J. Tu, S. Liu, W. Weng, K. Cheng, H. Wang, P. Du, G. Han, Mineralized collagen coatings formed by electrochemical deposition, Journal of Materials Science: Materials in Medicine 2013, 24, 2709-2718.

15. L. Kang, X. Liu, Z. Yue, Z. Chen, C. Baker, P. Winberg, G. Wallace, Fabrication and in vitro characterization of electrochemically compacted collagen/sulfated xylorhamnoglycuronan matrix for wound healing applications, Polymers 2018, 10, 415.

16. T.-U. Nguyen, C.A. Bashur, V. Kishore, Impact of elastin incorporation into electrochemically aligned collagen fibers on mechanical properties and smooth muscle cell phenotype, Biomedical Materials 2016, 11, 025008.

17. V. Kishore, J.E. Paderi, A. Akkus, K.M. Smith, D. Balachandran, S. Beaudoin, A. Panitch, O. Akkus, Incorporation of a decorin biomimetic enhances the mechanical properties of electrochemically aligned collagen threads, Acta biomaterialia 2011, 7, 2428-2436.

18. E. Cudjoe, M. Younesi, E. Cudjoe, O. Akkus, S.J. Rowan, Synthesis and fabrication of nanocomposite fibers of collagen-cellulose nanocrystals by coelectrocompaction, Biomacromolecules 2017, 18, 1259-1267.

19. M. Younesi, B.O. Donmez, A. Islam, O. Akkus, Heparinized collagen sutures for sustained delivery of PDGF-BB: delivery profile and effects on tendon-derived cells in-vitro, Acta biomaterialia 2016, 41, 100-109.

20. V. Kishore, R. Iyer, A. Frandsen, T.-U. Nguyen, In vitro characterization of electrochemically compacted collagen matrices for corneal applications, Biomedical Materials 2016, 11, 055008.

21. X. Zhao, Q. Lang, L. Yildirimer, Z.Y. Lin, W. Cui, N. Annabi, K.W. Ng, M.R. Dokmeci, A.M. Ghaemmaghami, A. Khademhosseini, Photocrosslinkable gelatin hydrogel for epidermal tissue engineering, Advanced healthcare materials 2016, 5, 108-118.

22. J.-M. Song, J.-H. Im, J.-H. Kang, D.-J. Kang, A simple method for hyaluronic acid quantification in culture broth, Carbohydrate polymers 2009, 78, 633-634.

23. J.B. Park, S. Roderic, Lakes, Biomaterials: An Introduction, Plenum Press, New York, 1992.

24. A.J. Ryan, F.J. O'Brien, Insoluble elastin reduces collagen scaffold stiffness, improves viscoelastic properties, and induces a contractile phenotype in smooth muscle cells, Biomaterials 2015, 73, 296-307.

25. X. Liang, S.A. Boppart, Biomechanical properties of in vivo human skin from dynamic optical coherence elastography, IEEE Transactions on Biomedical Engineering 2009, 57, 953-959.

26. A. Sadeghi-Avalshahr, S. Nokhasteh, A.M. Molavi, M. Khorsand-Ghayeni, M. Mahdavi-Shahri, Synthesis and characterization of collagen/PLGA biodegradable skin scaffold fibers, Regenerative biomaterials 2017, 4, 309-314.

27. A. van der Smissen, V. Hintze, D. Scharnweber, S. Moeller, M. Schnabelrauch, A. Majok, J.C. Simon, U. Anderegg, Growth promoting substrates for human dermal fibroblasts provided by artificial extracellular matrices composed of collagen I and sulfated glycosaminoglycans, Biomaterials 2011, 32, 8938-8946.

28. L.E. Tracy, R.A. Minasian, E. Caterson, Extracellular matrix and dermal fibroblast function in the healing wound, Advances in wound care 2016, 5, 119-136.

29. Z. Zhang, O. Ortiz, R. Goyal, J. Kohn, Biodegradable polymers, Handbook of Polymer Applications in Medicine and Medical Devices, Elsevier2014, pp. 303-335.

30. J.B. Leach, J.B. Wolinsky, P.J. Stone, J.Y. Wong, Crosslinked α-elastin biomaterials: towards a processable elastin mimetic scaffold, Acta biomaterialia 2005, 1, 155-164.

31. S.M. Mithieux, J.E. Rasko, A.S. Weiss, Synthetic elastin hydrogels derived from massive elastic assemblies of self-organized human protein monomers, Biomaterials 2004, 25, 4921-4927.

32. D.W. Lim, D.L. Nettles, L.A. Setton, A. Chilkoti, In situ cross-linking of elastin-like polypeptide block copolymers for tissue repair, Biomacromolecules 2007, 9, 222-230.

33. A.J. Hance, R.G. Crystal, Rigid control of synthesis of collagen types I and III by cells in culture, Nature 1977, 268, 152-154.

34. W. Cheng, R. Yan-hua, N. Fang-gang, Z. Guo-an, The content and ratio of type I and III collagen in skin differ with age and injury, African Journal of Biotechnology 2011, 10, 2524-2529.

35. A. Bailey, T. Sims, M. Le Lous, S. Bazin, Collagen polymorphism in experimental granulation tissue, Biochemical and biophysical research communications 1975, 66, 1160-1165.

36. M. Xue, C.J. Jackson, Extracellular matrix reorganization during wound healing and its impact on abnormal scarring, Advances in wound care 2015, 4, 119-136.

37. P.J. Nowatzki, D.A. Tirrell, Physical properties of artificial extracellular matrix protein films prepared by isocyanate crosslinking, Biomaterials 2004, 25, 1261-1267.

38. M.H. Kural, M. Cai, D. Tang, T. Gwyther, J. Zheng, K.L. Billiar, Planar biaxial characterization of diseased human coronary and carotid arteries for computational modeling, Journal of biomechanics 2012, 45, 790-798.

39. B. Li, J.H.-C. Wang, Fibroblasts and myofibroblasts in wound healing: force generation and measurement, Journal of tissue viability 2011, 20, 108-120.

40. J. Webber, S. Meran, R. Steadman, A. Phillips, Hyaluronan orchestrates transforming growth factor-β1-dependent maintenance of myofibroblast phenotype, Journal of Biological Chemistry 2009, 284, 9083-9092.

41. H. El-Mohri, Y. Wu, S. Mohanty, G. Ghosh, Impact of matrix stiffness on fibroblast function, Materials Science and Engineering: C 2017, 74, 146-151.

42. P. Kollmannsberger, C.M. Bidan, J.W. Dunlop, P. Fratzl, V. Vogel, Tensile forces drive a reversible fibroblast-to-myofibroblast transition during tissue growth in engineered clefts, Science advances 2018, 4, eaao4881.

43. M.E. Smithmyer, L.A. Sawicki, A.M. Kloxin, Hydrogel scaffolds as in vitro models to study fibroblast activation in wound healing and disease, Biomaterials science 2014, 2, 634-650.

44. K.L. Aya, R. Stern, Hyaluronan in wound healing: rediscovering a major player, Wound repair and regeneration 2014, 22, 579-593.

45. G. Kaya, I. Rodriguez, J.L. Jorcano, P. Vassalli, I. Stamenkovic, Selective suppression of CD44 in keratinocytes of mice bearing an antisense CD44 transgene driven by a tissue-specific promoter disrupts hyaluronate metabolism in the skin and impairs keratinocyte proliferation, Genes & development 1997, 11, 996-1007.

46. D.J. Tate, P.D. Oliver, M.V. Miceli, R. Stern, S. Shuster, D.A. Newsome, Age-dependent change in the hyaluronic acid content of the human chorioretinal complex, Archives of ophthalmology 1993, 111, 963-967.

47. D. Greiling, R. Clark, Fibronectin provides a conduit for fibroblast transmigration from collagenous stroma into fibrin clot provisional matrix, Journal of cell science 1997, 110, 861-870.

48. T. Lecuit, A.S. Yap, E-cadherin junctions as active mechanical integrators in tissue dynamics, Nature cell biology 2015, 17, 533-539.

49. A. Baroni, E. Buommino, V. De Gregorio, E. Ruocco, V. Ruocco, R. Wolf, Structure and function of the epidermis related to barrier properties, Clinics in dermatology 2012, 30, 257-262.

50. S. Nithya, T. Radhika, N. Jeddy, Loricrin–an overview, Journal of oral and maxillofacial pathology: JOMFP 2015, 19, 64.

51. M. Schäfer, S. Werner, The cornified envelope: a first line of defense against reactive oxygen species, Journal of Investigative Dermatology 2011, 131, 1409-1411.

# Chapter 6

# Conclusions and recommendations

## 6.1 Conclusions

The work presented in this thesis aimed to fabricate scaffolds for skin regeneration and wound healing applications. The key principle of this scaffold fabrication is to mimic the components and structure of natural skin ECM. As such, the materials used in this research are natural ECM components, including collagen, elastin, GAGs (hyaluronic acid), and GAG like marine polysaccharides: ulvan. The fabrication technique utilized here is electrocompaction. This produces densely packed, highly ordered collagen scaffolds that resemble the microstructure of natural ECM. The work described in the thesis is the first example of the using electrocompaction in skin regeneration and wound healing.

To mimic the function of natural skin ECM, the most straight forward and promising way is to utilize naturally occurred ECM components as the main material to fabricate scaffolds. In Chapter 1, roles of natural ECM components, including collagen, elastin, and GAGs, were reviewed and explained. Traditional and advanced fabrication methods for skin scaffolds were also reviewed. It is important to notice, even though the method of electrocompaction was explored in various areas, such as tendon repair, cartilage regeneration, even living machines. No work has been done to apply this method for skin regeneration which highlighted the importance of this research.

Chapter 2 outlined main experiments conducted in this research.

In chapter 3, the method of electrocompaction was applied for the first time in skin regeneration. Densely packed, highly ordered collagen sheets with a microstructure similar to that of natural skin ECM were fabricated using the method of electrocompaction. To mimic the major structure in natural skin tissue more closely, a GAG-like material-ulvan was coated onto this ECL scaffold. Physiochemical and biological characterization

demonstrated the feasibility of this method in fabricating skin scaffold, and showed the growth-supporting function of this scaffold to HDFs cells.

In chapter 4, a more biomimicry skin scaffold composed of naturally occurred skin ECM components, including collagen, elastin, and hyaluronic, were fabricated. One of the obstacles in this part was to incorporate these three types of molecule into the membrane uniformly. Naturally, due to similar properties, collagen and elastin are electrocompactable. However, HA was not electrocompactable. Thus, two fabrication procedures were conducted. One way is to do HA amination firstly and then co-electrocompact collagen, elastin, and HA. Another way is to co-electrocompact collagen and elastin, then couple HA into the collagen/elastin scaffolds. The second way was finally choose for later applications due to convenience and simplicity. A trail application of using electrocompacted collagen thread for nerve repair was also explored in this chapter.

In chapter 5, the ability of such a collagen/elastin/hyaluronic acid (CEH) scaffold in supporting dermis, epidermis, and full skin regeneration was investigated and demonstrated. The results confirmed its superior ability in supporting HDFs proliferation, inducing HDFs differentiation into myofibroblast, new ECM deposition in dermis. Epidermis regeneration supporting was also confirmed in terms of HaCaTs growth, stratification, and differentiation. After the organotypic co-culture of HDFs and HaCaTs on the CEH scaffold, a two-layered dermal/epidermal structure was also reconstructed. All these results demonstrated the superior potential of this CEH scaffold in the application of skin regeneration and wound healing.

In conclusion, in this research, the ECM component-based scaffolds were fabricated and evaluated for skin regeneration. The unique property of such scaffolds are densely packed, highly ordered collagen bundles that can mimic the intrinsic structural and compositional

property of natural skin ECM. By integrating the ECM cue, the ECM-like CEH scaffold demonstrated its superior ability in supporting skin cell function and skin regeneration.

While further research will be necessary, current findings of this research demonstrate the superior ability of such scaffolds in supporting dermis, epidermis, and full skin regeneration. The proposed study will provide a strong base for further advancing exploration and clinical application of skin tissue engineering.

## 6.2 Future work

With the ability of the CEH scaffold in supporting skin regeneration being proved, further detailed in vitro and in vivo studies will still be required to better elucidate the scaffold-cell interactions. More work could be done to improve the performance of the biomimicry scaffolds in skin repair and regeneration.

Incorporation of growth factors into the scaffold represents another promising area to explore [1]. Growth factors are critical extracellular cues during the wound healing process [2]. Supplements of exogenous growth factors hold tremendous potentials to induce faster re-epithelialization and wound healing process. Essential growth factors involved in the wound healing process include platelet-derived growth factor (PDGF) [3], epidermal growth factor (EGF) [4], transforming growth factor - β [5], heparin-binding EGF-like growth factor and so on. Incorporating growth factors into the collagen-based scaffolds through co-electrocompaction should result in more advanced physiochemical and biological performances. By achieving an appropriate release profile, this will be of great interest in terms of the bioengineering of biomimetic and functional skin scaffolds.

The skin is a highly complicated and sensitive organ [6]. It is densely innervated with different structures, such as hair follicles, nerves, blood vessels, and melanin. These structures enabled various skin functions such as barrier function, perceptions, nutrients transportation [7]. For successful wound healing, it is of crucial importance that angiogenesis and nerve regeneration processes take place [8]. Tissue engineered skin with improved nerve regeneration property by the incorporation of Schwann cells was constructed [7]. A 3D pre-vascularized skin patch pre-loaded endothelial progenitor cells (EPCs) and adipose stem cells (ASCs) was reported to stimulate wound closure and induce vascular regeneration [9]. As such, the double-layered cellular constructs built in this

research could be employed as a model to investigate vascularization and nerve innervation. This could be done through co-culture with relevant cell types, such as human umbilical vein endothelial cells and neural stem cells.

An in vivo cutaneous wound healing model on immunodeficient mice could also be considered. Especially, as reported by Cubo et, al [10], a skin-humanized mice model was utilized to analysis the in vivo maturation and differentiation of a 3D printed skin patch. Such model were reported to be an excellent system to perform in vivo human skin experiments in long term.

## 6.3 References


1. Huang, Sha, and Xiaobing Fu. "Naturally derived materials-based cell and drug delivery systems in skin regeneration." *Journal of Controlled Release* 142.2 (2010): 149-159.

2. Moulin, Véronique. "Growth factors in skin wound healing." *European journal of cell biology* 68.1 (1995): 1-7.

3. Yang, Hee Seok, et al. "Enhanced skin wound healing by a sustained release of growth factors contained in platelet-rich plasma." *Experimental & molecular medicine* 43.11 (2011): 622-629.

4. Choi, Ji Suk, Kam W. Leong, and Hyuk Sang Yoo. "In vivo wound healing of diabetic ulcers using electrospun nanofibers immobilized with human epidermal growth factor (EGF)." *Biomaterials* 29.5 (2008): 587-596.

5. Jost, Monika, Csaba Kari, and Ulrich Rodeck. "The EGF receptor–an essential regulator of multiple epidermal functions." *European Journal of Dermatology* 10.7 (2000): 505-10.

6. Zaidi, Zohra, and Sean W. Lanigan. "Skin: structure and function." *Dermatology in Clinical Practice*. Springer, London, 2010. 1-15.

7. Blais, Mathieu, et al. "Concise review: tissue-engineered skin and nerve regeneration in burn treatment." *Stem cells translational medicine* 2.7 (2013): 545-551.

8. Li, William W., et al. "The role of therapeutic angiogenesis in tissue repair and regeneration." *Advances in skin & wound care* 18.9 (2005): 491-500.

9. Kim, Byoung Soo, et al. "3D cell printing of in vitro stabilized skin model and in vivo pre-vascularized skin patch using tissue-specific extracellular matrix bioink: a step towards advanced skin tissue engineering." *Biomaterials* 168 (2018): 38-53.

10. Cubo, Nieves, et al. "3D bioprinting of functional human skin: production and in vivo analysis." Biofabrication 9.1 (2016): 015006.